Harvard-Smithsonian Center for Astrophysics

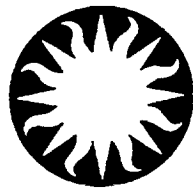

Preprint Series

No. 4621
(Received November 19, 1997)

THE EVOLUTION OF GAS AND STARS IN THE MERGER GALAXY NGC 1316 (FORNAX A)

G. Mackie and G. Fabbiano
Harvard-Smithsonian Center for Astrophysics

To appear in
Astronomical Journal
February 1998

HARVARD COLLEGE OBSERVATORY SMITHSONIAN ASTROPHYSICAL OBSERVATORY
60 Garden Street, Cambridge, Massachusetts 02138

An X-ray Catalog and Atlas of Galaxies by G. Fabbiano, D-W. Kim, and G. Trinchieri, Ap.J.Suppl. 1992, 80, 531-644.

The X-ray spectra of Galaxies: I. Spectral Fits of Individual Galaxies and X-ray Colors by D-W. Kim, G. Fabbiano, and G. Trinchieri, Ap.J.Suppl. 1992, 80, 531.

The X-ray Spectra of Galaxies: II. Average Spectral Properties and Emission Mechanisms by D-W. Kim, G. Fabbiano and G. Trinchieri, Ap.J. 1992, 393, 134.

Prepints are attached.

*A Multiparametric Analysis of the *Einstein* Sample of Early-type Galaxies. II: Galaxy Formation History and Properties of the ISM by P. Eskridge, G. Fabbiano, and D-W. Kim, Ap.J. 1995, 442, 2.

*A Multiparametric Analysis of the *Einstein* Sample of Early-type Galaxies. III: Comparisons with the κ Parameters, Ap.J. 1995, 448, 7-.

*ROSAT PSPC Observations of NGC 507/499: Central Cooling and Mass Determination, by D-W. Kim, and G. Fabbiano, Ap.J., 1995, 441, 182.

*ROSAT PSPC Observations of Two Dynamically Young Elliptical Galaxies: NGC 4125 and NGC 3610 by G. Fabbiano and F. Schweizer, Ap.J. 1995, 447, 572.

ASCA Spectra of the X-ray Faint S0 Galaxy NGC 4382 by D-W. Kim, G. Fabbiano, H. Matsumoto, K. Koyama, and G. Trinchieri, Ap.J. 1996, 468, 175.

ROSAT PSPC Observations of NGC4636: Interaction with Virgo Gas? by G. Trinchieri, D-W. Kim, G. Fabbiano, and C. Canizares, Ap.J. 1994, 428, 555.

*ROSAT PSPC Observations of two X-ray faint Early-type Galaxies: NGC 4365 and NGC 4382 by G. Fabbiano, D-W. Kim, G. Trinchieri, and C. Canizares, Ap.J. 1994, 429, 94.

*The very soft X-ray emission of X-ray faint early-type galaxies by S. Pellegrini and G. Fabbiano, Ap.J. 1994, 429, 105.

*Detection of Soft X-rays from SN 1993J Six Days after Outburst NATURE 1994, 367, 621.

X-ray Properties of Early-type Galaxies by G. Fabbiano, ESO proc. of the Elba Conference (J. Danziger, W.W. Zeilinger and K. Kjar, eds.), ESO proc. No. 45, p.617.

Coronal Stellar Emission in Galaxies by G. Fabbiano, in Physics of Solar and Stellar Coronae: G.S. Vaiana Memorial Symposium (J. F. Linsky and S. Serio, eds; Kluwer) 1993, p. 267.

Normal Galaxies and their X-ray Binary Populations by G. Fabbiano, to appear in "X-ray Binaries" (W. Lewin, J. van Paradijs, and E. van den Heuvel, eds; Cambridge Univ. Press), 1995.

X-ray continuum and iron K emission line from the radio galaxy 3C 390.3 by M. Inda, K. Makishima, Y. Kohmura, M. Tashiro, T. Ohashi, P. Barr, K. Hayashida, G.G.C. Palumbo, G. Trinchieri, M. Elvis, and G. Fabbiano, Ap.J. 1994, 420, 143.

High Resolution Optical and UV Observations of the Centers of NGC 1316 and NGC 3998 by G. Fabbiano, C. Fassnacht, and G. Trinchieri, Ap.J. 1994, 429, 94.

*The insignificance of "Heating flows" in "cooling flow" clusters of galaxies by C.R. Canizares, T.H. Markert, Sera Markoff, and J.P. Hughes, Ap.J.Lett. 1993, 405, 17.

This grant was instrumental on supporting a number of research projects, including the analysis of archival Einstein data, and ROSAT and ASCA observations. Highlights of this work include:

- The final production and publication of the Einstein galaxy catalog, resulting in a database of 450 galaxies observed in X-rays.
- X-ray spectral survey of galaxies observed with Einstein, which showed clear trends in galaxies of different morphology, pointing to different sources of the X-ray emission. This work also led to the discovery of different spectral properties in X-ray faint and X-ray bright E and S0, which was then followed up by ourselves and other authors with many ROSAT and ASCA papers.
- Multiwavelength correlation analyses of the Einstein E and S0 sample, which pointed out the combined effect of potential depth and shape in the galaxy's ability of retaining an extended hot gaseous halo.
- Multiwavelength correlation analyses of the Einstein Spiral and Irregular sample. This work was part of the Senior Thesis of A. Shapley, a Harvard undergraduate, now a graduate student in Caltech. This work was presented in a poster at the AAS Washington meeting (Jan 1998), and is beeing written up in three papers for publication.
- Investigations of the X-ray properties of X-ray faint galaxies, with both ROSAT and ASCA. This work clearly shows different spectral properties which we interpret as evidence of complex emission, including both the integrated emission of discrete X-ray sources, and a gaseous component in some cases. We also pointed out the possibility of a population of very soft soft sources in these galaxies.
- Investigation of the X-ray properties of X-ray bright galaxies, where the emission is dominated by hot extended halos, which can be used to measure the galaxy's mass.

A list of significant papers produced under support of this grant is given below.

*indicates paper previously supplied.

The Evolution of Gas and Stars in the Merger Galaxy NGC1316 (Fornax A) by G. Mackie and G. Fabbiano, Ap.J., Feb 1998.

ROSAT X-ray Observations of the Radio Galaxy NGC1316 (Fornax A) by D-W. Kim, G. Fabbiano, and G. Mackie, Ap.J. 1998.

*A Multiparametric Analysis of the *Einstein* Sample of Early-Type Galaxies. I. Luminosity and ISM Parameters by P. Eskridge, G. Fabbiano, and D-W. Kim, Ap.J.Supp. 1995, 97, 141-184.

The Evolution of Gas and Stars in the merger galaxy NGC 1316 (Fornax A)

G. Mackie[1] and G. Fabbiano
Harvard-Smithsonian Center for Astrophysics,
60 Garden Street, Cambridge, MA 02138

ABSTRACT

We present optical and archival X-ray data on the disturbed morphology radio elliptical NGC 1316 (Fornax A) that displays numerous low surface brightness shells, loops and tails. An extended (81x27″ or 9x3 kpc) emission line region (EELR) at a projected distance of 35 kpc from the nucleus has been discovered in a ~90x35 kpc, ~3.0x10^9 $L_{B\odot}$ tidal tail. The position and extreme size of the EELR suggest it is related to the merger process. We suggest that the ionization mechanism of the EELR is shock excitation, and the gas is remnant from the merger progenitor. X-ray emission is detected near two tidal tails. Hot, ~5 x 10^6K gas is probably the predominant gas component in the tidal tail ISM. However based on the current tidal tail (cold + warm + hot) gas mass, a large fraction of the tidal tail progenitor gas may already reside in the nucleus of NGC 1316. The numerous and varied tidal tail system suggests that a disk-disk or disk-E merger could have taken place $\geq$ 1 Gyr ago, whilst a low mass, gas rich galaxy started to merge $\sim$ 0.5 Gyr ago.

Subject headings: galaxies: structure — galaxies: photometry — galaxies: peculiar — galaxies: individual — galaxies: interactions — X-rays: galaxies

[1]Visiting Astronomer, Cerro Tololo Inter-American Observatory. CTIO is operated by AURA, Inc. under contract to the National Science Foundation.

Center for Astrophysics
Preprint Series No. 4621

THE EVOLUTION OF GAS AND STARS IN THE MERGER GALAXY NGC 1316 (FORNAX A)

G. Mackie and G. Fabbiano
Harvard-Smithsonian Center for Astrophysics

1. Introduction

NGC 1316 (Fornax A, PKS 0320-37, Arp 154) is one of the closest, D = 22.8 Mpc (adopting v_0=1713 km s^{-1}, Sandage and Tammann 1981, hereafter RSA, and H_0 = 75 km s^{-1} Mpc^{-1}) and brightest radio galaxies in the sky. Its catalogue morphological type is uncertain, being described as Sa pec (merger?) in RSA. It is located on the outskirts of the Fornax cluster, and is projected 3.7° from the centrally located cluster giant elliptical NGC 1399. Extensive optical observations of Schweizer (1980), hereafter S80, and Schweizer (1981) show NGC 1316 ($M_B \sim -22.7$) possessing a surprisingly small core radius and high central surface brightness for its luminosity. These unusual core properties alone may suggest a previous merger event (Kormendy 1987) has taken place. S80 showed NGC 1316 to be a D-type galaxy with an elliptical-like spheroid surrounded by a large envelope. Photographic plate imagery shows the envelope possessing numerous low surface brightness arcs or shells and loops, including a large loop that extends ~25′ S–SW (~170 kpc adopting 9″/kpc) from the galaxy nucleus. Long-slit spectroscopy by S80 shows a rapidly rotating ($v\sin i$ ~350 km s^{-1}) disk of ionized gas in the centre of the galaxy with a rotation axis almost 90° from the stellar rotation axis and a single giant H II region was discovered 6.7′ S of the nucleus.

NGC 1316 also shows activity that may be related to its dynamical history and environment. It displays low-ionization emission-line spectra in its nucleus (Veron-Cetty and Veron 1986; Phillips *et al.* 1986), as well as a steep spectrum radio core with dual–opposing jets (Geldzahler and Fomalont 1984). It has a double-lobe radio continuum structure (Ekers *et al.* 1983) with a diameter of ~35′ that exists primarily outside of the optical galaxy. HST FOC imaging by Fabbiano *et al.* (1994) shows that NGC 1316 possesses a UV-bright, unresolved nucleus. *ROSAT* HRI observations of hot gaseous emission in the central region of NGC 1316 by Kim *et al.* (1997) suggest a hot (10^7K) ISM exists with $M_{gas} \sim 10^9$ $M_\odot$ and sets a 3σ upper limit <9x10^{39} erg s^{-1} for a nuclear point-like source. Shaya *et al.* (1996) presented HST Planetary Camera V and I images that confirmed the existence of a small, 34 pc, core radius and found a central non-isothermal luminosity profile. The star cluster population appears to be quite normal in terms of colour and luminosity, with little sign of a young population, in contrast to other studies of merger galaxies (eg. NGC 1275, Holtzman *et al.* 1992; NGC 7252, Whitmore *et al.* 1993; NGC 4038/9, Whitmore and Schweizer 1995).

The origin of tidal tails such as those seen in NGC 1316 is firmly established. Toomre and Toomre (1972) and Toomre (1977) proposed that gravitational interactions between disk galaxies could form tidal features. Further, Toomre (1977) suggested that such disk-disk mergers could ultimately resemble ellipticals. Theoretical studies of equal mass disk-disk mergers by Barnes (1992) have strengthened the case of a merger origin for some ellipticals, whilst recent models (Barnes and Hernquist 1996) have included gas dynamics showing that large central concentrations of gas can form in the cores of merger remnants. Such predictions have been verified by the detection of large amounts of molecular gas in merger galaxies such as NGC 520 (Sanders *et al.* 1988), NGC 4038/9 (Stanford *et al.* 1990) and NGC 7252 (Dupraz *et al.* 1990).

Multi-wavelength observations of mergers can provide important constraints on the types of progenitors, the stellar and gaseous properties of tidal features and merger remnant and the ultimate fate of the remnant. Hibbard *et al.* (1994) presented optical, radio and X-ray observations of the merger remnant NGC 7252. Large amounts of H I exist in the tidal tails, showing inflow into the merger core although there is no H I in the main stellar body. X-ray emission is detected, centred on the main stellar body only. Computed X-ray luminosities suggest that the emission in NGC 7252 is larger than expected for a spiral, and lower than expected for an elliptical of the same blue luminosity. The lack of atomic hydrogen in the main body of the remnant, combined with the presence of warm ionized gas in the nucleus, and possible hot, ~10^{6-7}K, gas inferred from X-ray measurements, suggests an efficient mechanism converts H I into other gaseous phases. Hibbard and Mihos (1995) made N-body simulations of NGC 7252 in order to explain the H I observations. The kinematics of the H I showed a velocity reversal along the tails that could be successfully modelled as material in the base of the tails falling back to smaller radii of the merger remnant. A comprehensive H I, H II and R-band study of five mergers (including NGC 7252) is presented in Hibbard and van Gorkom (1996). Several trends are evident along the merging sequence including the presence of H I in the disks of the early mergers, and the scarcity of H I in the remnant bodies

of the more evolved systems. Efficient gas conversion appears to be a fundamental property along the disk-disk merger evolutionary sequence.

We present very deep CCD observations of NGC 1316 made with the CTIO Schmidt, and *ROSAT* archival X-ray images. In this paper the discovery of an extended, emission line region, at large radii from the nucleus of NGC 1316, yet located within a prominent low surface brightness tidal tail is presented. X-ray emission is detected, possibly for the first time, associated with two tidal tails. We shall discuss the stellar and gaseous properties of the two prominent tidal tails, the probable excitation mechanism of the extended emission line region, and the probable history of merger events in the system. The observations are described in §II. Reduction and analysis of the data is given in §III. A discussion of the results is given in §IV.

2. Optical Observations and Data Reduction

The CCD images presented in this paper were taken with the CTIO/University of Michigan Curtis Schmidt 0.6/0.9m telescope. The detector was a Thomson 1024x1024 CCD. The pixel size is 19μm square (1.835″) however vignetting limits the useable field size to about 30′. Multiple bias and dark images were taken. Flatfields were generated from twilight sky exposures each night. B band (λ_c = 4324Å, FWHM=1156Å; CTIO Harris set #2) exposures were taken on the night of 1994 November 10/11. The night was not photometric. Individual exposures were 900s with small shifts between successive exposures. The total exposure time was 11,700s. Narrowband (Hα+[NII]) exposures were taken on the night of 1994 November 11/12. The night was photometric. Individual exposures were typically 1200s with small telescope shifts between exposures. Total exposure times were 8100s each for the redshifted Hα+[NII] (λ 6563 + $\lambda\lambda$ 6548,6583) emission line filter (λ_c = 6606Å, FWHM=76Å), and continuum filter (λ_c = 6693Å, FWHM=81Å). Based on the half power points of the 6606Å line filter and assuming emission centred at 6563Å the filter will be sensitive to emission over the velocity range of 250–3700 km s^{-1}.

Images were bias subtracted, flatfielded, and added after registration by centroiding on bright stars. Since the night of 1994 November 10/11 was not photometric, B band standard star observations were not taken. The observations were calibrated using previous aperture photometry listed in Lauberts and Sadler (1984). Twelve previous B band photoelectric measurements with aperture diameter sizes ranging from 30.0 to 203.3″ were used to derive a zeropoint of the CCD data with a dispersion of 0.04 mag. The spectrophotometric standard HZ 4 was used to calibrate the narrow band images based on AB magnitudes (Oke 1994, priv. comm). The adopted magnitudes for HZ 4 were AB_{6606}=15.01 and AB_{6693}=14.81. The Hα+[NII] image was derived by subtracting a scaled, sky subtracted continuum image from the sky subtracted emission line image. PSF widths of stars in the on-line and continuum images were measured and they agreed within measuring errors. The adopted scaling was calculated from a linear least square fit to residuals of 25 field stars calculated from several scaling factors. Mean pixel values of the final Hα+[NII] image at large radii from the nucleus were consistent with zero. The Hα+[NII] image was smoothed with a Gaussian filter of σ = 3 pixels. A B-6693Å colour map was constructed from the B and narrowband red continuum filter (λ_c = 6693Å, FWHM=81Å) image. PSF widths of stars were matched via slight smoothing, and images were registered via centroiding on bright stars.

3. Analysis

3.1. B band images and NGC 1316 model

Figure 1 shows the NGC 1316 B band median filtered (stacked) image produced from 13 900s individual images. The galaxy ~6.4′ N of NGC 1316 is NGC 1317 (v_0=1893 km s^{-1} from RSA) that appears very regular, with no sign of structural disturbance. Figure 1 clearly shows the shells, ridges and loops of material at large radii. A prominent tidal tail originates SW of the main body of NGC 1316, then extends to the NW, ending in a straight feature. This is L_1 denoted by S80 (see also the sketch map, Figure 2 of S80). A second prominent tail, E of the nucleus, was denoted L_2. Other ripple features closer to the nucleus and fainter loops (L_3 and L_4 in S80, N and SW of L_2 respectively) are seen. In this paper we will concentrate on the two most prominent tails, L_1 and L_2.

This median image shows that the NW portion of L_1 is relatively narrow and quite straight, extending SE–NW. Progressing towards the SE, the loop then bends toward a P.A. of ~90° and becomes much wider. The faint light morphology suggests that this

section of L_1 is a distinct plateau from the main body of NGC 1316. L_2 is structurally more simple than L_1, and appears as a loop of material curving into the central region of NGC 1316. To isolate L_1 and L_2 from the envelope of NGC 1316, an isophotal model of NGC 1316 was made using IRAF [2] *ellipse* and *bmodel* tasks. Features such as NGC 1317 and the nuclear dust lane were masked from the fit. As well, clipping of the highest 10% of pixels in each isophotal fit was implemented to ignore faint light features such as the loops and shells themselves and any faint stars and galaxies that remained undetected by eye. The elliptical model extended to just outside the furthest extent of L_1 and L_2. The accuracy of the model is poor within 1′ of the nucleus due to the existence of the nuclear dust lane, however this does not effect the modelling near the tidal tails. The images displayed very good field flattening with small errors in the sky values (±0.4%) across the image.

Figure 2 shows the B band residual light derived from the median image (Figure 1) after isophotal model subtraction. This image clearly shows the complexity of low light features in the outer envelope of NGC 1316. The projected size of L_1 is ~90x35 kpc and the broadening of L_1 in the SE and its "plateau" nature as suggested by Figure 1 is confirmed. Its southern edge is quite sharp, although the main SE–NW component of L_1 can not be mistaken for a shell due to its extreme width and nearly uniform brightness. The apparent width of L_1 may be a projection effect, since tidal tails are usually flattened systems (Toomre and Toomre 1972). The majority of L_1 spans less than two magnitudes in surface brightness (25–27 B mag. arcsec^{-2}). L_2 is slightly shorter in projected size and much more loop-like than L_1, and shows a small variation in surface brightness (brighter at its S edge) yet is fainter overall than L_1.

The white (deficit) region in the nucleus of length 2′ at a P.A. of ~160° is the nuclear dust lane. Several extended, clumpy residual regions are seen within 2–3′ (NE, NW and SW) of the nucleus, as well as many shells. These regions are not artifacts of the isophotal model subtraction. The residual region to the NW at a P.A. of –40° contains the plume 'P' noted by S80 and subsequently suggested by Graham (1987) as a region of blue stars. The sketch map of Figure 2 in S80 suggests that L_2 joins this plume region, however it also seems possible that L_2 ends more abruptly in another residual region, NE of the nucleus, at a P.A. of 35°. A third residual region, 2.5′ SW of the nucleus could be associated with L_1. Overlayed on Figure 2 are lines showing the axis of stellar rotation at P.A. = 140° as determined by Bosma *et al.* (1985) and the direction of the two outer radio lobes (Ekers *et al.* 1983) at P.A. = 110°.

Tests showed that the parameters used to exclude extraneous faint features in the isophotal modelling were more important than flat fielding errors when determining the errors in the residual light components. By varying the amount of pixel clipping in each isophote (from our adopted 10%) and constraining the residual pixel value to be zero at large distances from the tidal features, we estimate our errors in the residual light of L_1 and L_2 to be ±30%. To estimate the stellar luminosity of L_1 the residual light was summed, after careful exclusion of bright (foreground) stars. An aperture of 90 x 37 kpc was used. An L_B (L_1) = 3.1x10^9 $L_{B\odot}$ or 2.2% of L_B (NGC 1316) is found. We have done a similar analysis to determine the optical luminosity of L_2. A 31 x 18 kpc aperture was used and L_B (L_2) = 2.6x10^9 $L_{B\odot}$ was derived. Profile fits to the broadband surface brightness (excluding the loops and ripples) of NGC 1316 support the findings in S80 that NGC 1316 follows an $r^{1/4}$-law very closely, suggesting that the main stellar body has relaxed to an equilibrium configuration. If L_1 and L_2 were formed by major merger events, with original luminosities well in excess of our calculated values above, our isophotal model could be overestimating the spheroidal light. This problem is inherent to any evolved merger system. Later results and discussion will however propose that the L_1 tidal system is probably a recent merger event, and therefore the derived luminosity is representative of the original pre-merger value.

3.2. The discovery and properties of the EELR

Figure 3 shows NGC 1316 with Hα+[NII] emission in greyscale overlayed with B band (total) contours of 23, 24, 25 and 26 mag. arcsec^{-2}. The newly discovered extended emission line region is labelled EELR, the giant H II region (2.6′ SE of the EELR) found in S80 is labelled SH2, and L_1 is also denoted. The positions of the EELR and SH2 relative to NGC 1316 are given in Table 1. The nuclear gas disk is seen, as is Hα+[NII] associated with NGC 1317. The EELR

[2] IRAF is distributed by the National Optical Astronomy Observatories, which is operated by the Association of Universities for Research in Astronomy, Inc. (AURA) under cooperative agreement with the National Science Foundation.

is situated ~5.3′ (35 kpc projected distance) SW of the nucleus of NGC 1316 and is located in the previously described plateau region of L_1. Comparison with the Figure 2 sketch map of S80 shows that the EELR is near a major dust lane. Inspection of the B band residual image shows strong extinction in the vicinity of the EELR that is structurally similar to the EELR. The position angle of the EELR, ~45°, is almost perpendicular to the predominant direction (SE–NW) of L_1. Very faint Hα+[NII] is also seen between the nuclear gas disk and NGC 1317, yet none is seen near L_2.

The SW quadrant of NGC 1316 is shown in Figure 4. Contours show Hα+[NII] emission, whilst greyscale depicts B band residual light (summed B image - isophotal model), clearly showing the intensity and structure of L_1. Several bright foreground stars are also seen in projection in L_1. The position of the EELR is at the central E edge of L_1. Interestingly, SH2 may be located in L_1 as well. There are no other bright, extended Hα+[NII] regions in L_1. The association between L_1 and the B band residual region, 2.5′ SW of the nucleus is shown more clearly, and suggests that it could be part of L_1. After excluding a foreground star, this region has a similar surface brightness to the main part of L_1. The other residual B band regions (NE and NW of the nucleus) are shown, as well as smaller (than the EELR) Hα+[NII] regions 2′ N of the nuclear gas disk and extending to the W. A close-up view of the EELR is given in Figure 5. The greyscale depicts Hα+[NII] emission, and contour levels at 2.0 and 4.0 x10^{-17} erg cm^{-2} s^{-1} arcsec^{-2} are also shown. A disturbed morphology is suggested, with its long axis extending along the NE-SW direction. The size of the ionized gas region is 81x27″ or 9x3 kpc. Central concentrations are evident along the major axis of the EELR and close-by, faint blobs of emission are also seen. The integrated flux of the EELR, $f_{H\alpha+[NII]}$ is 8.1x10^{-14} erg cm^{-2} s^{-1}.

3.3. The hot gas environment near L_1, L_2 and the EELR

A *ROSAT* Position Sensitive Proportional Counter (PSPC; Pfeffermann *et al.* 1987) image of NGC 1316 (FWHM ~ 25″) was extracted from the U.S. *ROSAT* data archive. This data has been previously used in a study of the X-ray emission associated with the outer radio lobes by Feigelson *et al.* (1995) who showed that the emission, predominantly beyond the field of view of our images, (see their Figure 2) can be explained by Inverse-Compton scattering. The total exposure time was 25.5 ksec. Figure 6 shows contours of PSPC Broadband (0.1-2.4 keV) emission at 3, 5, 10 and 20σ above background overlayed on the B band residual image, shown in greyscale. The PSPC data was binned to a pixel size of 15″ (approximately half of the PSPC FWHM; the PSPC instrumental pixel size is 0.5″) and smoothed with a Gaussian filter of $\sigma = 2$ pixels. The emission is dominated by X-rays from the main body of NGC 1316, however the X-ray emission at large radii is quite complex.

There is substantial X-ray emission cospatial with the higher surface brightness regions of L_1. The EELR is positioned (see arrow in Figure 6) on the N edge of this X-ray emission that extends S then W of NGC 1316. Other X-ray emission, that is cospatial with parts of L_2 (excluding the emission probably originating from the bright star SE of the main region) is seen. A third region of emission extends NW from NGC 1316, where there is little or no residual B band light at large radii. The X-ray emission that extends N from NGC 1316 overlaps with NGC 1317. There is no evidence of X-ray emission near the other loops or tails in the system.

An analysis of the PSPC data within 3′ of the nucleus (not including the emission near L_1 or L_2) has been done by Kim *et al.* (1997). The X-ray spectrum is consistent with hot gaseous emission, with an $L_X \sim 2 \times 10^{41}$ erg s^{-1} (for the Kim *et al.* 1997 adopted distance of 27.2 Mpc), and a possible hard component that could be due to low-mass binaries, contributing 20-30% of the flux. We concentrate on the X-ray emission at intermediate radii that has not been studied. The good correspondence of X-ray emission with both L_1 and L_2 tidal tails suggests a physical association. The origin of the emission could be binary sources and SNR in the tails and/or hot gas resulting from the merger process or from the evolution of the ISM in the tails. To investigate the origin of the X-ray emission, PSPC spectra have been extracted from the tidal tail regions (for the apertures used see Table 2). The background was taken well away from source emission (N. of NGC 1317), and vignetting corrections were applied to the data. The total PSPC spectral counts were 712±71 and 280±47 for the L_1 and L_2 regions respectively. Given the limited statistics of the data for the L_2 region, we concentrate on finding acceptable XSPEC spectral fits for the L_1 region emission. Table 2 summarizes our spectral fitting re-

sults.

We find that a single component Raymond and Smith (Raymond and Smith 1977; R-S hereafter) gaseous thermal model yields kT = 0.55 keV (with XSPEC 90% limits of 0.40-0.83 keV for 3 interesting parameters), N_H = 2.3 (1.2-3.5) x 10^{20} cm^{-2}, (consistent with the line of sight N_H = 2 x 10^{20} cm^{-2}; Fabbiano *et al.* 1992), and a very low metal abundance of 5.8 x 10^{-3} (0 - 4.1 x 10^{-2}) of solar. The fit returns a χ^2 of 17.5 for 25 degrees of freedom (d.o.f.). A statistically similar fit to the spectra can be achieved by using a single component Bremsstrahlung model. This model could represent a population of discrete X-ray sources (ie. binaries) in the tidal tails. The fit yields kT = 0.54(0.39-0.80; for 2 interesting parameters) keV, N_H = 2.7(1.7-3.8) x 10^{20} cm^{-2} (again consistent with the line of sight value), and a χ^2 of 19.2 for 26 d.o.f. Both single component models return similar X-ray luminosities (see Table 2) of ~2 x 10^{40} erg s^{-1}. Other model fits have been attempted although none are as good as the single model fits above. An R-S model with fixed line of sight absorption and solar abundance returns an unacceptable χ^2 of 67.3 for 28 d.o.f. A combined R-S (solar abundance) and Bremsstrahlung (kT = 5 keV; a temperature typically used to describe a hard X-ray binary component) model with fixed line of sight absorption, gives a soft R-S temperature of 0.16 keV and returns a χ^2 of 27.9 for 28 d.o.f.

The range of kT suggested by the single model fits (see Table 2) shows that the X-ray emission of L_1 is significantly softer than that expected from a population of evolved stellar sources (see Fabbiano 1989 and refs. therein) suggesting the emission is from a hot ISM. This is not surprising since the expected emission from a population of binary X-ray sources is L_X ~6 x 10^{38} erg s^{-1} in L_1 (using the average L_X-L_B relation of spirals in Fabbiano *et al.* 1992), which is a factor ~10 less than the above calculated luminosities. We adopt an area of 45 x 35 kpc (consistent with the area of X-ray emission in L_1) and a depth of 5 kpc, which assumes that the hot gas is coexistent with the tidal tail, and that the tail is seen face-on, consistent with most tails being flat or ribbon-like (Toomre and Toomre 1972). We adopt the cooling function of Wang and Helfand (1991) used for the LMC and a hot gas L_X ~2 x 10^{40} erg s^{-1} to derive an electron density of $n_e \sim 2.4 \times 10^{-3}\ \eta^{-1/2}$ cm^{-3}, where η is the gas volume filling factor. The mass of hot, ~5 x 10^6K gas in L_1 is then ~ 5 x $10^8\ \eta^{-1/2}$ $M_\odot$. Uncertainties in the volume would suggest an error of 2-3 could exist in our mass estimate. The implied shock velocity for this temperature of gas is ~380 km s^{-1}, much higher than observed for the H I infall velocity at the base of the tidal tails in NGC 7252 (Hibbard *et al.* 1994).

4. Discussion

4.1. Stellar and gaseous content of L_1 and L_2: Clues to the nature of the progenitors

We can attempt to derive the stellar and gas contents of the L_1 progenitor based on the properties of the L_1 tidal tail. We have determined that the luminosity of L_1 is 3.1x10^9 $L_{B\odot}$ with an error of ±30%. There is no evidence of recent star formation due to passage through NGC 1316 (see Section 4.2 for a discussion about the global colour of L_1). The structural characteristics of L_1 (plateau, ridges or ripples and the sharp southern edge), imply that the progenitor was a dynamically "colder" galaxy than NGC 1316 (Quinn and Hernquist 1987). For the following discussion we shall assume that the derived luminosity of L_1 is representative of the total luminosity of its progenitor galaxy. Arguments given later in this section and in section 4.3 will propose that L_1 is substantially different structurally and in gas content from the other tidal tails that are more likely to be indicative of a major disk-disk or disk-E merger.

We can estimate an original H I mass for an L_1 progenitor based on the gas fraction estimates of spirals. Adopting the H I estimates in Table IV of Haynes and Giovanelli (1984) and allowing the possible morphological types of the L_1 progenitor to range from Sa-Sab through Scd-Sd, would suggest an initial H I mass ranging from 8.7x10^8-2.8x10^9 $M_\odot$. This gas mass is substantially more than that detected in observations. Early searches for H I gave upper limits only for NGC 1316. Reif *et al.* (1982) list an upper limit of 4.5 Jy km s^{-1}, whilst Jenkins (1983) derives a similar (to Reif *et al.* 1982) H I mass limit of <2x10^8 $M_\odot$. A VLA H I observation (van Gorkhom 1996 priv. comm.) detects several 10^7 $M_\odot$ of H I near SH2 but only an upper limit of ~1x10^7 $M_\odot$ for the region near the EELR. We can also estimate the amount of H I that could be associated with the dust lane near the EELR. We assume a Galactic gas-to-dust ratio of M_{gas}/M_{dust} = 100, and N_H = 5.8 x 10^{21} E_{B-V} atoms cm^{-2} (Bohlin *et al.* 1978). A_B is measured directly from our B band image and isophotal model, whilst we assume the dust is optically thick

across 5.9×10^7 pc^2. We adopt an R_B =4.10 (Goudfrooij *et al.* 1994b) and derive $M_{HI} = 1.1 \times 10^8$ $M_\odot$, that is substantially larger than the upper limit found near the EELR, but still less than the gas mass predicted from a spiral progenitor.

We determine the ionized gas content of the EELR. We derive $L(H\alpha) = 8.2 \times 10^5$ $L_\odot$ or 3.2×10^{39} erg s^{-1} which is is a factor of ~10 less than the expected $L(H\alpha)$ for a 3.1×10^9 $L_{B\odot}$ late-type spiral based on the $L(H\alpha)$-l_B regression fits of Trinchieri *et al.* (1989). We then convert this $L(H\alpha)$ to a mass, and determine $M_{HII} = 7.5 \times 10^3$ $M_\odot$. A summary of the EELR dust and gas properties is given in Table 3. Therefore, based on a late-type spiral progenitor for L_1 the H II content could be diminished by a factor of ~10, and the H I content, allowing for the range of spiral types, may be diminished by ~30-100. As discussed in Section 3.3, ~5 x 10^8 $M_\odot$ of hot, 6 x 10^6K, gas could also exist near L_1. This could be the first detection of hot gas associated with tidal tails. The presence of a hot ISM may suggest heating by strong shocks (consistent with a merger velocity of a few hundred km s^{-1}). This hot gas may shock heat any cold gas that is falling into the central regions, and can at least partially explain the dearth of H I. We estimate a cooling time, τ_c ~1 x 10^9 $\eta^{1/2}$ yrs, which is larger than our estimated merger lifetime (see Section 4.2) of 0.5 Gyr. The amount of total ISM is in excess of that expected from the outgassing of an evolving stellar population (Faber and Gallagher 1976) over the lifetime of the merger. We assume that the stellar population in the tidal tail is similar to early-type galaxies as assumed in Faber and Gallagher (1976), which is supported by the smooth optical stucture in the tail and the elliptical-like colour (see Section 4.2) across the majority of L_1. We derive an outgassed mass of ~3 x 10^7 $M_\odot$ based on the estimated L_B of L_1 and a 0.5 Gyr lifetime, being the estimated time since the start of the merger encounter. Hence the bulk of the observed gas must be from the pre-merger progenitor.

The existence of a hot ISM in a tidal tail is an important discovery. Other tidal tail systems do not show X-ray emission suggesting a low or non-existent hot gas content. The PSPC observation of NGC 4038/9 (Read *et al.* 1995) detects emission related to the two interacting disks that can be explained by almost equal amounts of discrete source and diffuse emission originating from ~4 x 10^6K gas. The Hibbard *et al.* (1994) PSPC observation of NGC 7252 shows emission centred on the merger remnant body only. Our observations show that in L_1 (and possibly L_2) a hot gas phase exists that is separate to the central hot gas associated with the main stellar body. The shock velocity needed to produce the ~5 x 10^6K gas in L_1, ~380 km s^{-1}, suggests a rapid interaction velocity well in excess of the gas infall velocities in NGC 7252 and may help explain the paucity of H I. We suggest that the extreme size (9 x 3 kpc) of the EELR, the large hot gas content and the extensive and unusual tail morphology (similar to low mass merger models of Hernquist and Quinn 1989) of L_1 support it being the ~0.5 Gyr old remnant of a low mass, gas rich disk galaxy.

The L_2 tail is fainter and much smoother than L_1 although the S section has a slightly higher surface brightness than the rest of the tail. We do not detect any H II emission nor is any H I detected. If the X-ray content in L_2 is similar to that in L_1, and adopting a gas volume of 30 kpc x 15 kpc x 5 kpc, by simple scaling of the ratio of PSPC counts, L_2 may contain ~1 x 10^8 $M_\odot$ of hot gas (see Table 4 for a summary). The smooth structural appearance may suggest a progenitor that is dynamically hotter than the L_1 progenitor. We suggest that L_2 is not necessarily associated with the event that formed L_1 but could be related to a previous disk-disk or disk-E merger. The likely merger history and tidal tail progenitors will be discussed further in Section 4.3.

4.2. The probable ionization mechanism of the EELR

The large size, 9 kpc x 3 kpc (a factor ~5 larger in surface area than SH2) and special (projected) position of the EELR in the high surface brightness region of L_1, argues against it simply being a giant H II region, and connects its existence with the L_1 merger event. Theoretical simulations of low mass mergers (Weil and Hernquist 1993) show that stellar and gaseous (T=10^4K) components *rapidly* segregate with the gas flowing quickly into the nucleus of the primary galaxy whilst the stellar tidal tail evolves. As an example, one model simulation, Figures 2, 3 and 6 of Weil and Hernquist (1993), shows that by a timestep of 60 units, a substantial amount of merger gas has reached the central regions of the primary galaxy, whilst the stellar merger component continues to display low surface brightness shells and loops out to a timestep of 200 units. Hence at least in this case it is possible that a large fraction of the gas rapidly

segregates from its stellar body within 30% of the total time that such stellar merger signatures (shells, loops, tails) are visible.

The stellar light extent of L_1 would *suggest* it is substantially dynamically evolved. We derive an age estimate of L_1 of $\sim 5 \times 10^8$ yrs based on the low mass merger models of Hernquist and Quinn (1988) and Hernquist and Quinn (1989). We compute our age estimate via Equation 2.1 of Hernquist and Quinn (1988), inputting mass estimates for NGC 1316 and the L_1 progenitor, and then comparing the timescale of appearance of similar model structures to that seen in L_1. The error in this age estimate is probably a factor of 2, given the uncertainties of the geometry of the encounter and the long lifetime of the fine structures. If our age estimate is correct then the evolved nature of the stellar component of L_1 should favour a scenario in which the majority of progenitor gas already resides in the nucleus of NGC 1316. Whilst we detect a substantial amount of warm (the EELR) and hot gas, it is possible that the present warm and H I gas content is a factor $\sim$10 and $\sim$30-100 smaller (see Section 4.1) respectively than their original values. CO observations of NGC 1316 by Sage and Galletta (1993) detect $\sim 1 \times 10^9$ $M_\odot$ of H_2 that is coextensive with dust in the central ionized gas disk. Velocities suggest that the ionized and molecular gas are corotating, and the observations support an external origin for the warm gas and H_2. Therefore it is possible that a large fraction of the incoming galaxies original gas has settled into the nucleus of NGC 1316, in agreement with the rapid segregation predictions of Weil and Hernquist (1993).

There is no indication of a concentrated, stellar remnant within L_1. Inspection of the B-6693Å colour map shows that the *predominant* colour of L_1 is similar to non-disturbed areas of NGC 1316 at similar radii. Small blue regions are seen but do not dominate the L_1 colour. Hence there appears to be no compelling evidence for a present epoch, high star formation rate. The argument for photoionization of the EELR by young stars or hot old stars appears weak due to the lack of any unusual colour near the EELR. Based on the above, and the existence of the nearby structurally similar dust lane, we suggest that the most probable ionization mechanism of the EELR is shock excitation of remnant cold gas of the L_1 progenitor. Spectroscopic observations are required to determine this conclusively and establish its dynamical properties.

4.3. A merger (or more?) in progress

The complicated structure of NGC 1316 hinders an accurate reconstruction of its merger history. The small amount of H I does not allow a dynamical study to be done as in Hibbard and Mihos (1995) for the tidal tails in NGC 7252, and hampers attempts to predict the merger progenitor types. S80 proposed the infall of several gas-rich galaxies over the past $\sim 2 \times 10^9$ yrs to explain the system. Similarities between numerical models and observed systems of disk-disk mergers and some features of NGC 1316 also suggest that it could be an old remnant of a major disk-disk merger. It is also possible that both processes are occurring. In the case of a major disk-disk merger the lack of well defined bright tidal tails at large radii (eg. as seen in NGC 7252, Schweizer 1982; NGC 4038/9, Toomre and Toomre 1972) and the lack of H I in the tidal tails would support it being a substantially evolved merger system. The central surface brightness profile (excluding the loops and ripples) of NGC 1316 was found to follow an $r^{1/4}$-law very closely, hence the main stellar body has relaxed to an equilibrium configuration. This again supports an evolved system. The existence of nuclear H_2 and warm gas and a central hot (10^7K) ISM (Kim *et al.* 1997) and a possible mass of $\sim 6 \times 10^8$ $M_\odot$ of $\sim 5 \times 10^6$K gas associated with two tidal tails would support an efficient and evolved conversion of H I into other phases as seen in other merger systems (Hibbard and van Gorkom 1996).

The very faint (S80 estimates 27-28 mag. arcsec^{-2} in B) loop of stellar material (denoted L_5 in S80) that extends 25′ S-SW of the galaxy (outside our CCD field of view but shown in Figure 9 in S80) and the shorter length loop L_2 that are opposing, may be associated with one merger event. Whilst two equal length tails are typically associated with the classical picture of a disk-disk merger (Toomre and Toomre 1972), it is possible (Balcells 1997) to produce two different length and surface brightness tails (ie. L_2 and L_5) by the merger of a single spiral with a pre-existing elliptical given a special impact trajectory. However, without such special impact parameters, the narrowness of the L_2 and L_5 features is hard to explain by an interaction with a dynamically hot elliptical that should typically produce broad features. L_2 has no detectable H I or H II which argues for it to be substantially evolved, whilst the gaseous content of L_5 is unknown although S80 does describe variations in its structure that may suggest associations of young

stars. Shorter tails can also be produced via a bulge-dominated progenitor, which is also consistent with the low cold and warm gas content in L_2.

The properties of L_1 suggest that it is a singular merger event. The structure of the tidal tail is remarkably similar to structures produced in the low mass merger models of Hernquist and Quinn (1989). The existence of a 9 x 3 kpc, $\sim 10^4$ $M_\odot$ of $\sim 10^4$K gas (the EELR) is unusual in a tidal tail. The position of the EELR in the highest surface brightness region of L_1 and its disk-like shape suggest that it could be the remnant of a cold gaseous disk. The gas content and optical structure and brightness range of L_1 are very different to both L_2 and L_5 again suggesting different origins. Could L_1 be related to a previous disk-disk or disk-E merger event? Schweizer and Seitzer (1992) have suggested that delayed splashbacks of material can occur for several Gyr after an initial merger event. A splashback event would probably show extensive, disturbed stellar light (and possibly cold and warm gas) at large radii which is not seen. The centrally located position of the EELR, and the clean, compact stellar structure of L_1 argues against it being a splashback event. The broader shape of L_1 to that of L_2 and L_5 should argue for a merger event with an evolved, hot system. We believe the observational evidence support L_1 being a $\sim$0.5 Gyr old remnant of a gas rich galaxy on a high velocity encounter with the halo of NGC 1316.

The varied and numerous fine structures and gaseous properties of NGC 1316 may also be consistent with separate merger events. However, a recent study suggests that a major disk-disk merger can produce fine structure features that have been previously associated with low mass mergers. Balcells (1997) has observed NGC 3656 and finds two, low surface brightness tails, and argues for a major disk-disk merger origin of shells and a minor axis dust lane. In NGC 3656 however, the tidal tails are similar in brightness and extent, and are very different to the complex and numerous tidal tail system of NGC 1316. The NGC 1316 tidal tail system comprises 5 tails or loops of varying morphology, which argues for more than one merger event. The existence of nuclear molecular gas and a warm gas disk, and special nuclear (small core radius, high surface brightness) properties also suggest that earlier merger events may have taken place before the L_1 event began. The location of NGC 1316 in a cluster may also provide opportunities for multiple mergers. Adopting a mean expansion velocity of 200 km s^{-1} for the L_5 tail infers a timescale of $\sim$1 Gyr. This is similar to the timescales of the merger remnants NGC 7252 and NGC 3921 (Schweizer and Seitzer 1992). The faintness and low H I contents of L_2 and L_5 tails compared to the tails of NGC 7252 and NGC 3921 may imply an even longer timescale for a disk-disk or disk-E merger. In contrast, using the same encounter velocity for the L_1 tail, a $\sim$5 x 10^8 yr dynamical age is derived which agrees with our previous age estimate for L_1 based on the models of Hernquist and Quinn (1988). If the shock velocity, $\sim$380 km s^{-1}, inferred from the hot gas temperature of the L_1 region is representative of the encounter velocity then the above estimate of the L_1 age may even be too large, by a factor of $\sim$2. Hence, whilst a significant amount of mass in NGC 1316 could have been deposited by an early disk-disk or disk-E merger, optical and X-ray observations presented here suggest that a recent, ongoing low mass, gas rich galaxy is still in the process of merging.

We would like to thank Arturo Gomez for assistance at the CTIO Schmidt, Bev Oke for providing spectrophotometric scan information, and Jacqueline van Gorkom for supplying information about her VLA observations of NGC 1316. We thank Brian McNamara for comments on an early draft of the manuscript. We also thank the referee for many constructive comments that greatly improved the paper. The IRAF and VISTA image and spectral reduction packages were used in this work. This work was supported by NASA grant NAGW-2681 (LTSA).

TABLE 1

COORDINATES AND OFFSETS OF FEATURES.

	R.A. (1950)	Dec. (1950)	Δ R.A. (″)	Δ Dec. (″)
NGC 1316[a]	03 20 47.2	−37 23 08		
EELR			148W	271S
SH2			44W	380S

[a]The position of NGC 1316 is that given for the bright optical core in Schweizer (1981). All other positions are relative offsets from the optical nucleus based on the CTIO Schmidt CCD images.

TABLE 2

X-RAY PROPERTIES OF THE L_1^a REGION.†

Model	N_H ($x10^{20}$ cm^{-2})	Abundance (units of ⊙)	kT_{R-S} (keV)	$kT_{Brem.}$ (keV)	χ^2/d.o.f./$\chi^2_{red.}$	Flux (erg cm^{-2} s^{-1})	L_X (erg s^{-1})
R-S	2.3(1.2-3.5)	5.8E-03(0-4.1E-02)	0.55(0.40-0.83)	...	17.5/25/0.70	2.7(1.6-4.8)E-13	1.7(1.0-3.0)E40
Brem.	2.7(1.7-3.8)	...	...	0.54(0.39-0.80)	19.2/26/0.74	2.8(1.7-4.6)E-13	1.7(1.1-2.9)E40

[a]712±71 PSPC (0.1 - 2.4 keV) counts were extracted for the L_1 region in a 375″ x 300″ aperture centred on 03 20 33.8 -37 29 00 (1950), compared to 280±47 for the L_2 region in a 210″ x 330″ aperture centred on 03 21 24.1 -37 24 41 (1950). Background was taken from a 750″ x 360″ region, north of NGC 1317, centred on 03 20 38.5 -37 10 15 (1950).

† Errors in brackets are 90% confidence for 3 interesting parameters (R-S model) and for 2 interesting parameters (Brem. model).

TABLE 3

ESTIMATED AND MEASURED MASSES OF THE EELR.

Mass	Amount
$M_{HI}^{\dagger}$	$1.1 \times 10^8\ M_\odot$
$M_{HI}^{\ddagger}$	$< 1 \times 10^7\ M_\odot$
M_{HII}	$7.5 \times 10^3\ M_\odot$

$M_{HI}^{\dagger}$ estimated from observed dust extinction and assumes $M_{gas}/M_{dust} = 100$.

$M_{HI}^{\ddagger}$ is upper limit from observation.

M_{HII} assumes a 33% contribution to $f_{H\alpha+[NII]}$ from [NII] (based on 14 spirals, mainly Sc's; Kennicutt 1983), and $L(H\alpha) = 2.96 \times 10^{16}\ f_{H\alpha}\ D(\mathrm{Mpc})^2\ L_\odot$, and $M_{HII} = 2.33 \times 10^3 \left(\frac{L(H\alpha)}{10^{39}\ \mathrm{erg\ s^{-1}}} \right) \left(\frac{10^3 \mathrm{cm^{-3}}}{n_e} \right) M_\odot$ (Osterbrock 1974, Case B recombination theory; Goudfrooij *et al.* 1994a), $n_e = 10^3\ \mathrm{cm^{-3}}$ (assuming an electron temperature of $\sim 10^4$K).

TABLE 4

OPTICAL LUMINOSITIES AND ESTIMATED HOT GAS MASSES OF L_1 AND L_2.

	L_1	L_2
L_B	$3.1 \times 10^9 \pm 30\%\ L_{B\odot}$	$2.6 \times 10^9 \pm 30\%\ L_{B\odot}$
$M_{X,gas}$	$\sim 5 \times 10^8\ M_\odot$	$\sim 1 \times 10^8\ M_\odot$

$M_{X,gas}$ for L_2 is estimated assuming a similar X-ray content to L_1 and a gas volume of 30 x 15 x 5 kpc.

REFERENCES

Balcells, M. 1997, ApJ, 486, L87.

Barnes, J.E. 1996, ApJ, 393, 484.

Barnes, J.E, and Hernquist, L. 1996, ApJ, 471, 115.

Bohlin, R.C., Savage, B.D. and Drake, J.F. 1978, ApJ, 224, 132.

Bosma, A., Smith, R.M., and Wellington, K.J. 1985, MNRAS, 212, 301.

Dupraz, C., Casoli, F., Combes, F. and Kazes, I. 1990, A&A, 228, L5.

Ekers, R.D., Goss, W.M., Wellington, K.J., Bosma, A., Smith, R.M., and Schweizer, F. 1983, A&A, 127, 361.

Fabbiano, G. 1989, ARA&A, 27, 87.

Fabbiano, G., Kim, D.-W. and Trinchieri, G. 1992, ApJS, 80, 531.

Fabbiano, G., Fassnacht, C. and Trinchieri, G. 1994, ApJ, 434, 67.

Faber, S.M. and Gallagher, J.S. 1976, ApJ, 204, 365.

Feigelson, E.D., Laurent-Muehleisen, S.A., Kollgaard, R.I., and Fomalont, E.B. 1995, ApJ, 449, L149.

Geldzahler, B.J., and Fomalont, E.B. 1984, AJ, 89, 1650.

Goudfrooij, P., Hansen, L., Jorgensen, H.E., and Norgaard-Nielsen, H.U. 1994a, A&AS, 105, 341.

Goudfrooij, P., de Jong, T., Hansen, L., and Norgaard-Nielsen, H.U. 1994b, MNRAS, 271, 833.

Graham, J.A. 1987, B.A.A.S., 19, 1048.

Haynes, M.P., and Giovanelli, R. 1984, AJ, 89, 758.

Hernquist, L. and Quinn, P.J. 1988, ApJ, 331, 682.

Hernquist, L. and Quinn, P.J. 1988, ApJ, 342, 1.

Hibbard, J.E., Guhathakurta, P., van Gorkom, J.H., and Schweizer, F. 1994, AJ, 107, 67.

Hibbard, J.E. and Mihos, J.C. 1995, AJ, 110, 140.

Hibbard, J.E. and van Gorkom, J.H. 1996, AJ, 111, 655.

Holtzman, J.A., Faber, S.M., Shaya, E.J., Lauer, T.R., Grothe, J., Hunter, D.A., Baum, W.A., Ewald, S.P., Hester, J.F., Light, R.M., Lynds, C.R., O'Neil, E.J., Jr., and Westphal, J.A. 1992, AJ, 103, 691.

Jenkins, C.R. 1983, MNRAS, 205, 1321.

Kennicutt, R.C. 1983, ApJ, 272, 54.

Kim, D.-W., Fabbiano, G., and Mackie, G. 1997, *in prep.*

Kormendy, J. 1987, in IAU #127 Structure and Dynamics of Elliptical Galaxies, ed. T. de Zeeuw. p. 17.

Lauberts, A., and Sadler, E. 1984, ESO Scientific Report No. 3, A Compilation of UBVRI Photometry for Galaxies in the ESO/Uppsala Catalogue. (ESO)

Osterbrock, D.E. 1974, Astrophysics of Gaseous Nebulae, (W.H. Freeman & Co., San Francisco)

Phillips, M.M., Jenkins, C.R., Dopita, M.A., Sadler, E.M. and Binette, L. 1986, AJ, 91, 1062.

Pfeffermann, E. *et al.* 1987, Proc. SPIE, 733, 519.

Quinn, P.J. and Hernquist, L. 1987, in IAU #127 Structure and Dynamics of Elliptical Galaxies, ed. T. de Zeeuw. p. 249.

Raymond, J.C. and Smith, B.W. 1977, ApJS, 35, 419. (R-S)

Read, A.M., Ponman, T.J. and Wolstencroft, R.D. 1995, MNRAS, 277, 397.

Reif, K., Mebold, U., Goss, W.M., van Woerden, H., and Siegman, B. 1982, A&AS, 50, 451.

Sage, L.J. and Galletta, G. 1993, ApJ, 419, 544.

Sandage, A., and Tammann, G.A. 1981, A Revised Shapely-Ames Catalog of Bright Galaxies, (Washington:Carnegie Institution of Washington) (RSA)

Sanders, D.B., Scoville, N.Z., Sargent, A.I. and Soifer, B.T. 1988, ApJ, 324, L55.

Schweizer, F. 1980, ApJ, 237, 303. (S80)

Schweizer, F. 1981, ApJ, 246, 722.

Schweizer, F. 1982, ApJ, 252, 455.

Schweizer, F. and Seitzer, P. 1992, AJ, 104, 1039.

Shaya, E.J., Dowling, D.M., Currie, D.G., Faber, S.M., Ajhar, E.A., Lauer, T.R., Groth, E.J., Grillmair, C.J., Lynds, C.R., O'Neil, E.J. 1996, AJ, 111, 2212.

Stanford, S.A., Sargent, A.I., Sanders, D.B. and Scoville, N.Z. 1990, ApJ, 349, 492.

Toomre, A., and Toomre, J. 1972, ApJ, 178, 623.

Toomre, A. 1977, in The Evolution of Galaxies and Stellar Populations, eds. B.M. Tinsley and R.B. Larson (Yale University, New Haven) p.401.

Trinchieri, G., Fabbiano, G., and Bandiera, R. 1989, ApJ, 342, 759.

Veron–Cetty, M.P., and Veron, P. 1986, A&AS, 66, 335.

Wang, Q. and Helfand, D.J. 1991, ApJ, 379, 327.

Weil, M.L. and Hernquist, L. 1993, ApJ, 405, 142.

White, R.E. and Sarazin, C.L. 1991, ApJ, 367, 476.

Whitmore, B.C., Schweizer, F., Leitherer, C., Borne, K., and Robert, C. 1993, AJ, 106, 1354.

Whitmore, B.C. and Schweizer, F. 1995, AJ, 109, 960.

This 2-column preprint was prepared with the AAS LaTeX macros v4.0.

Fig. 1.— B band image of NGC 1316. NGC 1317 is 6.4′ N of NGC 1316. Schweizers (1980) L_1 loop is W and SW of NGC 1316 and L_2 loop is E of NGC 1316.

Fig. 2.— B band residual image of NGC 1316. Loops L_1 and L_2 are denoted. The axis of stellar rotation and the direction of the outer radio lobes are indicated.

Fig. 3.— A Hα+[N II] image of NGC 1316 and environment (greyscale) overlayed with B band surface brightness contours of 23,24,25 and 26 mag. arcsec^{-2}. The EELR, SH2 and L_1 are indicated.

Fig. 4.—SW quadrant of NGC 1316. B band residual shown as greyscale. Overlayed is Hα+[N II] shown in solid contours (2.0 and 4.0x10^{-17} erg cm^{-2} s^{-1} arcsec^{-2}).

Fig. 5.— A subimage of Figure 3 showing the EELR in Hα+[N II] (greyscale). Overlayed are Hα+[N II] contours at flux levels of 2.0 and 4.0x10^{-17} erg cm^{-2} s^{-1} arcsec^{-2} .

Fig. 6.— B band residual light (greyscale), overlayed with *ROSAT* PSPC Broadband (0.1 - 2.4 keV) 3, 5, 10 and 20 σ contours. The arrow shows the position of the EELR.

NGC 1316 B median

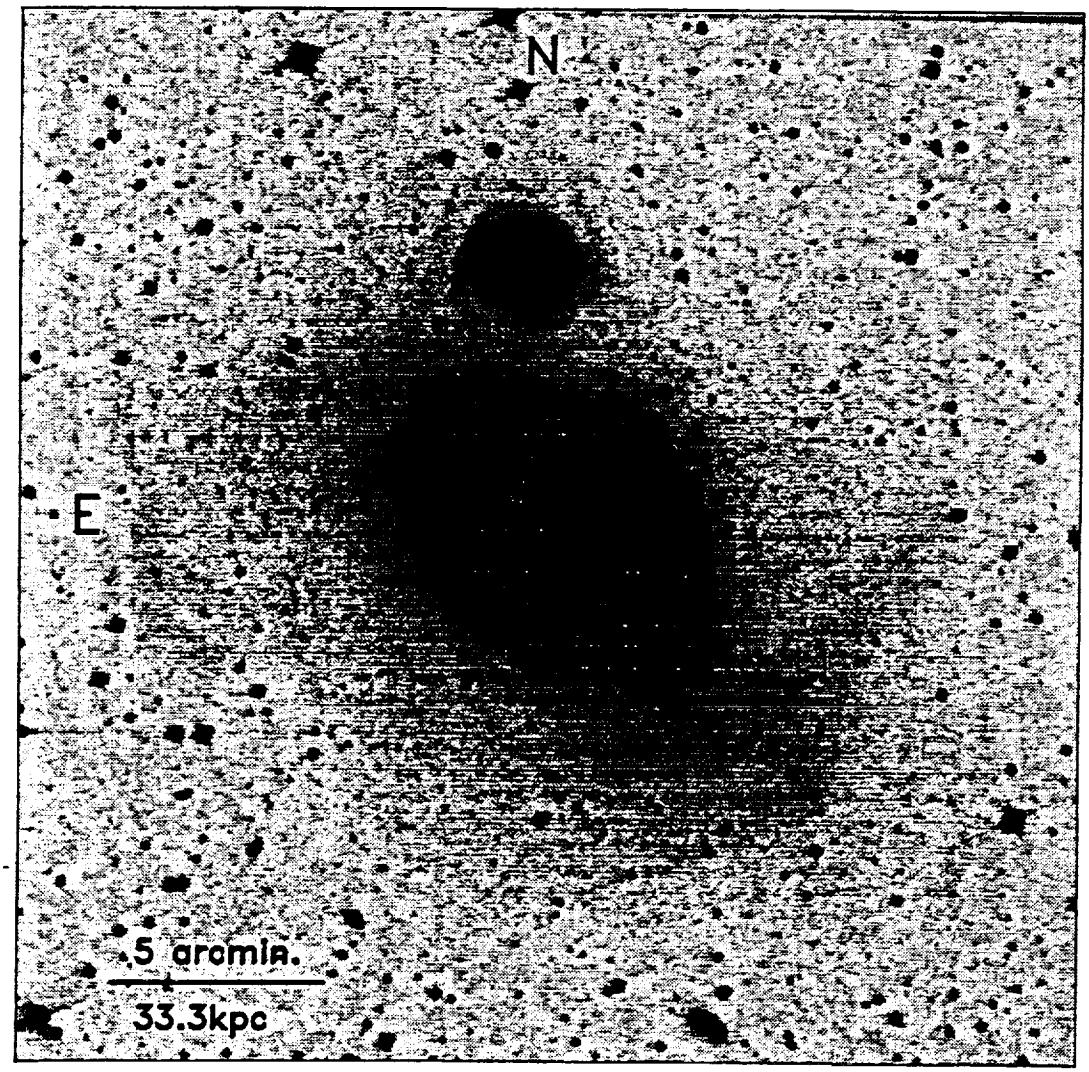

NGC 1316 B median − model

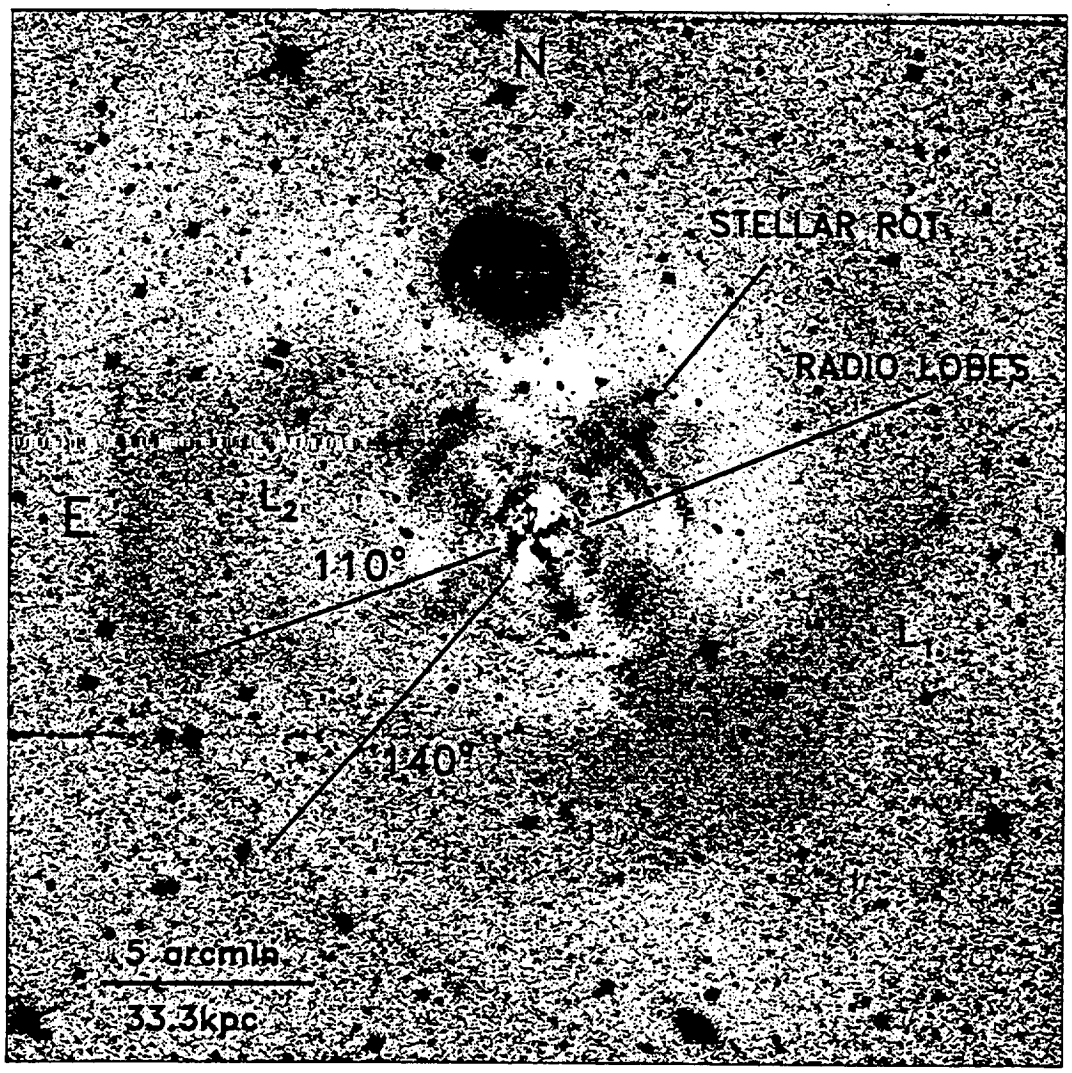

NGC 1316 Hα+[NII] greyscale
B 23,24,25,26 mag. sq. arcsec contours

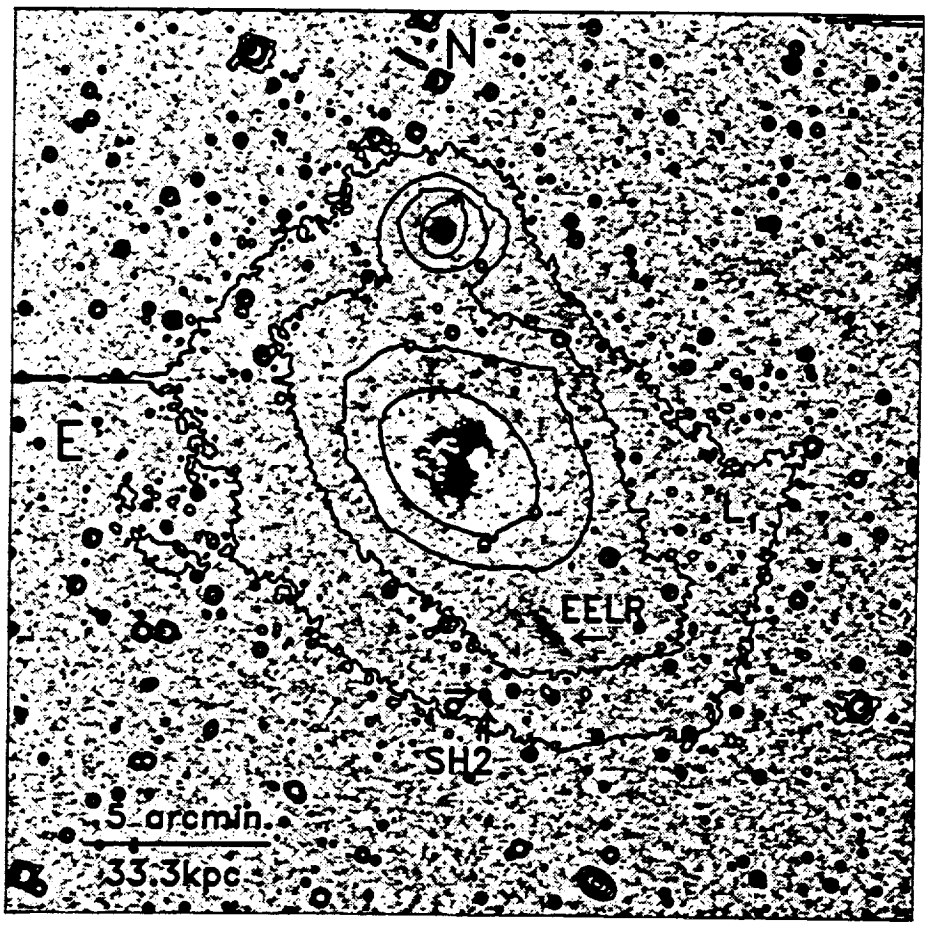

NGC 1316 and EELR
Hα+[NII] 2.0,4.0x10^{-17} erg cm^{-2} s^{-1} arcsec^{-2} solid contours
B residual greyscale

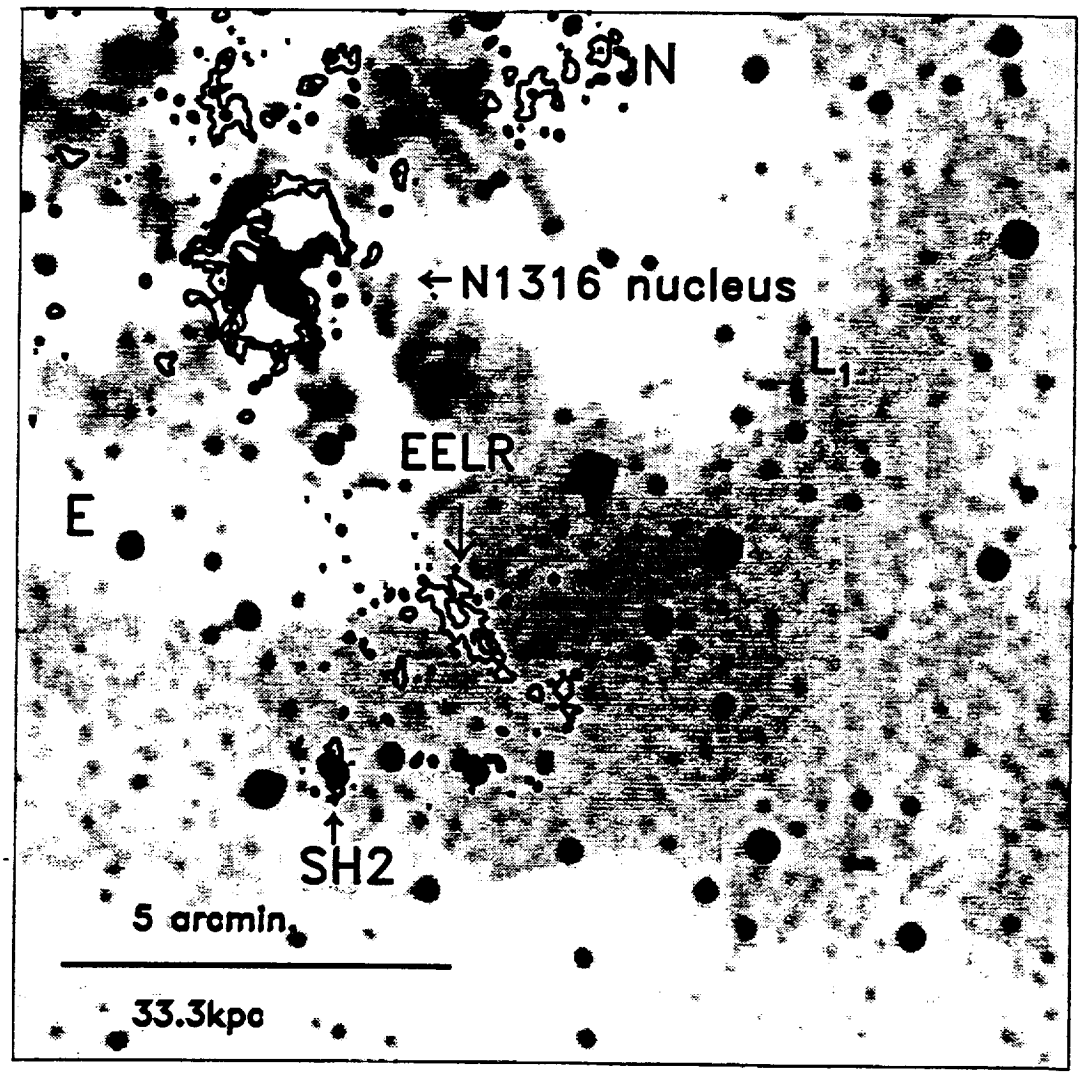

EELR Hα+[NII] greyscale
2.0,4.0x10^{-17} ergs cm^{-2} s^{-1} $arcsec^{-2}$ contours

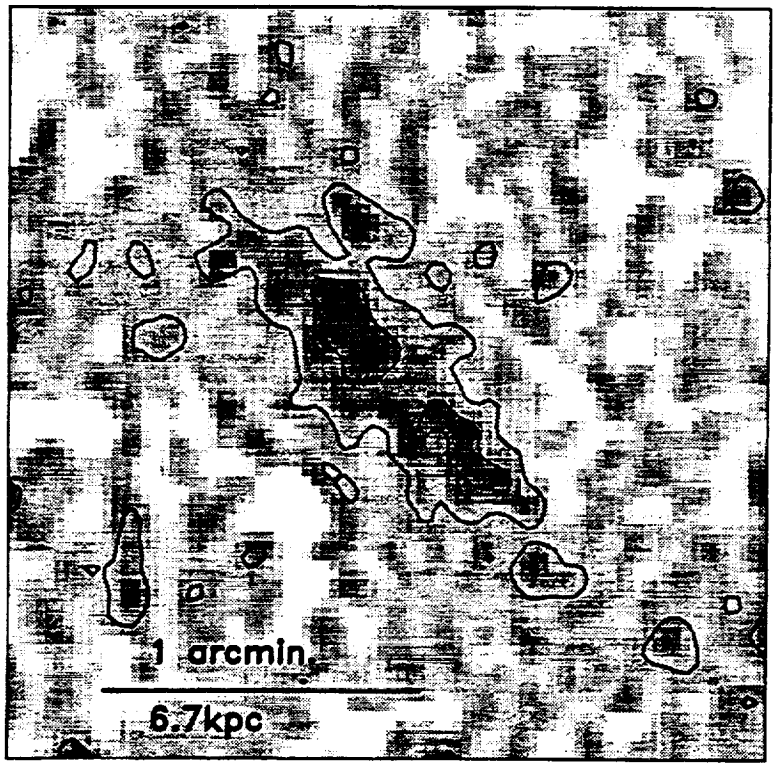

NGC 1316 B median − model greyscale
PSPC Broad (0.2−2.4keV) 3,5,10,20 σ contours

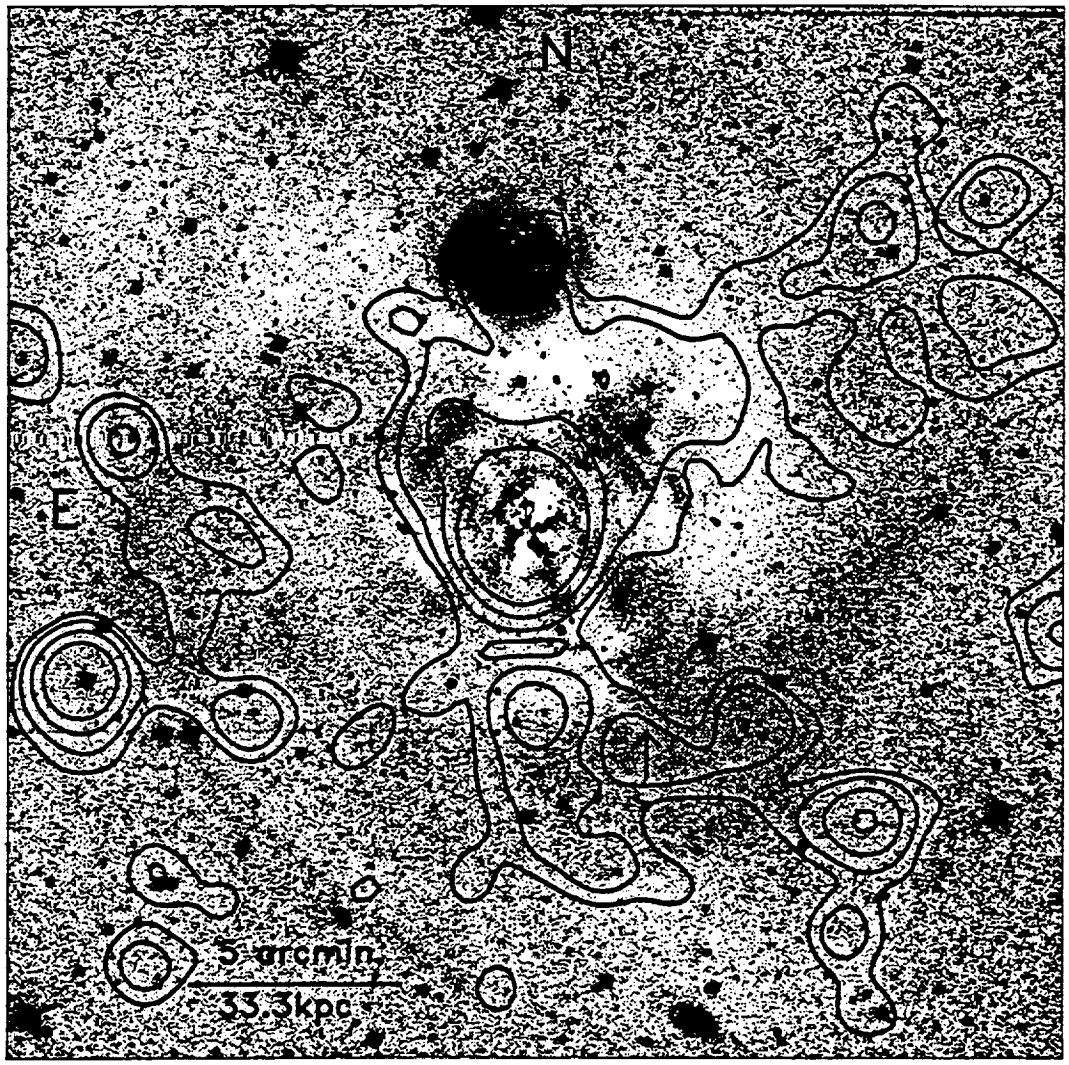

Harvard-Smithsonian Center for Astrophysics

Preprint Series

No. 4620
(Received November 13, 1997)

ROSAT X-RAY OBSERVATIONS OF THE RADIO GALAXY NGC 1316 (FORNAX A)

D.-W. Kim
Chungnam National University, South Korea
and
Harvard-Smithsonian Center for Astrophysics

and

G. Fabbiano and G. Mackie
Harvard-Smithsonian Center for Astrophysics

To appear in
The Astrophysical Journal

HARVARD COLLEGE OBSERVATORY SMITHSONIAN ASTROPHYSICAL OBSERVATORY
60 Garden Street, Cambridge, Massachusetts 02138

Center for Astrophysics
Preprint Series No. 4620

ROSAT X-RAY OBSERVATIONS OF THE RADIO GALAXY NGC 1316 (FORNAX A)

D.-W. Kim
Chungnam National University, Taejon, 305-764, South Korea; and
Harvard-Smithsonian Center for Astrophysics, 60 Garden Street, Cambridge, MA 02138

G. Fabbiano and G. Mackie[1]
Harvard-Smithsonian Center for Astrophysics, 60 Garden Street, Cambridge, MA 02138

November 10, 1997

1. Visiting Astronomer, Cerro Tololo Inter-American Observatory.

Abstract

We have observed NGC 1316 (Fornax A) with the ROSAT HRI. In this paper, we present the results of these observations and we complement them with the spectral analysis of the archival PSPC data. The spectral properties suggest the presence of a significant component of thermal X-ray emission ($> 60\%$), amounting to $\sim 10^9 M_\odot$ of hot ISM. Within $3'$ from the nucleus of NGC 1316, the HRI X-ray surface brightness falls as r^{-2}. In the inner $\sim 40''$, the X-ray surface brightness is significantly elongated ($\epsilon \sim 0.3$). This flattened X-ray feature is confirmed by a straightforward statistics test as well as moment analysis. By comparing the morphology of the X-ray emission with the distribution of optical dust patches, we find that the X-ray emission is significantly reduced at the locations where the dust patches are more pronounced, indicating that at least some of the X-ray photons are absorbed by the cold ISM. We also compare the distribution of the hot and cold ISM with that of the ionized gas, using recently obtained H_α CCD data. We find that the ionized gas is distributed roughly along the dust patches and follows the large scale X-ray distribution at $r > 1'$ from the nucleus. However, there is no one-to-one correspondence between ionized gas and hot gas. Both morphological relations and kinematics suggest different origins for hot and cold ISM. The radio jets in projection appear to pass perpendicularly through the central X-ray ellipsoid. Comparison of thermal and radio pressures suggests that the radio jets are confined by the surrounding hot gaseous medium.

1. INTRODUCTION

NGC 1316 (Fornax A, Arp 154) is a giant elliptical galaxy in the poor Fornax cluster. This galaxy exhibits many unusual features for an elliptical galaxy, including pronounced dust patches, H_α filaments, ripples and loops (e.g., Arp 1966; Schweizer 1980; Carter et al. 1983; Mackie and Fabbiano 1997). The distribution of the optical surface brightness reveals an extensive envelope, making NGC 1316 a typical D (or cD) galaxy (Schweizer 1980). It has one of the most pronounced shell systems observed in early type galaxies (Malin and Carter 1983). These features all point to a recent merging in NGC 1316 (e.g., Schweizer 1980).

In the radio (0.03 - 5 GHz), Fornax A is one of the brightest objects in the sky (L = 2×10^{42} erg sec^{-1}; Ekers et al. 1983). It contains giant radio lobes (Wade 1961), separated by $\sim 30'$ ($\sim$240 kpc), consisting of polarized, organized filaments (Fomalont et al. 1989). A faint bridge between the lobes is displaced to the south of the galaxy center and S-shaped nuclear radio jets are present, implying a significantly violent action in the galaxy history, as also suggested by the optical data (e.g., Ekers et al. 1983; Geldzahler and Fomalont 1984). The nucleus of NGC 1316 hosts a low-luminosity AGN: optically it has a LINER-type spectrum (Veron-Cetti and Veron 1986; Baum, Heckman and van Breugel 1992); it contains a radio core (Geldzahler and Fomalont 1984); and HST observations have revealed a nuclear UV-bright point source (Fabbiano, Fassnacht and Trinchieri 1994b). NGC 1316 also contains complex, multiphase ISM: it has been detected in optical emission lines from ionized gas (e.g., Schweizer 1980; Phillips et al. 1986; Veron-Cetti and Veron 1986), IRAS far infrared emission (Knapp et al. 1989) and CO lines of molecular gas (Wiklind and Henkel 1989; Sage and Galletta 1993).

In X-rays, NGC 1316 was detected with Einstein (Fabbiano, Kim and Trinchieri 1992) and belongs to a group with the lowest L_X/L_B ratio among E and S0 galaxies (Kim, Fabbiano and Trinchieri 1992b). Therefore, based on the global amount of X-ray emission, NGC 1316 does not necessarily contain a large amount of hot ISM (see Fabbiano, Gioia and Trinchieri 1988). In this, it is similar to other galaxies which may have experienced recent mergers (Hibbard et al. 1994; Fabbiano and Schweizer 1995). ROSAT PSPC (Feigelson et al. 1995) and ASCA observations (Kaneda et al. 1995) have revealed the presence of extended Inverse Compton X-ray emission at the locations of radio lobes.

In this paper, we discuss the results of a re-analysis of the archival ROSAT (Truemper 1983) PSPC observation of NGC 1316, and we report for the first time the results of high

resolution X-ray observation with the ROSAT HRI. The HRI has ~5 arcsec resolution (David et al 1993), comparable to that of ground-based radio and optical data. With these data we establish the presence of a hot ISM in NGC 1316 and we correlate its properties to that of the other phases of the ISM. We also explore possible interactions between this hot ISM and the active radio nucleus.

This paper is structured as follows: in section 2, we present the results of the ROSAT HRI (§2.1 and §2.2) and the ROSAT PSPC data analysis (§2.3); in section 3, we compare the X-ray data with the optical and radio data; finally, in section 4 we discuss the implications of our results.

2. X-RAY OBSERVATIONS

NGC 1316 was observed with the ROSAT HRI on Jan. 14, 1994 and Jul. 7-10, 1994 for a total exposure time ~40 ks (3/4 of total observations were obtained in the July run). The two data sets are consistent with each other within the observational uncertainty. We present the combined results except as mentioned in §2.1. The field of view of this observation also includes the companion elliptical galaxy NGC 1317 (Figure 1). The observational log and basic parameters of both galaxies are given in Table 1. NGC 1316 was also observed with the ROSAT PSPC (Feigelson et al. 1995), and we used the PSPC archival data to determine spectral parameters.

Given the limited statistics of our HRI observation, we have used various binning and smoothing factors to investigate both large scale (a few arcmin) and small scale ($\lesssim$ 1 arcmin) features. We used both IRAF and software we developed ourselves to analyze our data. We adopt a distance to NGC 1316 of 27.2 Mpc using $H_o = 50$ km s^{-1} Mpc^{-1} (Fabbiano et al. 1992).

To extract source data, the field background must be subtracted. We found that estimates from the background map generated by the standard ROSAT SASS processing and from local measures of the background in concentric annuli around the sources agree well with each other. We will present results obtained with the local background subtraction.

2.1 X-ray Emission Features and Sources

The entire observed field of view is shown in Figure 1, where the X-ray contour map is overlaid on the optical image obtained from the Digitized Optical Survey[2]. The X-ray

image was binned with a pixel size of 8″ and smoothed with a Gaussian of $\sigma = 16''$. The background is not subtracted. The octagonal shape indicates the boundary of the HRI detector. The figure shows a strong X-ray source at the center of the field, corresponding to the optical position of NGC 1316. Also X-ray emission is detected at the optical position of NGC 1317 (6.3″ to north of NGC 1316). Additionally, 10 point-like sources (above 3σ) are detected in the observed field. The source position, radius of the count extraction circle and X-ray count for each source are listed in order of RA in Table 2. The corresponding source numbers are marked in Figure 1. X-ray counts were extracted from circular regions centered on their X-ray centroids. The radius was determined with the radial profile of the X-ray surface brightness (§2.2.). Typically these radii extend to where the surface brightness is within ~3-4 % of the background. The background counts were extracted in annuli r=60″ - 200″, except for NGC 1316 where an annulus r=200″ - 400″ is used.

---

2. The Digitized Sky Survey was produced at the Space Telescope Science Institute under U.S. Government grant NAG W-2166. The images of these surveys are based on photographic data obtained using the Oschin Schmidt Telescope on Palomar Mountain and the UK Schmidt Telescope.

With the HRI observation of NGC 1316 we can trace the X-ray emission out to 170″, or 22.4 kpc at an adopted distance of 27.2 Mpc (see §2.2). However, the X-ray emission is extended at least to 1000″ (Fabbiano et al. 1992; Feigelson et al. 1995). The other sources (including NGC 1317) are point-like. Except for NGC 1316 and 1317, the sources are not identified with known objects in the SIMBAD catalog.

Source 2 and 12 are possibly variable. Their count rates from the two HRI observing epochs (Table 1) are significantly different (above 3 σ), while count rates of other sources are consistent within the count errors between the two observations (see Table 3). The small numbers of source counts do not warrant further temporal analysis.

The number of serendipitous sources (omitting the target galaxy) found in this observation is consistent with the expected number of background sources. According to the LogN-LogS function (Hasinger et al. 1993), we would have about 9 sources within a circular area of radius 15′ and a limiting flux 1.8×10^{-14} erg sec^{-1} cm^{-2} in 0.5-2.0 keV, which corresponds to the faintest among detected sources (Table 2) for a power law spectrum with $\alpha_E = 1$.

Figure 2 provides a close-up view of the NGC 1316 X-ray image which was binned with a pixel size of $2''$ and smoothed with a Gaussian of $\sigma = 4''$, corresponding to FWHM $= 11.3''$ for an on-axis point source. This image covers a $3' \times 3'$ field which falls inside the optical galaxy ($12' \times 8.5'$ in $D_{25} \times d_{25}$; see Table 1). Inside the central arcmin, the X-ray emission is elongated along the NE-SW direction, following the optical major axis (PA=50°; RC3), while in a larger scale ($\sim 2'$), the X-ray emission is extended along the N-S direction. This extension is more pronounced toward the north (see also Figure 1).

The observed NE-SW elongation inside r $\sim 1'$ is intriguing if real because it may be related to a disk forming in the rotating cooling flow (§4.2) and because the radio jet in projection appears to propagate perpendicular to the direction of this elongation (§4.3). To determine its statistical significance, we first applied a straightforward test by comparing counts and errors in angular sectors at different position angles. We then applied more sophisticated tests: a Monte Carlo simulation and moment analysis. Figure 3 compares the counts at different position angles and gives the significance of differences. Overall the difference between counts extracted in the NE-SW (PA=30-70°, 210-250°) and NW-SE (PA=120-160°, 300-340°) is very significant with a signal to noise ratio of 7.7 σ within r $< 40''$.

To estimate whether the flattening of the X-ray isophotes at small radii is due to chance positioning of a few noise 'blobs' from an underlying spherical distribution, we have run a Monte Carlo simulation. This involves: (1) choosing a spherical model; (2) creating a set of 'observations' in which Poisson noise is added to the model and each X-ray is distributed taking into account the HRI PRF; and (3) then determining the chance probability of occurrence of the observed features. We generated a smooth model image by adopting the X-ray radial profile determined in §2.2 under the assumption of spherical symmetry. Then we normalized the model image and added background counts to match with our HRI observation. We produced a set of 100 'observations' with a pixel size of $2''$ (as in Figure 2) by estimating Poisson deviate for each pixel value and distributing the photon according to the PRF. To estimate how often we obtain an elliptical surface brightness by chance, we examined simulated images after smoothing with the same Gaussian σ as in Figure 2. Out of 100 images, no ellipticity as significant as that of Figure 2 is seen. In our simulations, we also added serendipitous sources at random positions according to the LogN-LogS function (Hasinger et al. 1993) to verify whether a few undetected point sources can mimic our observed features. However the results do not change appreciably. In conclusion, the chance probability to generate the observed, elongated distribution of

the inner X-ray surface brightness out of a circularly symmetrical distribution is less than 1%.

To parameterize the X-ray surface brightness distribution, we have applied a moment analysis (see fore details, Buote and Canizares 1994 and Carter and Metcalfe 1980). Ellipticities (ϵ) and position angles of the semi-major axis (θ) are iteratively determined by computing two-dimensional moments of inertia within elliptical apertures. We used an unsmoothed, raw image (2″ pixel) with background included. The measured ellipse parameters with a semi-major axis varying from 10″ to 50″ are $\epsilon = 0.28 \pm 0.05$ and $\theta = 56° \pm 8°$. We have also applied ellipse fitting (e.g., Jedrzejewski 1987), using the IRAF/STSDAS package to the smoothed image in Figure 2. The derived position angle and ellipticity are consistent with those determined by the moment analysis within their uncertainties.

Figure 4 shows the central region in greater detail with a pixel size of 1″ and smoothed with a Gaussian of $\sigma = 2''$ which corresponds to an on-axis beam of 6.9″ FWHM. In this scale the core surface brightness divides into double peaks, separated by 7.3″. The optical center (RC3) is close (within arcsec) to the X-ray centroid determined with the image in Figure 2 and falls in the middle of the double peaks shown in Figure 4. Also noticeable are larger scale valleys at PA $\simeq 120°$ and PA $\simeq 320°$ which apparently bisect the core if extended to the center.

The double peaks and the SE-NW X-ray valleys are not caused by telescope aspect problems. We used only data obtained in the July run (see Table 1), to avoid a possible mismatch of the galaxy centers in the two observations due to aspect uncertainties, although source positions differ by less than 2″. The data obtained in the January run also present the same features but with larger statistical noise. To further check potential aspect problems, we applied the same binning and smoothing to point-like sources within the observed field. Sources 4, 7, and 8 which are within 5′ from the field center [therefore the HRI PRF is similar to the on-axis one (David et al. 1993)] are all circularly shaped while sources 2 and 12, both at 11′ off-axis distance (the PRF may not be circular), exhibit randomly elongated distribution.

The observed features are very interesting, because the radio jet (Geldzahler and Fomalont 1984) in projection appears to pass through the X-ray valleys (§3). However, the relatively low X-ray counts obtained in this high resolution image may produce an artificial feature by chance positioning of a few noise 'blobs'. To explore this possibility, we have rerun a Monte Carlo simulation as described above. Out of 100 simulations with

a resolution same as Figure 4 (1″ pixel and σ=2″), 3 images exhibit double peaks and valleys, although not as significant as the observed. This simulation results imply that the existence of the double peaks and the X-ray valleys, although suggestive, is not conclusive and it is required to be confirmed by a deeper observation.

2.2 Radial Profile

Figure 5 shows the radial profile of the X-ray surface brightness measured in concentric rings centered on the NGC 1316 X-ray centroid (Table 2). The raw, background and net counts are indicated by open squares, a solid line and filled squares, respectively. The emission is extended out to 170″, 22 kpc at the adopted distance of 27.2 Mpc. To this profile, we fitted a King approximation model, $\Sigma_X \sim (1 + (\frac{r}{a})^2)^{-3\beta+0.5}$, convolved with the HRI point response function. [In the case of gaseous emission, β is related to a true isothermal value by $\beta_i = 1.5 \times \beta$ (e.g., Sarazin 1988)]. Best-fit model, fit residuals, and confidence contours are shown in Figure 6. The best fit parameters and 90% confidence range with 2 interesting parameters (in parentheses) are: core radius a = 4.1″ (3.1–5.0″) and slope β = 0.51 (0.49–0.54), yielding χ^2 = 14.8 for 9 degrees of freedom. The estimated slope corresponds to $\Sigma_X \sim r^{-2.06\,(1.94-2.24)}$ for $r >> a$. This is close to that of the optical brightness distribution. Using the data in Schweizer (1981), we estimated the slope of the V_4 (5300-6400Å) surface brightness in r = 30″ to 300″ to be 2.02 ± 0.06. The radial slope measured with the red continuum image (§3) does not differ sinificantly. We also used the PSPC data to derive the radial profile of the X-ray surface brightness. Using the radial profile within r=180″ (to minimize the contribution of extended IC emission; see §2.3 and Feigelson et al. 1995), and a background count rate estimated at r=1800-2400″ (with vignetting correction), we find $\Sigma_X \sim r^{-2.25\,(2.12-2.45)}$, consistent with the HRI profile.

Fits to the radial profiles at the position angles of Figure 3, which take into account the central flattening of the surface brightness give slightly steeper slope [β = 0.56 (0.52–0.61)] and slightly larger core radius [a = 6.2″ (4.1–8.2)] along the direction of flattening, whereas the opposite is true along the perpendicular direction [β = 0.46 (0.43–0.50) and a = 1.8″ (< 3.8)].

A central point source that may be the X-ray counterpart of the radio AGN was not detected with our HRI observations (see the HRI PRF indicated as a dashed line in Figure 5; see also Figure 4). To estimate an upper limit to a central point source, we applied the King model plus the HRI point spread function in fitting the radial profile and determined how strong a central source can be added without having χ^2 too large. We derive an upper

limit (90%) for the central source of about 5% of the total counts, which corresponds to a flux of 1.0×10^{-13} erg sec^{-1} cm^{-2} in 0.1-2.4 keV and a luminosity of 9×10^{39} erg sec^{-1}. Here we assumed a power law with an energy index α_E=0.7 and line-of-sight N_H. Of course a more luminous AGN would be allowed in the presence of large intrinsic N_H.

The spectral analysis of the extended X-ray emission associated with NGC 1316 (§2.3) suggests that over 60% of the flux is likely to be of gaseous origin. In the assumption that most of the extended emission is due to a hot ISM, we have derived its 3-dimensional density distribution, using a direct deprojection method (Kriss, Cioffi and Canizares 1983), where the emissivity (or density) is inwardly measured by subtracting the contribution of successive spherical layers. We implicitly assume that the hot gas is homogeneous and that the physical status of the gas at a given radius can be represented by one temperature and density. The deprojected density profile is shown in Figure 7a. We have assumed T = 0.8 keV (§2.3). The density profile corresponding to β=0.51, i.e., $n_e \sim r^{-1.53}$ is also shown as a dashed line in the figure.

Using the deprojected density distribution, we estimate the cooling time and gas pressure as a function of radius (Figure 7b). The cooling time is given as $\tau_c = 1.5 \frac{nkT}{n_e n_H \Lambda}$, where n, n_e and n_H are the total particle density, electron density, and Hydrogen density, respectively and Λ is the cooling function. The constant is in the range of 1 to 2.5, depending on its definition (see Sarazin 1988). The cooling time in the center is $\sim 10^8$ years, much smaller than the Hubble time; it reaches 10^{10} years at $\sim 180''$. To estimate the cooling function, we assumed solar metal abundances. With the PSPC spectral data (§2.3), the metal abundances cannot be determined unambiguously (see also e.g., Trinchieri et al. 1994; Fabbiano et al. 1994a). The cooling time in the central region is still much shorter than the Hubble time even with a zero metal abundance model. We also estimate the thermal gas pressure using the measured density and assuming kT = 0.8 keV (Figure 8).

We point out that these radial dependences of density, cooling time and pressure are only indicative average values. Because of the complexity of the surface brightness distribution in the inner regions, we would expect a range of these physical parameters at each radius, reflecting the clumpiness of the hot ISM. Also as remarked earlier, we cannot study separately the properties of the different components of the emission suggested by the PSPC data.

2.3 ROSAT PSPC Spectral Properties

In order to determine the X-ray spectral properties, we have used the ROSAT PSPC data obtained from the public archives. The method of data reduction is similar to that of the PSPC observations of NGC 507 (Kim and Fabbiano 1995). Because the X-ray emission is extended at least out to 1000″ (see Feigelson et al. (1995) for discussions of the extended structure of X-ray emission), we determined the background at r=1800-2400″ and applied vignetting correction to each energy channel. Since we are interested in the galaxy emission, we have analyzed the X-ray emission within 180″ from the center. Feigelson et al. (1995) found Inverse Compton (IC) radiation at the location of the extended radio lobes. The slope of the X-ray radial profile changes abruptly at r$\sim$180″, indicating that the X-ray emission in the central region has a different origin from that of the extended X-ray emission (Feigelson et al. 1995). To check for possible contribution of IC radiation to the X-ray emission within r $<$ 180″, we also estimated the background using portions of the field within the PSPC support structure (r $\sim$1000″) where the diffuse emission is least. However, the results are not significantly different.

Using XSPEC, we found that the X-ray spectra within 180″ can be well reproduced either by a one-temperature, low abundance model (kT $\simeq$ 0.6-0.7 keV and $\sim$10% solar abundance) or by a two-temperature, solar-abundance model ($kT_1 \simeq$ 0.1-0.2 keV and $kT_2 \simeq$ 0.8-0.9 keV at 90% confidence). In both cases, the acceptable range of N_H is consistent with the Galactic line-of-sight value (2×10^{20} cm^{-2}). The best fit parameters and acceptable ranges with N_H fixed at the line-of-sight value are listed in Table 4. Although we prefer the two-component model rather than the almost zero-abundance model (see §5.1), both models suggest a significant amount of hot gaseous emission, because a significantly higher kT would be expected from a population of LMXB (see the analysis of the M31 bulge data by Fabbiano, Trinchieri and van Speybroeck 1987). We do not see any radial variations in the spectral parameters (temperature and N_H) with the PSPC observations (Table 4).

The absorption-corrected X-ray flux for the best fit parameters is 2×10^{-12} erg sec^{-1} cm^{-2} (see Table 5), corresponding to a X-ray luminosity of 1.8×10^{41} erg sec^{-1} at the adopted distance of 27.2 Mpc. The HRI flux is consistent with the *Einstein* IPC flux (see Table 1). For the two-component model, the X-ray flux of the very soft component is $\sim$40% of the total flux in 0.1-2.4 keV, similar to those seen in other X-ray faint early type galaxies (Fabbiano et al. 1994a, Fabbiano and Schweizer 1995). These results indicate the presence of hot ISM contributing at least 60% of the total X-ray emission even if the soft component is fully of stellar origin.

The analysis of the HRI image (§2.2) shows that a nuclear point source cannot contribute significantly to the emission in the ROSAT band. Therefore the spectral parameters (even in the outermost bin) are representative of an extended emission component. To estimate the upper limits of hard X-ray emission from low-mass binaries to this emission [as seen in the bulges of spirals (Fabbiano 1989) and in ellipticals (Matsushita et al. 1994; Matsumoto et al. 1997)], we added a hard Bremsstrahlung component in the spectral fitting and determined the acceptable range of its normalization. Its temperature was allowed to vary between 3 and 20 keV. The 90% upper limit of the hard component is 15% of the total flux in 0.1-2.4 keV for a one-temperature, low abundance model and 20% for a two-temperature, solar-abundance model. Even if we restrict our analysis to the central 1 arcmin region, the contribution of the hard component is less than 20% for a 1-component model and 30% for a 2-component model. This upper limit corresponds to fluxes of $3-4\times10^{-13}$ erg sec^{-1} cm^{-2} and luminosities of $3-4\times10^{40}$ erg sec^{-1} (Table 5). The X-ray to optical luminosity ratio is then $L_X/L_B \leq 2-3\times10^{29}$ erg sec^{-1} $L_\odot{}^{-1}$ and is consistent with that of the bulge of M31 where the X-ray emission is dominated by a population of individual bright X-ray sources (e.g., Trinchieri and Fabbiano 1991) and with those of hard components in other early type galaxies observed with ASCA (Matsumoto et al. 1997).

3. COMPARISON WITH OTHER WAVELENGTH DATA

Figures 9, 10 and 11 compare the high resolution HRI contour map of Figure 2 with the distribution of dust (Schweizer 1980), ionized gas, and radio continuum (Geldzahler and Fomalont 1984), respectively. Although the low signal-to-ratio nature of the X-ray data is such that a definitive, quantitative comparison can not be done, there are some qualitative trends that it is worth to mention.

In general, the hot and cold ISM are related in the sense that the X-ray emission is significantly reduced at the locations where the dust patches are more pronounced. In particular, a dust lane is found in the central SE X-ray valley, suggesting the possibility of absorption.

Because the ionized gas may be originated from the cooling hot gas, the distribution of ionized gas provides further clues of the relationship between cold and hot ISM. Narrow-band CCD images were taken on the photometric night of 1994 November 11/12. The CTIO/University of Michigan Curtis Schmidt 0.6/0.9m telescope was used with a Thomson

1024x1024 CCD. Pixel size is 19μm square (1.835″) however vignetting limits the useable field size to about 30′. Total exposure times were 8100s each for the redshifted (v=1801 km/s) $H\alpha$ + [NII] (λ 6563 + $\lambda\lambda$ 6548,6583) emission line filter (λ_c = 6606Å , FWHM=76Å), and continuum filter (λ_c = 6693Å , FWHM=81Å). Bias and dark frames were taken. Flatfields were generated from twilight sky exposures. The spectrophotometric standard HZ 4 was used to calibrate the narrow band images based on AB magnitudes (Oke 1994, private communication). The adopted magnitudes were AB_{6606}=15.01 and AB_{6693}=14.81. The $H\alpha$ + [NII] image was derived by subtracting a scaled, sky subtracted continuum image from the sky subtracted emission line image. The adopted scaling was calculated from a linear least square fit to residuals of 25 field stars calculated from several scaling factors. The mean pixel value of the $H\alpha$ + [NII] image at large radii of the optical galaxy was also consistently near zero. The distribution of ionized gas is shown in Figure 10, superposed on the X-ray image (same as Figure 2). The overall distribution of the ionized gas is similar to that of the dust, ie., aligned toward north-south, slightly turned to NW and SE (clockwise), as observed in other early type galaxies with cold ISM (Kim 1989). The peak of the northern blob (40^s.5, 11′.8) falls in between the dust patches, likely due to dust absorption. The eastern part of the southern blob generally follows the distribution of the dust patch. Comparing the distributions of hot and warm ISM, we also find an overall similarity (e.g., N-S extension), but there is not always a one-to-one correspondence.

Figure 11a shows the radio jets superposed on the X-ray image (same as Figure 2). This radio image was reproduced from the Figure 2b in Geldzahler and Fomalont (1984), which was obtained with the VLA and has 4″ resolution at 1.5 GHz. The direction of the radio jet is in projection perpendicular to the direction of NE-SW elongation of the central X-ray distribution. If confirmed, the X-ray valleys (seen in Figure 4) may imply even more striking relations in that both sides of the radio jets in projection coincide with the X-ray valleys at PA$\simeq$120° and PA$\simeq$320° (Figure 11b), suggesting that the radio jets are interacting with the surrounding hot gaseous medium as seen in Cygnus A (Carilli, Perley and Harris 1994).

These connections need to be checked with future high resolution observations. The AXAF CCD detector will provide 1″ resolution data with spectral resolution as well, which will be ideally suited for this type of investigation.

4. DISCUSSION

4.1 The Nature of X-ray Emission of NGC 1316

The X-ray emission of E and S0 galaxies can be due to different sources (see Fabbiano 1989): a hot gaseous halo dominating the emission in the X-ray bright early type galaxies; integrated stellar X-ray binary emission, seen in the bulges of spirals (see Fabbiano 1989) and confirmed in ellipticals with ASCA (Matsushita et al. 1994; Matsumoto et al. 1997); a nuclear source, seen in bright radio galaxies (Fabbiano et al. 1984; Worrall and Birkinshaw 1994); and a very soft component, seen in X-ray-faint early type galaxies (Kim et al. 1992b; Fabbiano et al. 1994a; Kim et al. 1996) of debatable nature (e.g., Pellegrini and Fabbiano 1994). NGC 1316 is both an X-ray faint D (maybe cD) galaxy and a radio galaxy, therefore its X-ray emission is likely to be complex.

With the HRI imaging data and the PSPC spectral data, we can limit the contribution from the nuclear component and stellar binary component respectively as being relatively unimportant to the detected X-ray emission (Table 5). The upper limit to the nuclear X-ray emission obtained with the HRI image (§2.2) is $L_X \leq 9 \times 10^{39}$ erg sec^{-1}, which is about 5% of the total luminosity. Of course a more luminous nuclear source could be present and not visible if the nuclear N_H is much higher than the line of sight one. With the PSPC spectra, we can pose an upper limit to the hard stellar component of 20-30% of the total flux in 0.1-2.4 keV ($L_X \leq 3-4 \times 10^{40}$ erg sec^{-1}; §2.3). This is consistent with the expected hard X-ray emission from a 'bulge' population of X-ray sources (e.g., scaling from the M31 bulge; Trinchieri and Fabbiano 1991). Individual typical X-ray binary sources would not be detectable at the luminosity threshold of our observation (a few x 10^{39} erg sec^{-1}).

The PSPC spectrum of NGC 1316 (§2.3) suggests that most of the X-ray emission within 3′ is due to a hot ISM in this galaxy. Although with the PSPC data we cannot unequivocally define the emission model, the spectral fits require the presence of a ~0.7-0.9 keV thermal emission (Table 4). The X-ray spectrum of NGC 1316 resembles that of other X-ray faint early type galaxies. X-ray spectra of those galaxies observed both with the IPC (Kim et al. 1992a) and the PSPC (e.g., Fabbiano et al. 1994a) present an excess of counts in the lowest energy channels, when compared to those of X-ray bright E and S0. This type of spectrum can either be fitted with a metal-free single-temperature optically-thin model, or with two (or more) component models (see Fabbiano et al. 1994a; Pellegrini and Fabbiano 1994; Fabbiano and Schweizer 1995). Recent ASCA measurements of the spectrum of the X-ray faint galaxy NGC 4382 (Kim et al. 1996) reject the single-component metal-free model in that galaxy. The two component model, in the case of NGC 1316, would consist of a very soft component of kT ~ 0.1-0.2 keV (which could be of stellar origin, e.g., Pellegrini and Fabbiano 1994), and a harder (kT ~ 0.7-1.0 keV), almost solar

metallicity ISM. It is interesting that the abundance of the ISM determined from this two-component model is near to the optical metallicity of this galaxy (e.g., Gorgas, Efstathiou and Salamanca 1990). However, based on more general ASCA results on galaxies (e.g., Loewenstein et al. 1994; Arimoto et al. 1996), the latter may just be a coincidence.

Although a hot ISM is present, the total amount of hot gas is $\sim 10^9\ M_\odot$, only a fraction of that present in X-ray bright early type galaxies with a comparable optical luminosity (for example, $M_{gas} \sim 2 \times 10^{10}\ M_\odot$ in NGC 4636; Trinchieri et al. 1994). NGC 1316 clearly has not been accumulating all the gas ejected from the evolved stars during a Hubble time, which would be $\sim 3 \times 10^{10}\ M_\odot$. This is not surprising since this galaxy may have undergone recent merging events (see Schweizer 1980). Recent mergers (Hibbard et al. 1994) and dynamically young ellipticals (Fabbiano and Schweizer 1995) also tend to be relatively empty of hot ISM. It may be a coincidence, but the mass of the hot ISM is comparable with what would be expected from stellar accumulation in $\sim$1 Gyr, which may be the age of merger (Schweizer 1980). In a recent paper discussing the optical and X-ray emission at larger radii, Mackie and Fabbiano (1997) find $\sim 3 \times 10^8\ M_\odot$ of hot ISM spatially coincident with the tidal tails in the outskirts of NGC 1316.

4.2 Multi-phase ISM

The comparison between X-ray and optical data reveals that the distribution of the X-ray emission is related with that of dust patches (§3.1.). The X-ray emission is weak where dust is seen and X-ray blobs are often surrounded by dust patches. The X-ray valleys running toward NW and SE from the center (Figure 4), if confirmed, may be real low density regions in the hot ISM, because they are not coincident with dust patches, except in the central SE region. The ionized gas is overall cospatial with the dust patches. However, the northern blob of the ionized gas falls in between dust patches, while the southern blob coexists with dust, indicating some of the line emission is absorbed by the dust.

The origin of the ionized gas (i.e., ionization mechanism) is unclear in early type galaxies. The emission lines often indicate LINER-type nuclear activity rather than HII regions, judged by for example the relative line strengths $H\alpha$ to [NII] flux ratio (e.g., Kim 1989). It has also been suggested that the gas is photo-ionized by post AGB stars (Trinchieri and di Serego Alighieri 1991). In the case of galaxies containing significant amounts of hot ISM, the ionized gas may also be the result of cooling flows (e.g., Sarazin 1988), but this is unlikely in NGC 1316.

In NGC 1316, the kinematics of the ionized gas revealed that the gas is rapidly (up to 350 km sec^{-1}) rotating along the minor axis (PA=127-142°; Schweizer 1980), while the stellar system rotates along the major axis (PA=50°; Bosma, Smith and Wellington 1985). The same is true for molecular gas (Sage and Galletta 1993). This suggests an external origin for the cold and ionized ISM, perhaps connected with the merging episode (Schweizer 1980; Mackie and Fabbiano 1997) and argues against the idea that the ionized/cold gas is originated from cooling hot gas. In the latter case both hot and cold/warm gas would be expected to have the same kinematics as the stars, since the hot ISM is likely to originate from stellar evolution. Different origins of warm gas (likely cold gas and dust as well) and hot gas may be further supported by our HRI observations in that the central X-ray flattening, possibly a disk would rotate along the major axis and that the morphological relationships between the ionized gas and the X-ray emission are lacking. Therefore, it is likely that the cold and warm ISM might be acquired externally by mergers and infalls occurred $\sim 10^9$ years ago, while the hot gas has been accumulated since the latest merger.

If the infalling, cooling hot ISM carries angular momentum it may form an accretion disk, which could be extending out to a 10 kpc radius (see Kley and Mathews 1995; Brighenti and Mathews 1996). The NE-SW flattened isophotes of NGC 1316 (Figure 2) may represent such a disk. However, because the isophotes are measured at radii less than the optical effective radius, the stellar potential needs not be round at these radii. Therefore, the observed elongation may be consistent with hydrostatic gas in the stellar potential (or with a modest amount of dark matter).

4.3 Is the radio jet thermally confined?

Interestingly, the observed elongation in the hot gas structure is approximately perpendicular to the radio jet of NGC 1316. The possibility of thermal confinement is supported by the radial behaviour of the jet/ISM energetics. We estimated the radio jet pressure corresponding to the minimum energy using the radio map by Geldzahler and Fomalont (1984) (see Feigelson et al. 1995 for the validity of the minimum energy argument). We applied the prescription for a Gaussian jet given in Killeen, Bicknell and Ekers (1986a; see also Pacholczyk 1970). We also used the cylindrical jet approximation (see Perley, Willis and Scott 1979), but the results do not change significantly. We assumed that: the jet and the magnetic field are perpendicular to the line of sight; the energy of relativistic electrons is equal to that of protons and ions; the radio spectrum is a power law from 10 MHz to 10 GHz with a slope α=0.7; and the volume filling factor is unity. The estimated jet pressure is compared with the thermal pressure in Figure 8. At 6 - 24″ from the cen-

ter, the jet pressure for both NW and SE jets is an order of magnitude lower than the thermal pressure. Radio and thermal pressure are supposed to be in balance in the case of thermal confinement. However, as discussed by Killeen et al. (1988) the radio minimum pressure could be easily underestimated (see also Pacholczyk 1970) while the similarity of the radial behaviour of radio and X-ray pressures argues for thermal confinement. This apparent contradiction between the thermal gas and minimum radio pressures has also been reported in similar cases where radio jets are expanding through the hot gaseous environment (e.g., Bohringer et al. 1993; Carilli, Perley and Harris 1994).

The possibility (suggested by Figure 8) that the jet is thermally confined inside a relatively small region reinforces the suggested lack of causal connection between the jet and the extended lobes (Ekers et al. 1983). It is possible that active events took place some time ago, probably induced by a merger ($\sim 10^9$ years ago; Schweizer 1980) and now the nucleus is relatively weak and the radio lobes are slowly cooling (see also Ekers et al. 1983). This idea is also supported by the relative power ($\sim 1/2500$) of the jets to the extended radio lobes, which is a few hundred times lower than that of a typical early type galaxy (Slee et al. 1994); the lack of strong optical emission lines (see Schweizer 1980); the absence of a connection between the jet and the lobe (Geldzahler and Fomalont 1984); and the morphology of the lobes (Fomalont et al. 1989).

The double peaks and X-ray valleys seen in Figure 4, if confirmed, will provide more direct evidence for interaction between the hot gas and the radio jet. Both sides of the radio jets in projection appear to pass through the X-ray valleys which may play a role as nozzles in collimating the jets.

4.4 The Nucleus

Fabbiano et al. (1984) found a relationship between radio core power and X-ray luminosity in a sample of 3CR galaxies, indicating that both radio and X-ray emission are of non-thermal nuclear origin. This relationship holds down to radio faint galaxies (Fabbiano et al. 1989). Recently, with ROSAT observations, Worrall and Birkinshaw (1994) spatially decomposed central X-ray point sources from the diffuse, extended emission in several radio galaxies and confirmed the linear relationship between core radio and central X-ray emission in low-power radio galaxies. Although the X-ray core of NGC 1316 is not detected, the ratio between the X-ray upper limit (corresponding to $l_{1keV} \leq 6.3 \times 10^{21}$ erg s^{-1} Hz^{-1}) and the radio core emission ($l_{5GHz} = 2 \times 10^{28}$ erg s^{-1} Hz^{-1}, form Geldzahler and Fomalont 1984) is consistent with the linear relationship between these quantities discussed above.

A comparison of the spectral energy distribution (SED) of the NGC 1316 nucleus with those of other LINER galaxies can be found in Fabbiano and Juda (1997). It is worth noting the possible similarity between the nuclear sources of NGC 3998 and NGC 1316 (both early type galaxies). They both present a bright UV point-like source discovered with HST, and their SED differ from those of bright AGN (see also Fabbiano et al. 1994b). A better coverage of the nuclear emission of these faint AGN will be necessary to understand the emission mechanism.

5. CONCLUSION

We have presented the analysis of the high spatial resolution image and of the X-ray spectrum of NGC 1316 (Fornax A) obtained with the ROSAT HRI and PSPC. The results lead to the following conclusions:

(1) The X-ray emission of NGC 1316 is extended. No point sources are detected within the galaxy at a luminosity threshold of a few x 10^{39} erg sec^{-1}. The radial profile of the X-ray surface brightness falls as r^{-2}, which is close to the optical light distribution. No gradient of the X-ray emission temperature is seen. Within the central 40″, the X-ray isophotes are flattened along the optical major axis. In a larger scale (1-2′), the X-ray emission is extended toward N-S, in agreement with the PSPC report of Inverse Compton emission (Feigelson et al. 1995).

(2) The X-ray spectrum of NGC 1316 (r < 180″) can be reproduced either by a single-temperature low-abundance model (kT = 0.7 keV and 10% solar) or by a two-temperature, solar-abundance model (kT_1 = 0.1-0.2 keV and kT_2 = 0.8-0.9 keV). These results indicate the presence of hot gaseous component contributing to >60% of the total X-ray emission. We set an upper limit of ~20% of the total emission due to a hard component from LMXB in NGC 1316, consistent with an extrapolation based on the bulge of M31 as well as those of early type galaxies observed with ASCA. The total X-ray emission is 2×10^{41} erg sec^{-1} in the 0.1-2.4 keV band and $M_{gas} \sim 10^9 M_\odot$. The relatively small amount of hot ISM present in this X-ray faint galaxy [by comparison with that of X-ray bright E and S0 such as NGC 4636 and NGC 4472 (e.g., Fabbiano et al. 1992)] is consistent with observations of other systems that may have undergone relatively recent merging (Fabbiano and Schweizer 1995).

(3) The X-ray emission is significantly reduced at the locations where the dust patches

are more pronounced, indicating that some of the X-ray emission may be absorbed by the internal cold ISM in NGC 1316. The ionized gas is generally distributed along with the dust patches. Some features of the ionized gas appear to be related with a hot ISM but there is no one-to-one correspondence. Both morphological relations and kinematics suggest that the hot and cold/warm ISM may not have the same origin. The cold/warm ISM might be acquired externally by mergers/infalls, while the hot ISM has been accumulated since the latest merger.

(4) In projection, the direction of the radio jets is perpendicular to the central NW-SE elongation of the X-ray emission. The thermal pressure is higher than the jet equipartition pressure by an order of magnitude. However, the radial behaviour of thermal and radio pressures are similar, suggesting the possibility of thermal confinement.

(5) Although a nuclear source is not detected in X-rays, the upper limit ($L_X \leq 9 \times 10^{39}$ erg sec^{-1}) is consistent with the expectations, based on the extrapolation from low-power radio galaxies (Worrall and Birkinshaw 1994).

ACKNOWLEDGMENTS

This work was supported by NASA grants NAG 5-2152 (ROSAT), NAGW 2681 (LTSA), NASA contract NAS8-39073 (AXAF Science Center) and by Non Directed Research Fund, Korea Research Foundation. This research has made use of SIMBAD which is operated by the Centre de Donnees astronomiques de Strasbourg (CDS), France. We thank the referee and Greg Bothun for their comments on the original draft.

REFERENCES

Arimoto, N., Matsuchita, K., Ishimaru, Y., Ohashi, T., & Renzini, A. 1996 preprint

Arp, H. 1966, ApJS, 14, 1

Baum, S. A., Heckman, T. M. & van Breugel, W. 1992, ApJ, 389, 208

Begelman, M. C., Blandford, R. D., & Rees, M. J. 1984, Rev. Mod. Phys. 56, 255

Bohringer, H., Voges, W., Fabian, A. C., Edge, A. C., & Neumann, D. M. 1993, MNRAS, 264, L25

Bosma, A., Smith, R. M. & Wellington, K.J. 1985, MNRAS, 212, 301

Brighenti, & Mathews, W. 1996, preprint

Buote, D. A., & Canizares, C. R. 1994, ApJ, 427, 86.

Carilli, C. L., Perley, R. A., & Harris, D. E. 1994, MNRAS, 270, 173

Carter, D., Jorden, P.R., Thorne, D.J., Wall, J.V. & Straede, J.C. 1983 MNRAS, 205, 377

Carter, D., and Metcalfe, N. 1980, MNRAS, 191, 325

David, L. P., Harnden, F. R., Kearns, K. E., & Zombeck, M. V. 1993, The ROSAT High Resolution Imager (US ROSAT Science Data Center/SAO)

de Vaucouleurs, G., de Vaucouleurs, H., Corwin, H. G., Buta, R. J., Paturel, G., & Fouque, P. 1991 *Third Reference Catalogue of Bright Galaxies*, (**RC3**), (New York: Springer-Verlag)

Ekers, R. D., Gross, W. M., Wellington, K. J., Bosma, A., Smith, R. M., & Schweizer, F. 1983, AA, 127, 361

Fabbiano, G. 1989, ARAA, 27, 87

Fabbiano, G., Miller, L., Trinchieri, G., Longair, M., & Elvis, M. 1984, ApJ, 277, 115

Fabbiano, G., Gioia, I. M., & Trinchieri, G. 1988, ApJ,324,749

Fabbiano, G., Gioia, I. M., & Trinchieri, G. 1989, ApJ, 347, 127

Fabbiano, G., Kim, D.-W., & Trinchieri, G. 1992, ApJS, 80, 531

Fabbiano, G., Kim, D.-W., & Trinchieri, G. 1994a, ApJ, 429, 94

Fabbiano, G., Fassnacht, C., & Trinchieri, G., 1994b, ApJ, 434, 67

Fabbiano, G., & Schweizer, F. 1995, ApJ, 447, 572

Fabbiano, G., & Juda, G. 1997, in preparation.

Fabbiano, G., Trinchieri, G., and van Speybroeck, L. 1987, ApJ, 316, 127

Faber, S. M., and Gallagher, J. S. 1979, ARAA, 17, 135

Feigelson, E.D., Laurent-Muehleisen, S.A., Kollgaard, R.I., & Fomalont, E. B. 1995, ApJ, 449, L149

Fomalont, E. B., Ebnerter, K. A., van Breugel,J. M., & Ekers, R. D. 1989, ApJ, 346, L17

Geldzahler, B. J., & Fomalont, E. B. 1984, AJ, 89, 1650

Gorgas J., Efstathiou G. & Aragon Salamanca, A. 1990, MNRAS, 245, 217

Hasinger, G., Burg, R., Giacconi, R., Hartner, G., Schmidt, M., Trumper, J., & Zamorani, G. 1993, AA, 275, 1

Hibbard, J. E., Guhathakurta, P., van Gorkom, J. H., Schweizer, F. 1994, AJ, 107, 67

Jedrzejewski, R. I. 1987, MNRAS 226, 747

Kaneda, H., Tashiro, M., Ikebe, Y., Ishiski, Y., Kubo, H., Makishima, K., Ohashi, T., Saito, Y., Tabara, H., and Takahashi, T. 1995, ApJ, 453, L13

Killeen, N. E. B., Bicknell, G. V., & Ekers, R. D. 1986a, ApJ, 302, 306

Killeen, N. E. B., Bicknell, G. V., & Carter, D. 1986b, ApJ, 309, 45

Killeen, N. E. B., Bicknell, G. V., & Ekers, R. D. 1988, ApJ, 325, 180

Kim, D.-W. 1989, ApJ, 346, 653

Kim, D.-W., Fabbiano, G., & Trinchieri, G. 1992a, ApJS. 80, 645

Kim, D.-W., Fabbiano, G., & Trinchieri, G. 1992b, ApJ. 393, 134

Kim, D.-W., & Fabbiano, G., 1995, ApJ, 441, 182

Kim, D.-W., Fabbiano, G., Matsumoto, H, Koyama, K., & Trinchieri, G. 1996, ApJ, 468, 175.

Kley, W. & Mathews, W. 1995, ApJ, 438, 100

Knapp, G. R., Turner, E. L., & Cunniffe, P. E. 1985, AJ, 90, 454

Knapp, G. R., Guhathakurta, P., Kim, D.-W., & Jura, M. 1989, ApJS, 70, 329

Kriss, G. A., Cioffi, D. F., & Canizares, C. R. 1983, ApJ, 272, 439

Loewenstein, M., Mushotzky, R. F., Tamura, T., Ikebe, Y., Makishima, K., Matsushita, K., Awaki, H., & Serlemitsos, P. J. 1994, ApJ, 436, L75.

Mackie, G., & Fabbiano, G. 1997, AJ submitted

Malin, D. F., & Carter, D. 1983, ApJ, 274, 534

Matsushita, K., Makishima, K., Awaki, H., Canizares, C. R., Fabian, A. C., Fukazawa, Y., Loewinstein, M., Matsumoto, H. Mihara, T., Mushotzky, R. F., Ohashi, T., Ricker, G. R., Serlemitsos, P. J., Tsuru, T., Tsusaka, Y., & Yamazaki, T 1994, ApJ, 436, L41

Matsumoto, H., Koyama, K., Awaki, H., Tsuru, T., Loewenstein, M., and Matsushita, K. 1997, ApJ, 482, 133.

Pacholczyk, A. G. 1970, *Radio Astrophysics* (San Francisco: Freeman)

Pellegrini, S. & Fabbiano, G. 1994, ApJ, 429, 105

Perley, R. A., Willis, A. G., & Scott, J. S. 1979, Nature, 281, 437

Phillips, M. M., Jenkins, C. R., Dopita, M. A., Sadler, E. M. & Binette, L. 1986, AJ, 91, 1062

Sage, L.J. & Galletta, G., 1993, ApJ, 419, 544

Sarazin, C. L. 1988 *X-ray emissions from clusters of galaxies* (Cambridge: Cambridge

University press)
Schweizer, F., 1980, ApJ, 237, 303
Schweizer, F., 1981, ApJ, 246, 722
Slee O. B., Sadler E. M., Reynolds, J. E. & Ekers R.D. 1994, MNRAS, 269, 928
Truemper, J. 1983, Adv. Space Res. 2, 241
Trinchieri, G. & Fabbiano, G. 1991, ApJ, 382, 82
Trinchieri, G. & di Serego Alighieri, S. 1991, AJ, 101, 1647
Trinchieri, G., Kim, D.-W., Fabbiano, G. & Canizares, C. R. 1994, ApJ, 428, 555
Veron-Cetty, M. P. & Veron, P. 1986 , AAS, 66, 335
Wade, C. M. 1961, Pub. NRAO, 1, 99
Wiklind, T. & Henkel, C. 1989, AA, 225, 1
Worrall, D. M., & Birkinshaw, M. 1994, ApJ, 427, 134

Table 1

Basic parameters

	NGC 1316	NGC 1317
RA (J2000)[a]	3 22 41.6	3 22 44.7
DEC (J2000)[a]	-37 12 28	-37 6 10
B_T^o (mag)[a]	9.40	11.81
D (Mpc)[b]	27.2	27.2
D_{25} (arcsec)[a]	721	165
N_H (cm^{-2})[c]	2.0 x 10^{20}	2.0 x 10^{20}
HRI Observed Date[d]	Jan. 14, 1994	Jan. 14, 1994
HRI Exp time (sec)[d]	11038	11038
HRI Observed Date[e]	Jul. 7-10, 1994	Jul. 7-10, 1994
HRI Exp time (sec)[e]	29403	29403
PSPC Observed Date	Jan. 13-20, 1992	Jan. 13-20, 1992
PSPC Exp time (sec)	25500	25500
Log Fx (IPC) erg sec^{-1} cm^{-2}[f]	2.0 x 10^{-12}	<2.7 x 10^{-13}

a. Right Ascension (RA), declination (DEC), total face-on B magnitude (B_T^o), and major isophotal diameter measured at B = 25 magnitude $arcsec^{-2}$(D_{25}) taken from de Vaucouleurs et al. 1991 (RC3)

b. Distance from Fabbiano et al. 1992.

c. Galactic line of sight HI column density from Starks et al. 1992.

d. Sequence number 600255n00

e. Sequence number 600255a01

f. IPC flux from Fabbiano et al. 1992. Fluxes were estimated in a energy range of 0.2–4.0 keV for a Raymond-Smith model with solar abundance, kT=1keV and line of sight N_H. The count extraction radii are r=450″ for NGC 1316.

Table 2

X-ray sources

source number	X Y pixel	radius[c] arcsec	offaxis arcmin	vignetting correction	net cnts	error	Fx[e] 10^{-13}
1	5599.86 3823.70	30	12.9	1.076	67.44	15.77	0.53
2	5075.38 4998.42	25	10.9	1.055	89.45[d]	14.96	0.69
3	4468.47 4499.67	30	4.4	1.012	48.61	15.52	0.36
4	4104.82 3607.70	25	4.7	1.013	86.11	15.30	0.64
5[a]	4076.98 4108.50	170	—	—	2047.79	85.77	14.99
6[b]	4009.78 4862.26	20	6.2	1.020	120.29	15.05	0.90
7	3842.10 4436.98	25	3.4	1.008	35.52	13.19	0.26
8	3702.10 3687.70	30	5.1	1.015	68.92	16.08	0.51
9	3296.79 3583.91	15	8.1	1.033	31.89	9.79	0.24
10	3041.20 3157.04	25	12.0	1.065	53.90	13.76	0.42
11	2959.06 4396.66	20	9.7	1.045	44.42	11.83	0.34
12	2823.38 3703.22	20	11.2	1.057	201.14[d]	17.81	1.56

a. NGC 1316

b. NGC 1317

c. Background counts were extrated in annuli (r=200″- 400″ for NGC 1316; r=60″-200″ for all other sources).

d. variable (see Table 3).

e. Fluxes were estimated in a energy range of 0.1–2.4 keV for a Raymond-Smith model with solar abundance, $kT = 1$ keV and line of sight N_H. Vignetting correction was applied.

Table 3

Variable Sources

source	Jan. 94		Jul. 94		difference
number	rate	err	rate	err	σ
2	-0.47	0.56	3.22	0.46	5.09
12	7.81	1.04	3.92	0.46	3.41

Rates and errors are in unit of counts in 1,000 seconds.

Table 4

SPECTRAL FIT OF PSPC DATA[a]

2-Component fit with solar abundance[b]

radius ($''$)	kT_1 (keV)	kT_2 (keV)	Norm[c]	χ^2	degrees of freedom
0-60	0.16 (0.13-0.20)	0.83 (0.76-0.90)	1.68 (1.44-1.88)	26.61	23
60-180	0.15 (0.11-0.17)	0.86 (0.72-1.04)	0.74 (0.54-1.03)	17.89	23
0-180	0.16 (0.14-0.17)	0.84 (0.79-0.89)	1.23 (1.08-1.38)	25.34	23

1-component fit with varying abundance[d]

radius ($''$)	kT (keV)	Abundance (solar)	χ^2	degrees of freedom
0-60	0.70 (0.65-0.77)	0.12 (0.10-0.15)	14.36	24
60-180	0.59 (0.48-0.70)	0.03 (0.02-0.05)	21.14	24
0-180	0.68 (0.63-0.73)	0.08 (0.06-0.10)	12.99	24

a. N_H is fixed at the Galactic line-of-sight value, 2×10^{20} cm^{-2}.

b. Errors are at 90% confidence with 3 interesting parameters.

c. Normalization of the second component relative to the first component.

d. Errors are at 90% confidence with 2 interesting parameters.

Table 5

X-RAY FLUX AND LUMINOSITY[a]

	Flux[b]	Luminosity[c]
1-component model		
total	$1.9(\pm0.2) \times 10^{-12}$	$1.7(\pm0.2) \times 10^{41}$
upper limit of hard binary component	2.9×10^{-13}	2.6×10^{40}
upper limit of nuclear component[d]	1.0×10^{-13}	8.9×10^{39}
2-component model		
total	$2.0(\pm0.2) \times 10^{-12}$	$1.8(\pm0.2) \times 10^{41}$
0.2 keV component	$8.1(\pm1.0) \times 10^{-13}$	$7.2(\pm0.9) \times 10^{40}$
0.8 keV component	$1.2(\pm0.1) \times 10^{-12}$	$1.1(\pm0.1) \times 10^{41}$
upper limit of hard binary component	4.0×10^{-13}	3.6×10^{40}
upper limit of nuclear component[d]	1.0×10^{-13}	8.9×10^{39}

a. The data with r $<$ 180″ are used and the errors are based on the acceptable range of normalization at 90%

b. Absorption-corrected flux in unit of erg sec^{-1} cm^{-2} in 0.1-2.4 keV.

c. Distance = 27.2Mpc

d. Estimated from the HRI image

Figure Captions

Figure 1. The entire field of view of this HRI observation (NGC 1316 and NGC 1317). The X-ray contours are overlaid on the optical image obtained from the Digital Sky Survey. X-ray image is binned with a pixel size of 8 arcsec, background-subtracted and smoothed with a Gaussian of σ = 16 arcsec. The octagonal shape indicates the boundary of the HRI detector. The source numbers are ordered by an increasing RA (see Table 2). RA and Dec are in J2000.

Figure 2. A close-up view of the X-ray image (with a pixel size of 2″ and a Gaussian σ of 4″). The contours indicate isophotes at 5% to 95% of the peak with 8 steps. RA and Dec are in J2000.

Figure 3. (a) Radial distribution of X-ray counts extracted in different angular sectors. The filled circles are for the NE-SW sector (PA=30-70°, 210-250°) and the open circles are for NW-SE (PA=120-160°, 300-340°). (b) The significance of count differences between two angular sectors.

Figure 4. same as Figure 2 but with a pixel size of 1″ and a Gaussian σ of 2″. The data obtained only in the July run are used. The contours indicate isophotes at 6% to 85% of the peak with 8 steps.

Figure 5. Radial distribution of X-ray counts determined with the raw, unsmoothed image. Raw, background (determined at r=200–400″), and net counts are indicated by open squares, a solid line and filled squares with error bars.

Figure 6. Radial profile of X-ray surface brightness and best fit model prediction.

Figure 7. (a) Deprojected density and (b) cooling time as a function of radius. The density profile corresponding to β=0.51 ($n_e \sim r^{-1.53}$) is shown as a dashed line.

Figure 8. Thermal gas pressure as a function of radius. The minimum radio pressure along the jets is also plotted with filled circles (the NW jet) and open circles (the SE jet).

Figure 9. Distribution of dust patches (from Schweizer 1980) overlaid onto the X-ray image (same as Figure 2).

Figure 10. Distribution of ionized gas overlaid onto the X-ray image. The continuum-subtracted $H\alpha$ + [NII] image was smoothed with a 2 pixel (full width) gaussian filter

and the X-ray image is the same as Figure 2.

Figure 11. Radio jet overlaid onto the X-ray image. The radio map was taken from Geldzahler and Fomalont (1984). The X-ray image is the same as (a) Figure 2 and (b) Figure 4.

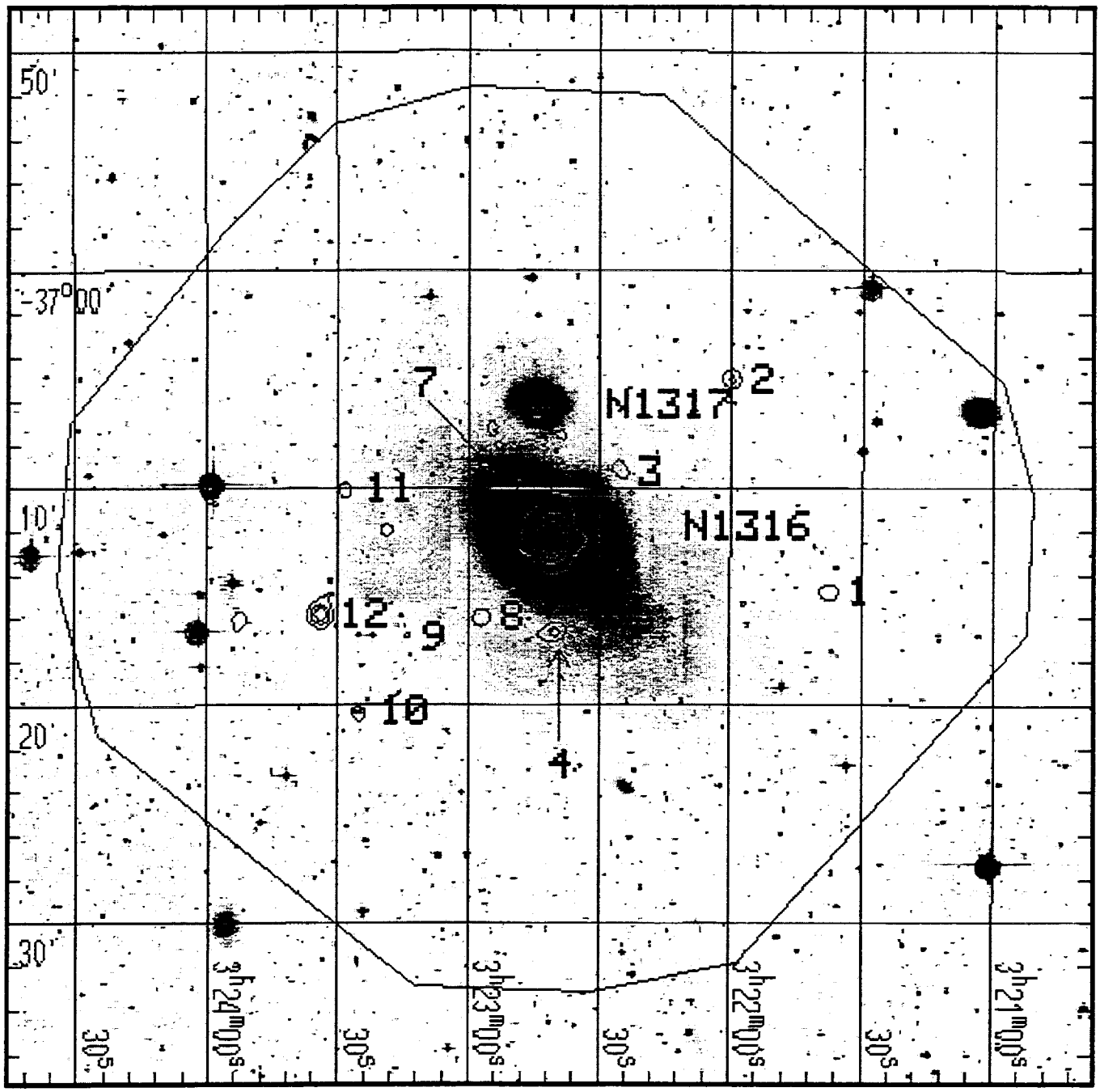
50'
-37°00'
10'
20'
30'
7
N1317
2
3
11
N1316
1
12
9
8
10
4
3h24m00s
30s
3h23m00s
30s
3h22m00s
30s
3h21m00s

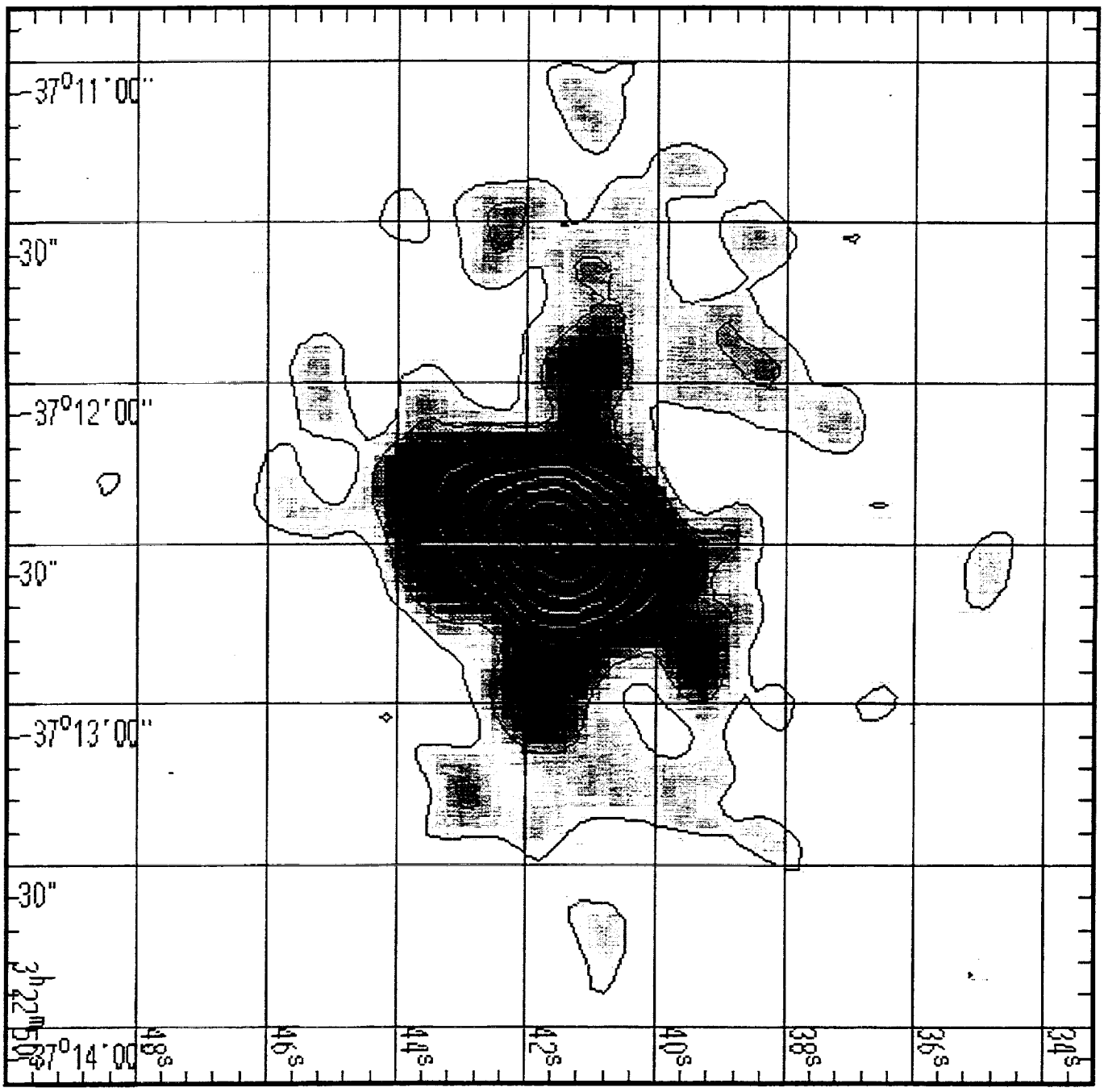
37°11'00"
30"
37°12'00"
30"
37°13'00"
30"
3h22m50s
37°14'00"
48s
46s
44s
42s
40s
38s
36s
34s

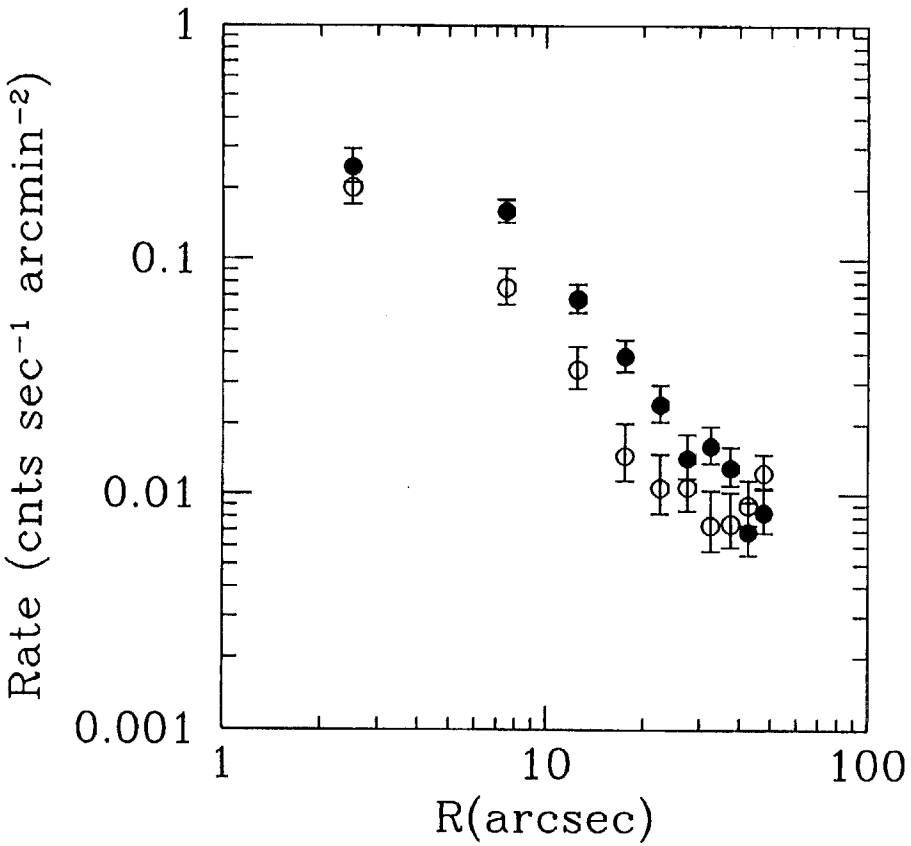
1
0.1
0.01
0.001
Rate (cnts sec^{-1} arcmin^{-2})
1
10
100
R(arcsec)

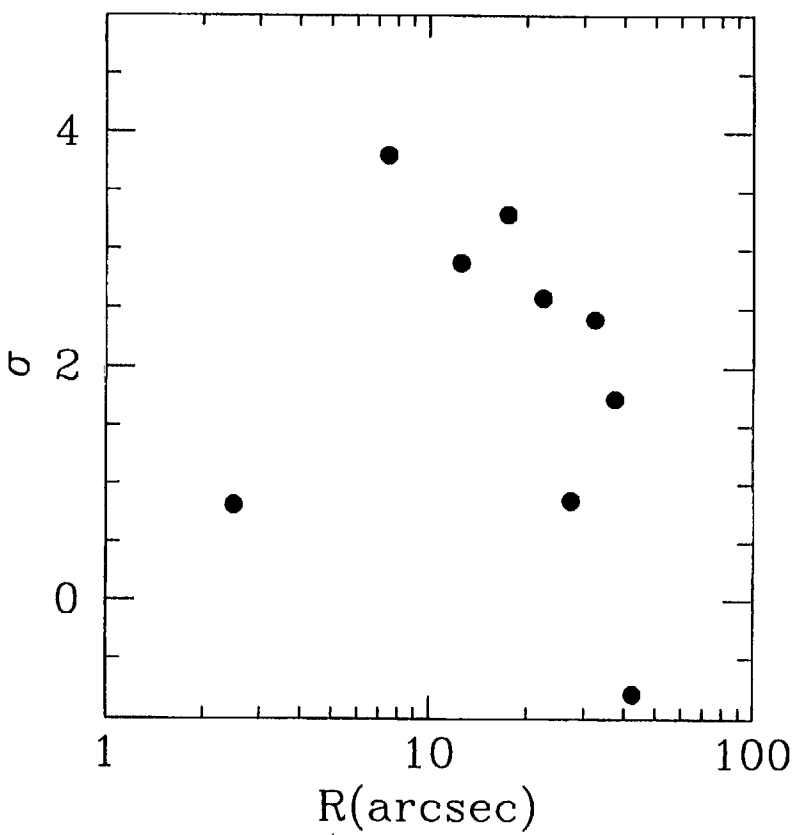
4
2
0
σ
1
10
100
R(arcsec)

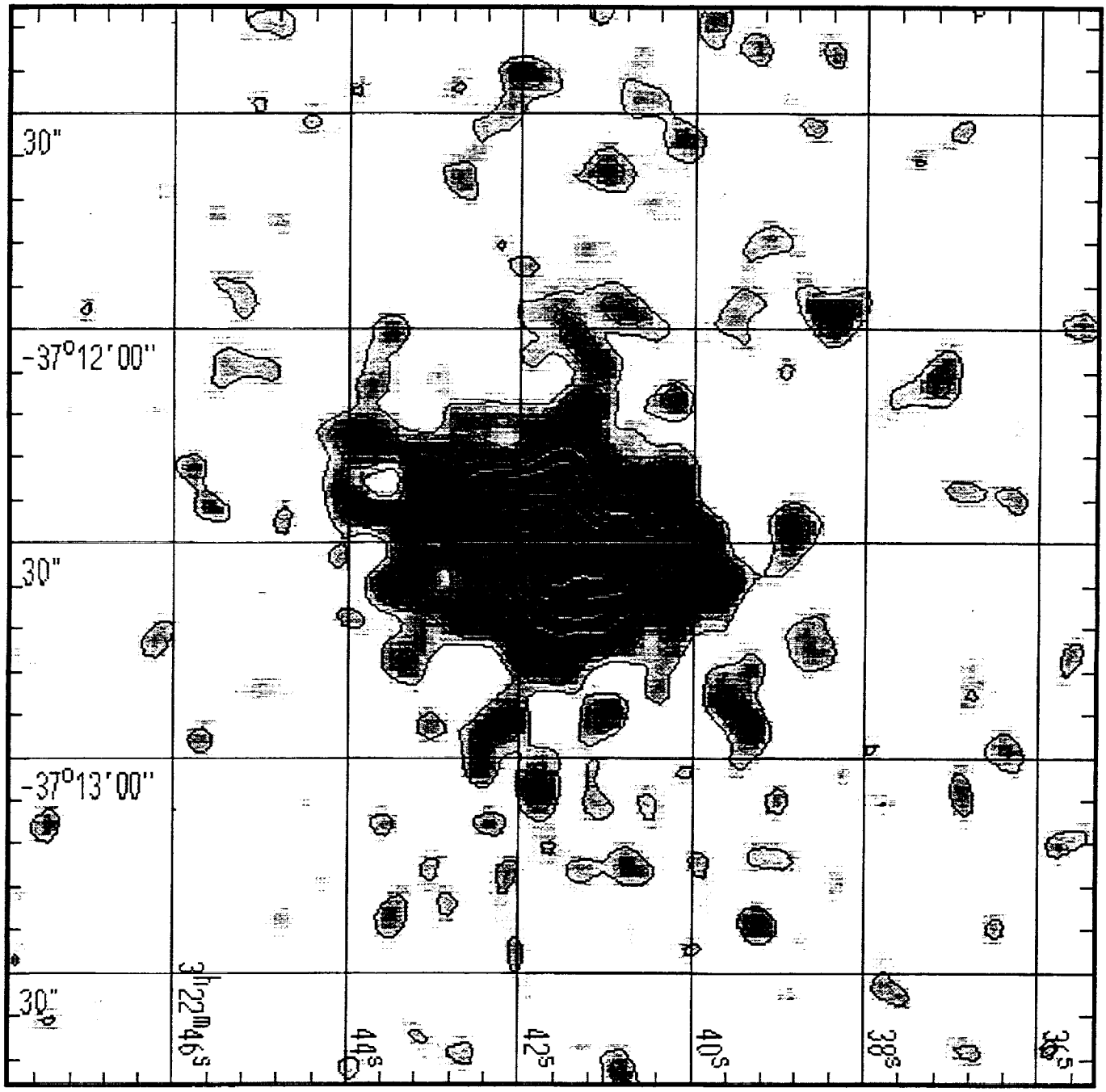
30"
-37°12'00"
30"
-37°13'00"
30"
3h22m46s
44s
42s
40s
38s
36s

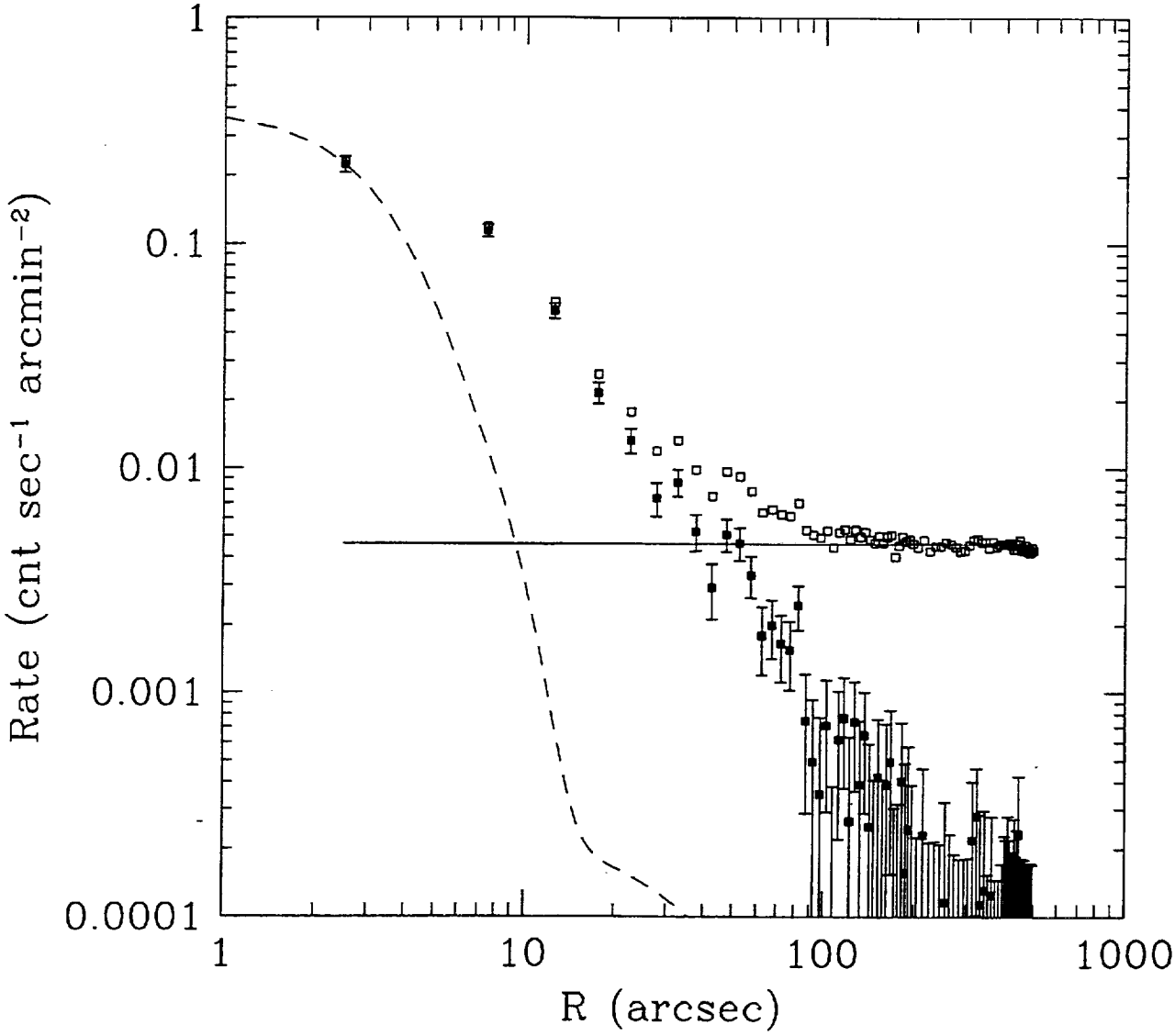
1
0.1
0.01
0.001
0.0001
Rate (cnt sec^{-1} arcmin^{-2})
1
10
100
1000
R (arcsec)

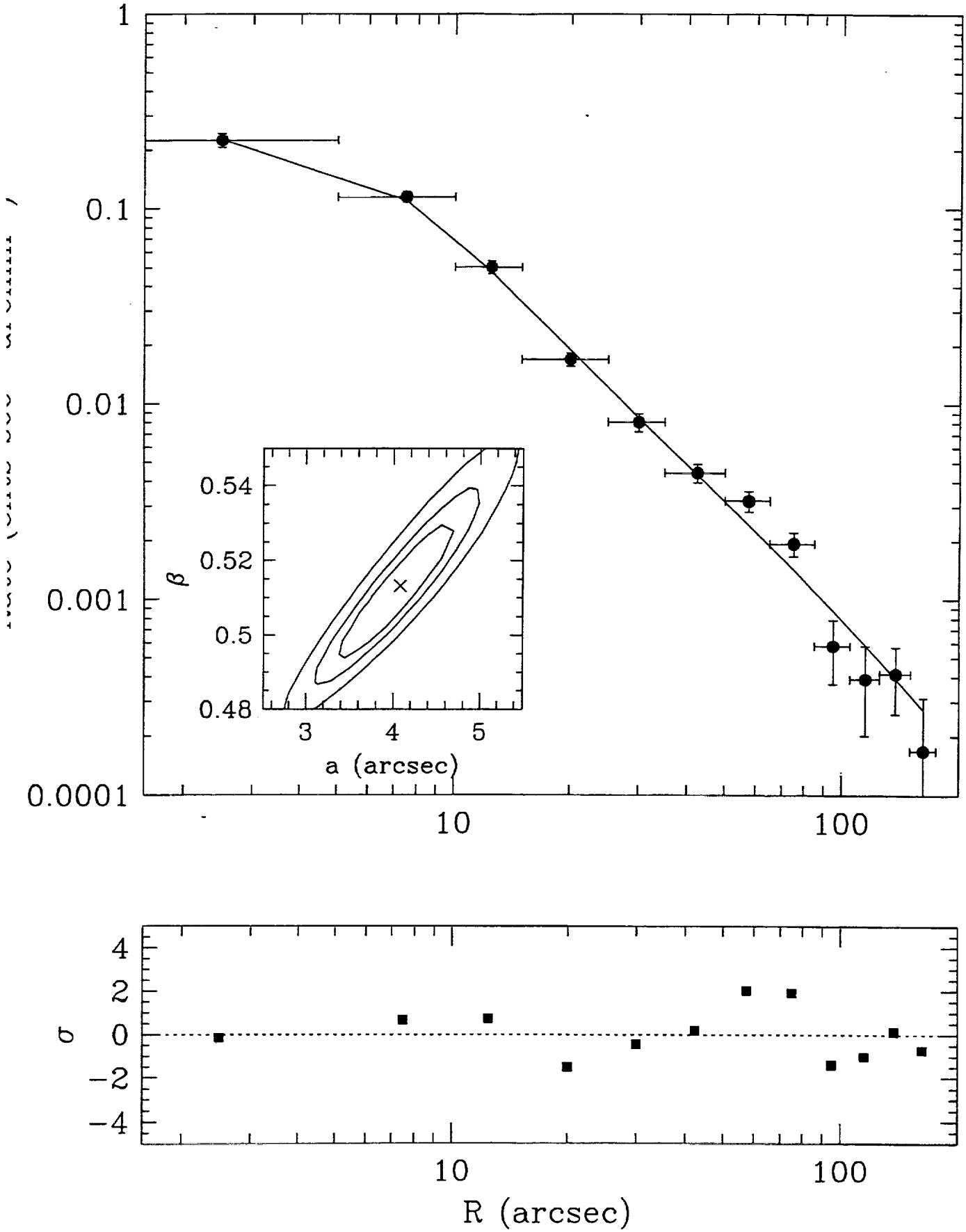
1
0.1
0.01
0.001
0.0001
10
100
0.54
0.52
0.5
0.48
β
3
4
5
a (arcsec)
4
2
0
−2
−4
σ
10
100
R (arcsec)

Figure 6

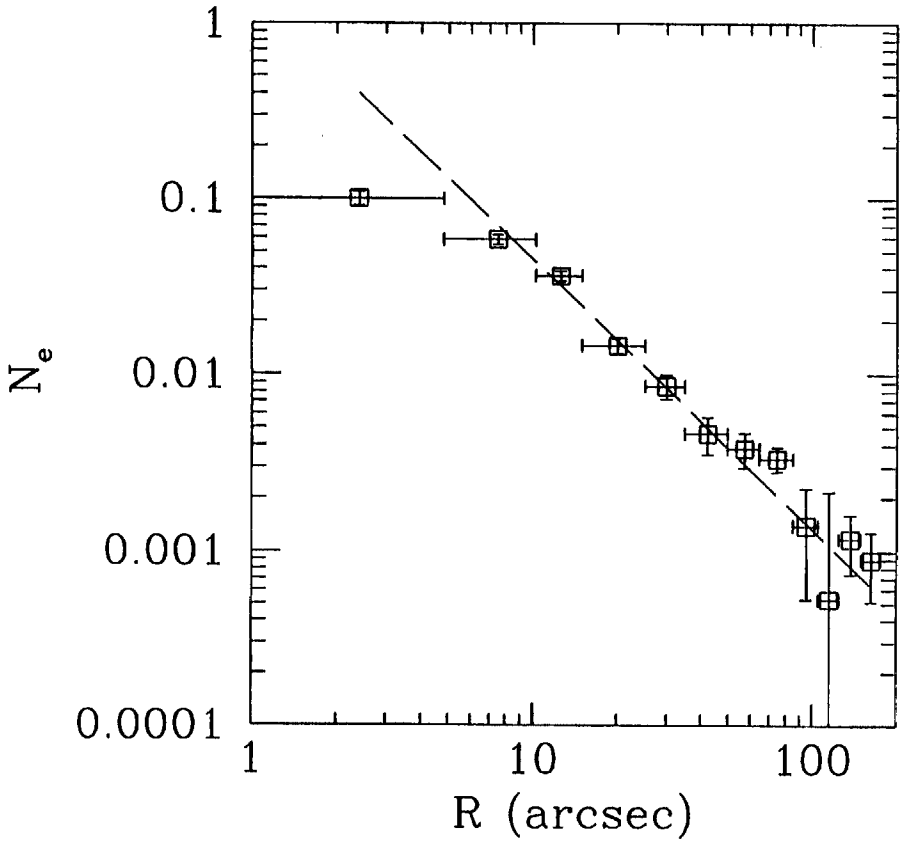
1
0.1
0.01
0.001
0.0001
N_e
1
10
100
R (arcsec)

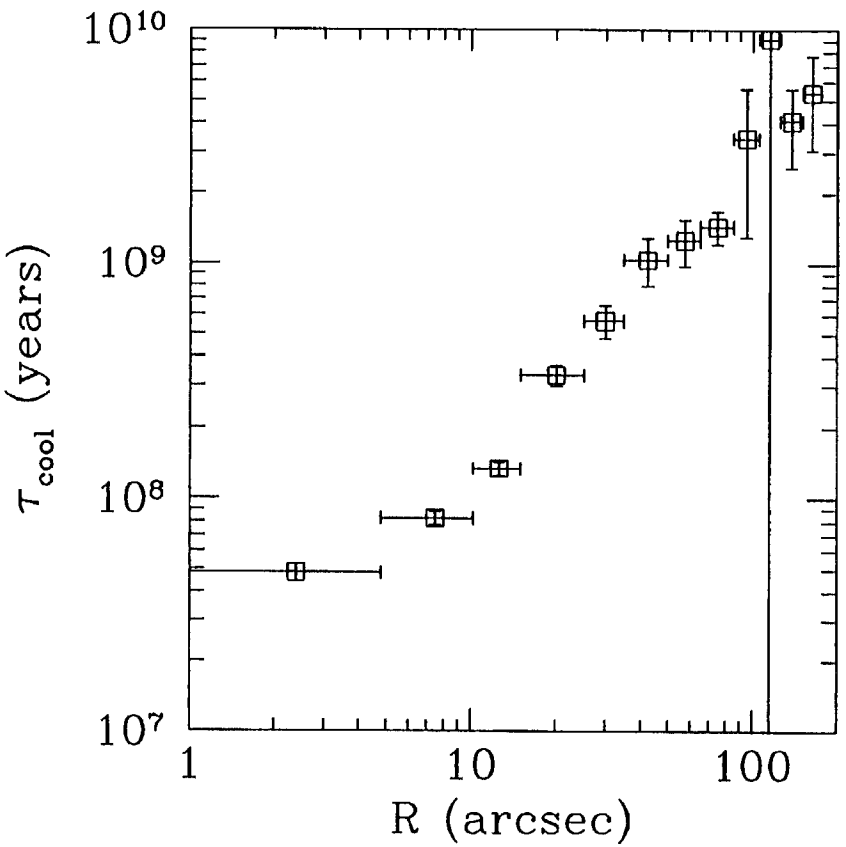
10^{10}
10^9
10^8
10^7
τ_{cool} (years)
1
10
100
R (arcsec)

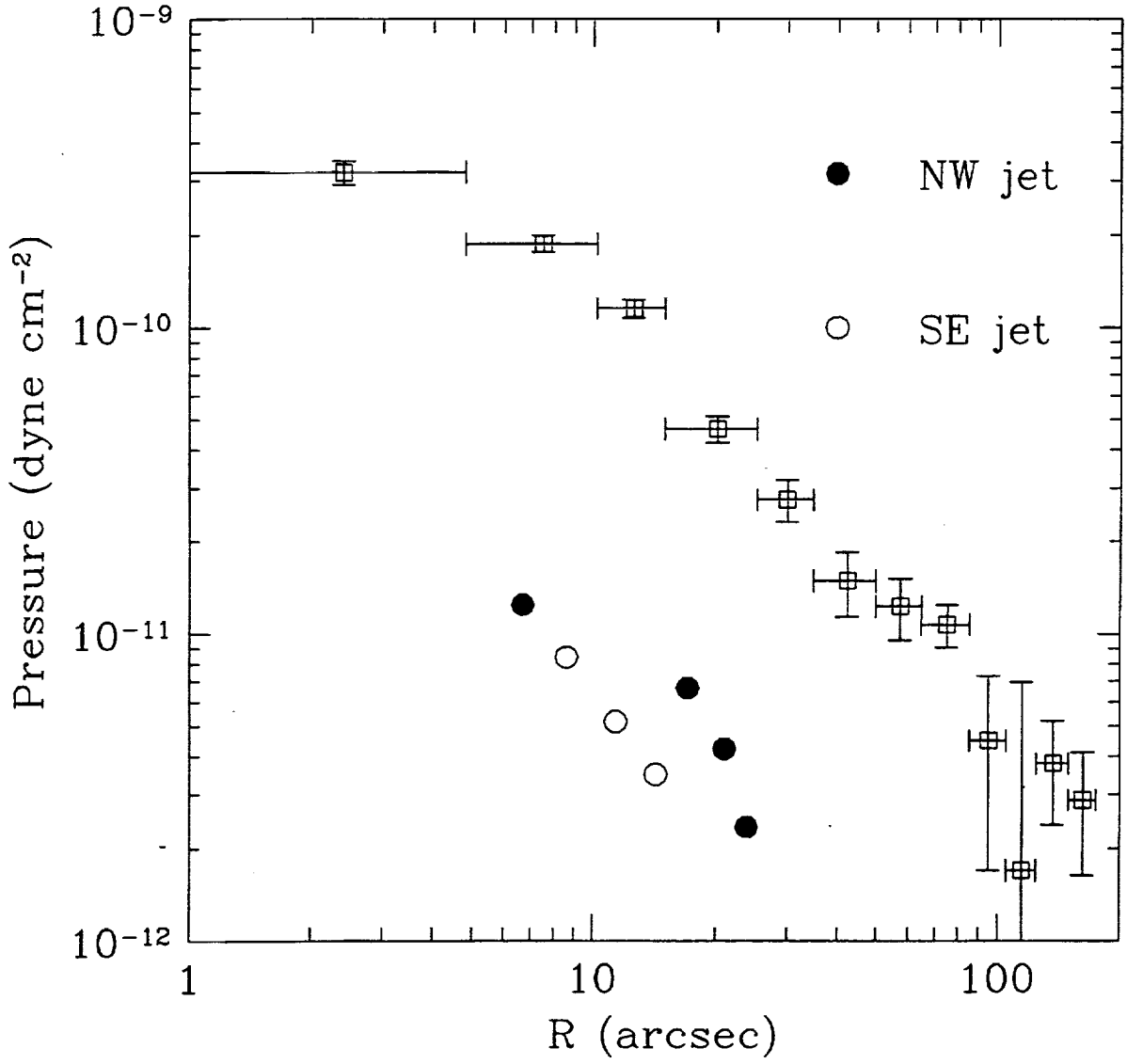
10^{-9}
10^{-10}
10^{-11}
10^{-12}
Pressure (dyne cm^{-2})
NW jet
SE jet
1
10
100
R (arcsec)

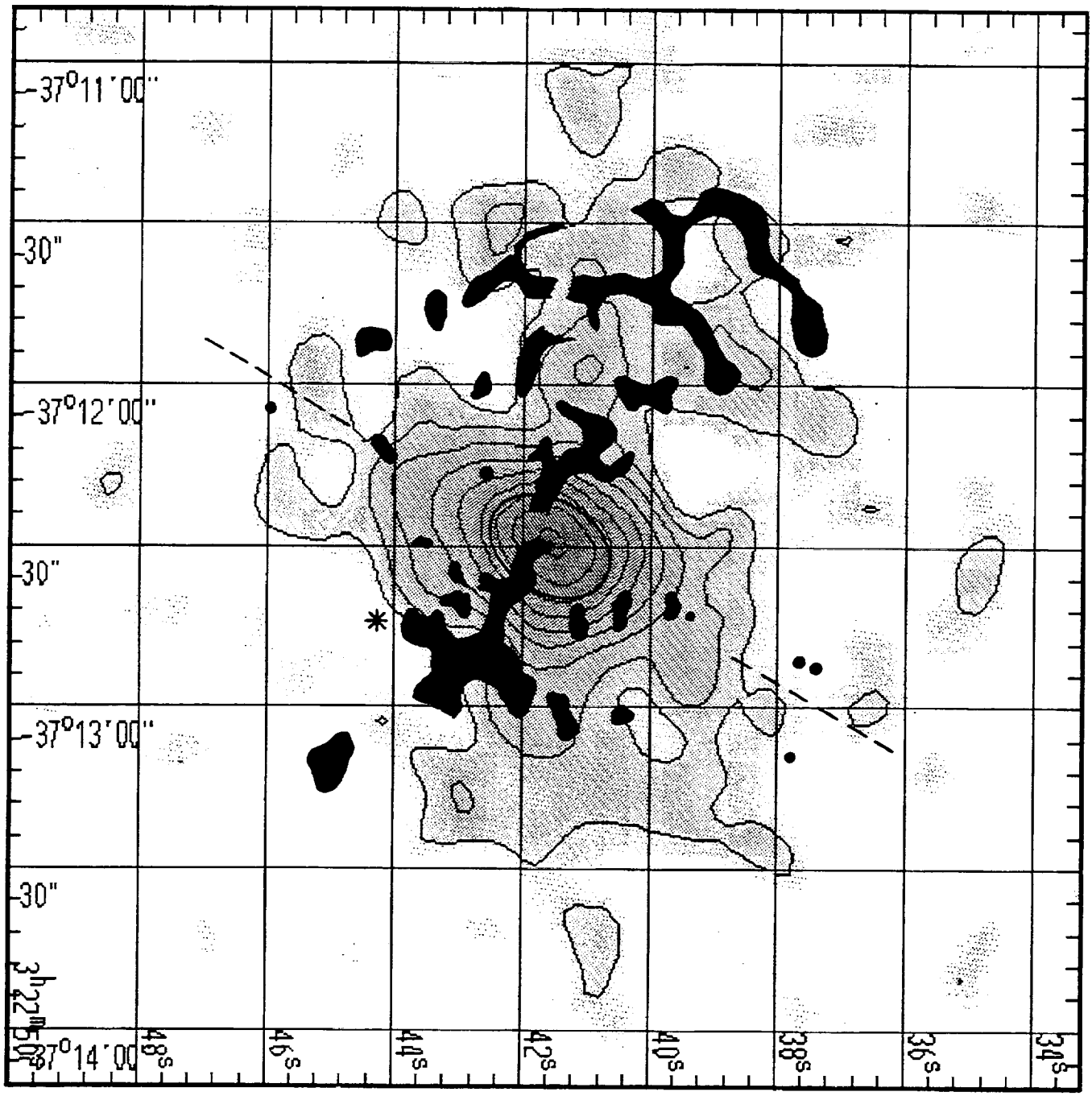
37°11'00"
30"
37°12'00"
30"
37°13'00"
30"
3h22m50s
37°14'00
48s
46s
44s
42s
40s
38s
36s
34s

Figure 9

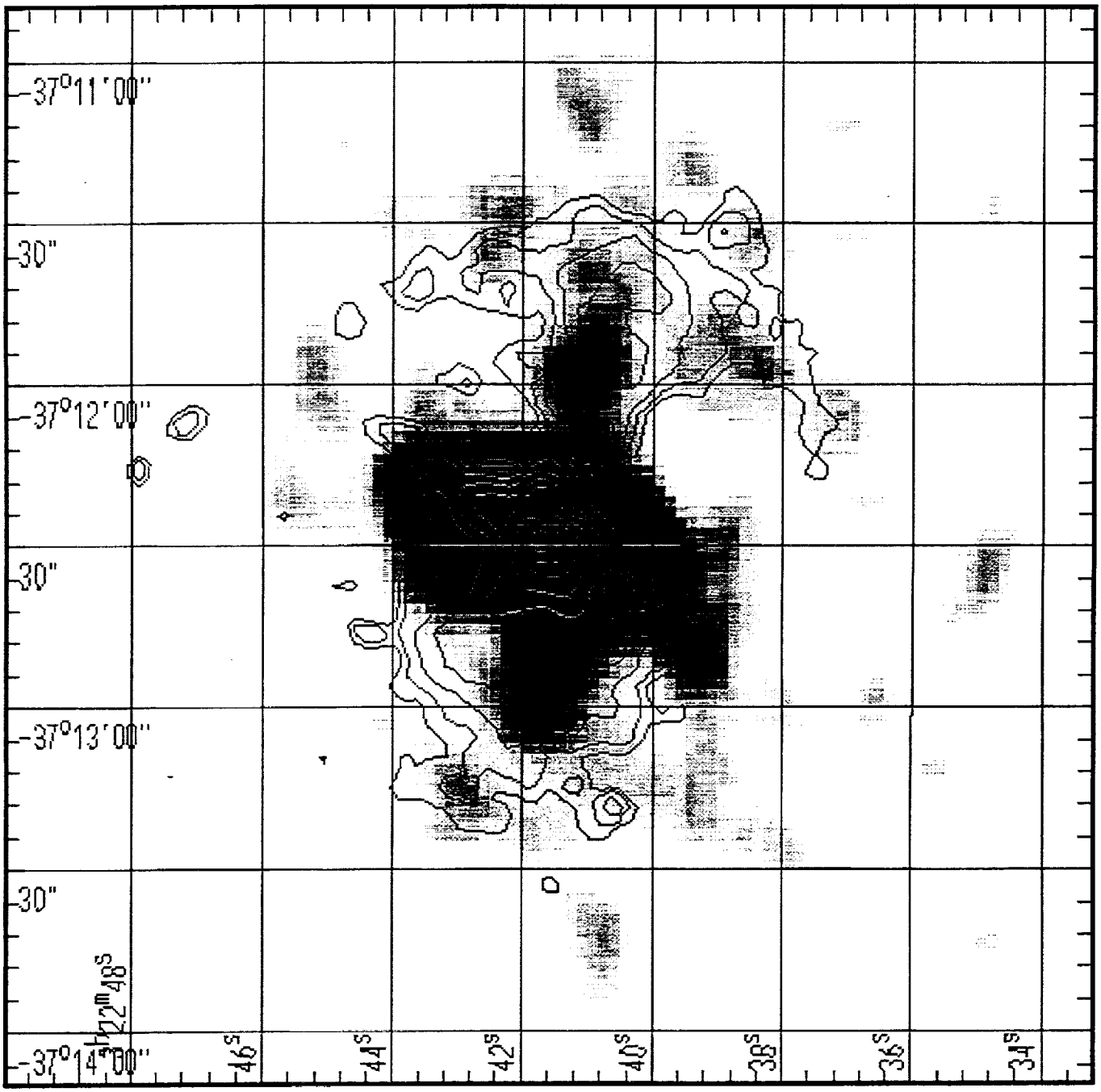
-37°11'00"
30"
-37°12'00"
30"
-37°13'00"
30"
-37°14'00"
12h12m48s
46s
44s
42s
40s
38s
36s
34s

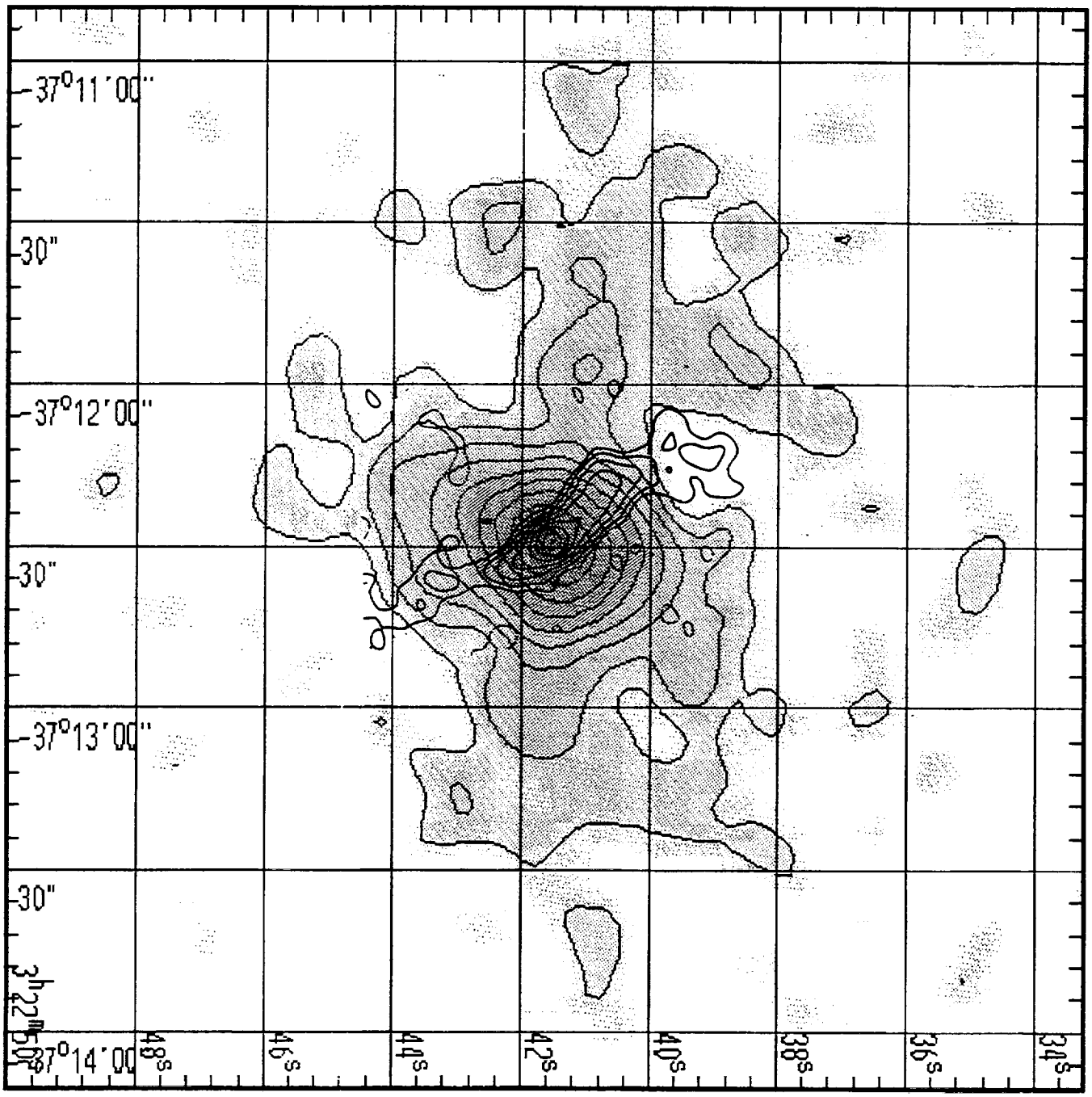
37°11'00"
30"
37°12'00"
30"
37°13'00"
30"
3h27m50s
37°14'00
48s
46s
44s
42s
40s
38s
36s
34s

Figure 11a

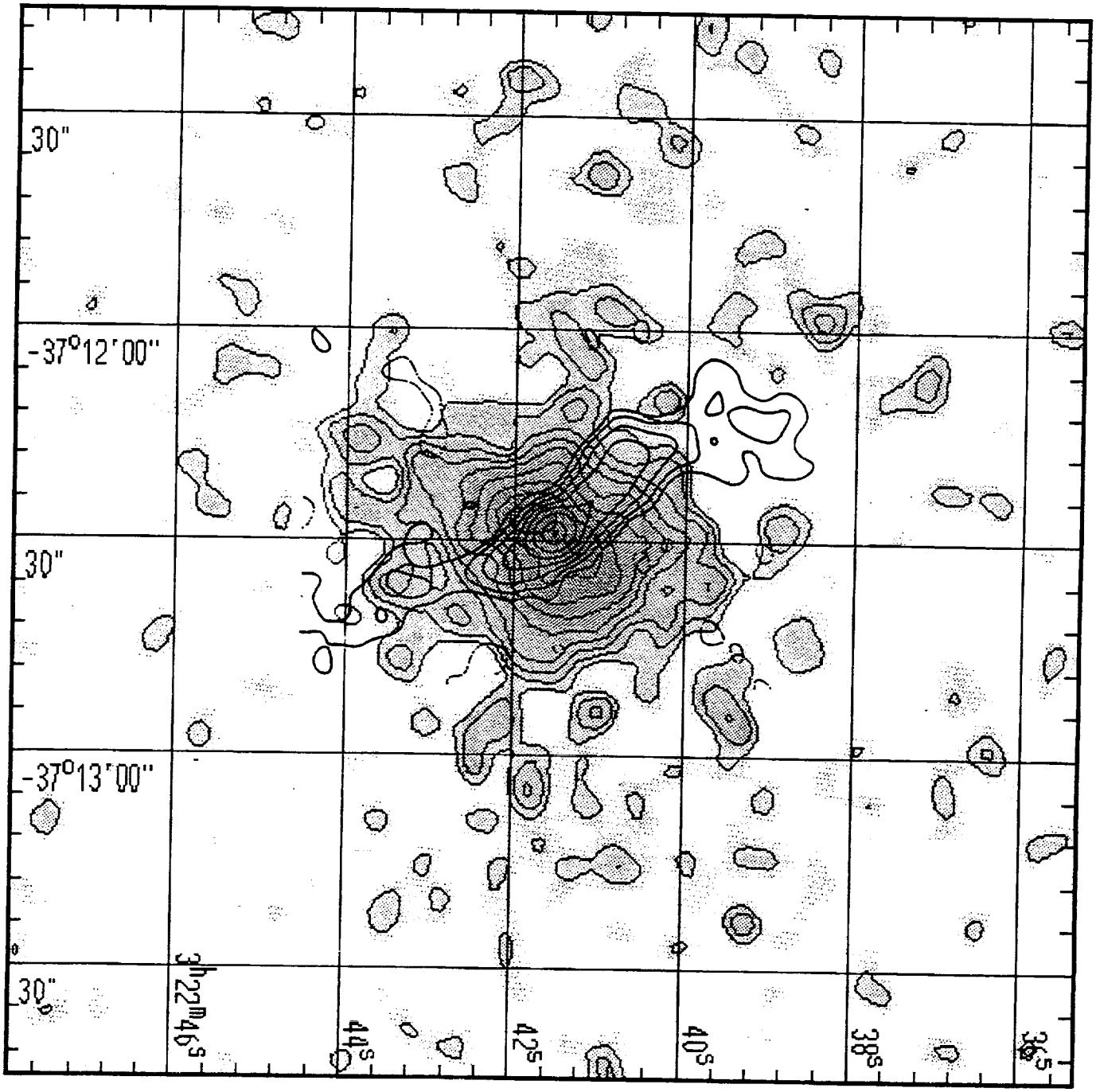

Figure 11 b

THE ASTROPHYSICAL JOURNAL SUPPLEMENT SERIES, 97:141–184, 1995 March

A MULTIPARAMETRIC ANALYSIS OF THE *EINSTEIN* SAMPLE OF EARLY-TYPE GALAXIES. I. LUMINOSITY AND ISM PARAMETERS

PAUL B. ESKRIDGE[1] AND GIUSEPPINA FABBIANO
Harvard-Smithsonian Center for Astrophysics, 60 Garden Street, Cambridge, MA 02138; paul@hera.astr.ua.edu, pepi@cfa.harvard.edu

AND

DONG-WOO KIM
Harvard-Smithsonian Center for Astrophysics, 60 Garden Street, Cambridge, MA 02138; and Department of Astronomy and Space Science, Chungnam National University, Taejon, 305-764, South Korea; kim@cfa.harvard.edu
Received 1994 May 16; accepted 1994 July 28

ABSTRACT

We have conducted bivariate and multivariate statistical analysis of data measuring the luminosity and interstellar medium of the *Einstein* sample of early-type galaxies (presented by Fabbiano, Kim, & Trinchieri 1992). We find a strong nonlinear correlation between L_B and L_X, with a power-law slope of 1.8 ± 0.1, steepening to 2.0 ± 0.2 if we do not consider the Local Group dwarf galaxies M32 and NGC 205. Considering only galaxies with $\log L_X \leq 40.5$, we instead find a slope of 1.0 ± 0.2 (with or without the Local Group dwarfs). Although E and S0 galaxies have consistent slopes for their L_B-L_X relationships, the mean values of the distribution functions of both L_X and L_X/L_B for the S0 galaxies are lower than those for the E galaxies at the 2.8 σ and 3.5 σ levels, respectively. We find clear evidence for a correlation between L_X and the X-ray color C_{21}, defined by Kim, Fabbiano, & Trinchieri (1992b), which indicates that X-ray luminosity is correlated with the spectral shape below 1 keV in the sense that low-L_X systems have relatively large contributions from a soft component compared with high-L_X systems. We find evidence from our analysis of the 12 μm *IRAS* data for our sample that our S0 sample has excess 12 μm emission compared with the E sample, scaled by their optical luminosities. This may be due to emission from dust heated in star-forming regions in S0 disks. This interpretation is reinforced by the existence of a strong L_{12}-L_{100} correlation for our S0 sample that is not found for the E galaxies, and by an analysis of optical-IR colors. We find steep slopes for power-law relationships between radio luminosity and optical, X-ray, and far-IR (FIR) properties. This last point argues that the presence of an FIR-emitting interstellar medium (ISM) in early-type galaxies is coupled to their ability to generate nonthermal radio continuum, as previously argued by, e.g., Walsh et al. (1989). We also find that, for a given L_{100}, galaxies with larger L_X/L_B tend to be stronger nonthermal radio sources, as originally suggested by Kim & Fabbiano (1990). We note that, while L_B is most strongly correlated with L_6, the *total* radio luminosity, both L_X and L_X/L_B are more strongly correlated with L_{6cm}, the *core* radio luminosity. These points support the argument (proposed by Fabbiano, Gioia, & Trinchieri 1989) that radio cores in early-type galaxies are fueled by the hot ISM.

Subject headings: galaxies: elliptical and lenticular, cD — galaxies: general — galaxies: ISM — X-rays: galaxies

1. INTRODUCTION

The classic view of early-type (E and S0) galaxies, as put forth in the preface to the Hubble Atlas (Sandage 1961) is that of pure Population II stellar systems, with little or (ideally) no optical signatures of an interstellar medium (ISM). It was already clear by then that a significant fraction of luminous early-type galaxies do indeed possess some quantity of optical emission-line gas (Mayall 1939; Humason, Mayall, & Sandage 1956). Furthermore, as the angular resolution of radio telescopes improved throughout the 1950s and 1960s, it also became clear that many early-type galaxies are powerful radio continuum sources (e.g., Maltby & Moffet 1962). It was thus obvious that they contain relativistic electrons, moving under the influence of magnetic fields (e.g., Hoyle 1960). By the 1970s, a few early-type galaxies were also known to have some amount of H I gas, based on 21 cm line observations (e.g., Bottinelli & Gouguenheim 1977; Gallagher et al. 1977; White & Gardner 1977; Knapp, Gallagher, & Faber 1978; Fosbur al. 1978). However, all available evidence pointed toward v small mass fractions for the ISM in early-type galaxies.

That this was, in fact, a serious problem was pointed ou a landmark paper by Faber & Gallagher (1976). They no that the stellar populations of early-type galaxies are do nated by old stars, and that stars lose a significant amoun mass in the course of stellar evolution. Thus a typical ea type galaxy ($L_B \approx 10^{10}\ L_\odot$) *should* contain $\approx 10^9\ M_\odot$ of I if this material were not either converted into new stars (considered a major sink either then or now) or swept from system by some internal or external process.

For a number of years, theoretical work focused on the la possibility, the main mechanisms considered being ram-p sure stripping due to interactions of the early-type galaxies w the intracluster medium of their host clusters (Gunn & G 1972; Gisler 1976; Frank & Gisler 1976) and galactic wi generated by energy input from supernovae (Johnson & /

[1] Current address: Department of Physics and Astronomy, University of Alabama, Tuscaloosa, AL 35487.

A MULTIPARAMETRIC ANALYSIS OF THE *EINSTEIN* SAMPLE OF EARLY-TYPE GALAXIES. II. GALAXY FORMATION HISTORY AND PROPERTIES OF THE INTERSTELLAR MEDIUM

PAUL B. ESKRIDGE[1,2] AND GIUSEPPINA FABBIANO[3]
Harvard-Smithsonian Center for Astrophysics, 60 Garden Street, Cambridge, MA 02138

AND

DONG-WOO KIM[4]
Harvard-Smithsonian Center for Astrophysics; and Department of Astronomy and Space Science, Chungnam National University, Taejon, 305-764, South Korea

Received 1994 July 22; accepted 1994 October 12

ABSTRACT

We have conducted bivariate and multivariate statistical analysis of data measuring the integrated luminosity, shape, and potential depth of the *Einstein* sample of early-type galaxies (presented by Fabbiano et al. 1992). We find significant correlations between the X-ray properties and the axial ratios (a/b) of our sample, such that the roundest systems tend to have the highest L_X and L_X/L_B. The most radio-loud objects are also the roundest. We confirm the assertion of Bender et al. (1989) that galaxies with high L_X are boxy (have negative a_4). Both a/b and a_4 are correlated with L_B, but not with *IRAS* 12 μm and 100 μm luminosities. There are strong correlations between L_X, Mg_2, and σ_v in the sense that those systems with the deepest potential wells have the highest L_X and Mg_2. Thus the depth of the potential well appears to govern both the ability to retain an ISM at the present epoch and to retain the enriched ejecta of early star formation bursts. Both L_X/L_B and L_6 (the 6 cm radio luminosity) show threshold effects with σ_v, exhibiting sharp increases at $\log(\sigma_v) \approx 2.2$. Finally, there is clearly an interrelationship between the various stellar and structural parameters: The scatter in the bivariate relationships between the shape parameters (a/b and a_4) and the depth parameter (σ_v) is a function of abundance in the sense that, for a given a_4 or a/b, the systems with the highest σ_v also have the highest Mg_2. Furthermore, for a constant σ_v, disky galaxies tend to have higher Mg_2 than boxy ones. Alternatively, for a given abundance, boxy ellipticals tend to be more massive than disky ellipticals. One possibility is that early-type galaxies of a given mass, originating from mergers (boxy ellipticals), have *lower* abundances than "primordial" (disky) early-type galaxies. Another is that disky inner isophotes are due not to primordial dissipational collapse, but to either the self-gravitating inner disks of captured spirals or the dissipational collapse of new disk structures from the premerger ISM. The high measured nuclear Mg_2 values would thus be due to enrichment from secondary bursts of star formation triggered by the merging event.

Subject headings: galaxies: elliptical and lenticular, cD — galaxies: ISM — galaxies: structure — X-rays: galaxies

1. INTRODUCTION

The connection between the structural and stellar properties of galaxies and the nature of their interstellar medium (ISM) was first discussed by Spitzer (1954). The basic situation, as it was understood ~35 years ago, was laid out by Sandage (1961). Our ability to observe, and thus our understanding of, the ISM has increased enormously since then. Current observational techniques allow us to collect data on the solid phase of the ISM (dust grains), as well as gas phases ranging from cold molecular cloud cores ($T \sim 10$ K, $n \sim 10^6$ cm^{-3}) to X-ray–emitting gas ($T \sim 10^{6-7}$ K, $n \gtrsim 0.1$ cm^{-3}). Our understanding of the relationships between ISM properties and the structural and stellar properties of galaxies is thus undergoing a concomitant rapid development.

Early-type (E and S0) galaxies, once considered devoid of intestellar gas, are now known to possess rich and complex ISM. Although many early-type galaxies exhibit the ISM tracers more traditionally associated with late-type galaxies (e.g., Huchtmeier & Richter 1989 and Eder, Giovane Haynes 1991 for H I; Sage & Wrobel 1989 and Thronson 1989 for CO; Goudfrooij et al. 1994 for Hα; Knapp et al for FIR), X-ray observations, beginning with the *Ei Observatory* (Giacconi et al. 1979) have demonstrated th ISM in luminous early-type galaxies is typically dominat a hot ISM (see Fabbiano 1989 and references therein).

In the previous paper of this series (Eskridge, Fabbia Kim 1995, hereafter P1), we presented an analysis of the properties of the *Einstein* sample of early-type ga (Fabbiano, Kim, & Trinchieri 1992, hereafter P0). The results of P1 are as follows: In agreement with previous st (see Fabbiano 1989 and references therein), we find a s correlation between L_B and L_X, with a power-law slo 1.8 ± 0.1. However, this is actually a combination of a sl relation for the fainter galaxies [$\log(L_X) \leq 40.5$] and a sl relation for the more luminous galaxies. This result is c tent with previous work indicating that X-ray–faint early galaxies do not retain any significant quantities of hot (Trinchieri & Fabbiano 1985; Fabbiano, Gioia, & Trin 1989, hereafter FGT). In this case, their X-ray emission sl be dominated by the integrated output of discrete sc similar to those found in the bulge of M31 (van Speybro al. 1979). The X-ray emission from more distant spiral bul

[1] Current address: Department of Physics and Astronomy, University of Alabama, Tuscaloosa, AL 35487.
[2] paul@bera.astr.ua.edu.
[3] pepi@cfa.harvard.edu.
[4] kim@cfa.harvard.edu.

A MULTIPARAMETRIC ANALYSIS OF THE EINSTEIN SAMPLE OF EARLY-TYPE GALAXIES

III: COMPARISONS WITH THE κ-PARAMETERS

Paul B. Eskridge[1],

Harvard-Smithsonian Center for Astrophysics
60 Garden Street
Cambridge, MA 02138
and
Department of Physics and Astronomy[2]
University of Alabama
Tuscaloosa, AL 35487

Giuseppina Fabbiano[1],

Harvard-Smithsonian Center for Astrophysics

and Dong-Woo Kim[1]

Harvard-Smithsonian Center for Astrophysics
and
Department of Astronomy and Space Science
Chungnam National University
Taejon, 305-764, S. Korea

Accepted for publication in the 20 July 1995 issue of **The Astrophysical Journal**

1: Internet addresses:
paul@hera.astr.ua.edu
pepi@cfa.harvard.edu
kim@cfa.harvard.edu
2: Current address

Abstract

We have extended our bivariate and multivariate statistical analysis of the *Einstein* sample of early-type galaxies (Fabbiano *et al.*, 1992; Eskridge *et al.*, 1995a,b) to include a consideration of the κ parameters defined by Bender *et al.* (1992). The κ parameters are defined such that κ_1 scales with virial mass, κ_3 scales with inner M/L ratio, and κ_2 is perpendicular to both κ_1 and κ_3. The κ_1–κ_3 plane is essentially edge-on to the Bender *et al.* (1992) formulation of the fundamental plane, and the parameter $\delta\kappa_3$ describes the scatter about that plane. We find that L_B, L_X, and L_6 are all strongly correlated with κ_1. Partial Spearman rank analysis shows these trends to be independent of the correlations between the luminosities. There are also significant bivariate trends of both L_X and L_6 with κ_3. Partial Spearman rank analysis indicates that the L_X–κ_3 is the dominant one, thus arguing for a connection between the prominence of x-ray coronae and the inner M/L. This suggests that galaxies with central excesses of dark matter also have more massive extended dark matter halos, providing a mechanism for retaining larger amounts of hot ISM. We find evidence for a correlation between Mg_2 and $\delta\kappa_3$ that is independent of correlations of these two parameters with σ_v, and is enhanced when tested for constant a_4. The strengthening of the Mg_2–$\delta\kappa_3$ correlation when tested for constant a_4 indicates an underlying connection between the scatter about the fundamental plane, and the type II SN enrichment history of the central regions of elliptical galaxies that is independent of the details of the central structure of individual galaxies. This suggests that the Mg_2–$\delta\kappa_3$ trend is not related to the Mg_2 enhancements associated with kinematically decoupled cores seen in some disky elliptical galaxies (e.g., Bender & Surma 1992). It may be that systems with higher inner M/L_e (at a given mass) were more able to retain the metals generated in early epochs of star formation. Alternatively, systems experiencing more active or prolonged star formation may have produced an excess of baryonic dark matter from stellar remnants that is reflected in their higher M/L_e.

Subject Headings: galaxies: elliptical and lenticular, cD — galaxies: evolution — galaxies: general — galaxies: ISM — galaxies: structure – x-rays: galaxies

1. Introduction

The *Einstein* sample of early-type galaxies (Fabbiano *et al.*, 1992, hereafter P0) is the largest currently available sample of E and S0 galaxies observed in x-rays. There are *Einstein* observations of 148 normal or nearly normal early-type galaxies in the sample. We have been using this sample to explore the relationships of x-ray properties of E/S0 galaxies to other tracers of the ISM (Eskridge *et al.*, 1995a, hereafter P1) and to observables related to the structure and stellar populations of the sample (Eskridge *et al.*, 1995b,

Harvard-Smithsonian Center for Astrophysics

Preprint Series

No. 3947
(Received September 19, 1994)

ROSAT PSPC OBSERVATIONS OF THE EARLY TYPE GALAXIES NGC 507 AND NGC 499: CENTRAL COOLING AND MASS DETERMINATION

Dong-Woo Kim
Harvard-Smithsonian Center for Astrophysics
and
Chungnam National University, South Korea

and

G. Fabbiano
Harvard-Smithsonian Center for Astrophysics

To appear in
The Astrophysical Journal
March 1, 1995

HARVARD COLLEGE OBSERVATORY SMITHSONIAN ASTROPHYSICAL OBSERVATORY
60 Garden Street, Cambridge, Massachusetts 02138

ABSTRACT

We present the results of a deep observation of NGC 507 and NGC 499 with the ROSAT PSPC. The X-ray emission of NGC 507 is extended at least out to 1000 arcsec (458 kpc at a distance of 94.5 Mpc). The radial profile of X-ray surface brightness goes as $\Sigma_X \sim r^{-1.8}$ outside the core region. The radial profile is a function of energy such that the softer X-rays have a smaller core radius and a flatter slope. Spectral analysis reveals that the emission temperature, with an average of 1 keV, peaks at an intermediate radius of 2-3 arcmin and falls toward the center (possibly decreases outward as well). The absorption column density is consistent with the Galactic line-of-sight value. The X-ray emission of NGC 499 is extended to 300 arcsec and suggests a similarly cooler core. The cooler cores of NGC 507 and NGC 499 are strong evidence of the presence of cooling flows in these galaxies. Assuming hydrostatic equilibrium outside the cooling radius, the estimated mass to light ratio of NGC 507 is 97 $\pm$ 16 within 458 kpc, indicative of the presence of a heavy halo. Similarly the mass to light ratio of NGC 499 is 89 $\pm$ 14 within 137 kpc. Near the edge of the X-ray emitting region of NGC 507 we detect 19 soft, unresolved sources. These sources do not have optical counterparts and are significantly in excess of the expected number of background serendipitous sources. We speculate that they may represent cooling clumps in the halo of NGC 507. If there are many undetected cooling clumps distributed at large radii, then the radial profile of the X-ray surface brightness does not directly reflect the potential, adding uncertainty to the measurement of the binding mass; the gas mass could also be overestimated.

Harvard-Smithsonian Center for Astrophysics

Preprint Series

No. 4026
(Received January 26, 1995)

ROSAT PSPC OBSERVATIONS OF TWO DYNAMICALLY YOUNG ELLIPTICAL GALAXIES: NGC 4125 AND NGC 3610

G. Fabbiano
Harvard-Smithsonian Center for Astrophysics

and

François Schweizer
Department of Terrestrial Magnetism, Carnegie Institution of Washington

To appear in
The Astrophysical Journal
July 10, 1995

HARVARD COLLEGE OBSERVATORY SMITHSONIAN ASTROPHYSICAL OBSERVATORY
60 Garden Street, Cambridge, Massachusetts 02138

Abstract

We present the results of ROSAT PSPC X-ray observations of NGC 4125 and NGC 3610. These two galaxies are among the best representatives of a newly recognized class of elliptical galaxies that may be the product of recent mergers. NGC 4125 shows two plumes or disks crossing at right angles; NGC 3610 has the richest fine structure of all ellipticals catalogued by Schweizer and Seitzer. Our X-ray observations show that these galaxies do not retain large gaseous halos, contrary to the suggested link between merging and X-ray brightness. Their X-ray luminosities (0.1 –2 keV) are in the range $10^{40-41} ergs\ s^{-1}$, low compared with those of hot-gas-rich ellipticals. The X-ray to optical ratio of NGC 3610 is in the range of those of X-ray faint ellipticals, consistent with the value found for the bulge of M31, where the X-ray emission is dominated by low-mass binaries; its X-ray spectrum is also comparable with those of X-ray faint ellipticals, presenting significant very soft excess emission. The X-ray to optical ratio of NGC 4125 is larger, and might suggest the presence of some hot ISM. This suggestion is supported by the spectrum of NGC 4125, which shows evidence of Fe L emission. This spectrum can be fitted with either a low abundance single temperature Raymond model, or with a two-temperature model with solar abundances. Further work is needed to firmly resolve the question of gaseous versus stellar X-ray emission in NGC 4125.

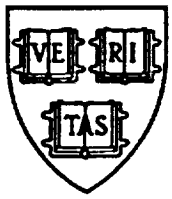

Harvard-Smithsonian Center for Astrophysics

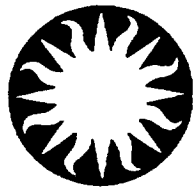

Preprint Series

No. 4298
(Received April 15, 1996)

ASCA SPECTRA OF THE X-RAY-FAINT S0 GALAXY NGC 4382

D.-W. Kim
Chungnam National University, South Korea
and
Harvard-Smithsonian Center for Astrophysics

G. Fabbiano
Harvard-Smithsonian Center for Astrophysics

H. Matsumoto and K. Koyama
Kyoto University, Japan

and

G. Trinchieri
Osservatorio Astrofisico di Brera, Italy
and
Harvard-Smithsonian Center for Astrophysics

To appear in
The Astrophysical Journal
September 1996

HARVARD COLLEGE OBSERVATORY SMITHSONIAN ASTROPHYSICAL OBSERVATORY
60 Garden Street, Cambridge, Massachusetts 02138

Center for Astrophysics
Preprint Series No. 4298

ASCA Spectra of the X-ray-faint S0 Galaxy NGC 4382

D.-W. Kim
Chungnam National University, Taejon 305-764, South Korea
and
Harvard-Smithsonian Center for Astrophysics

G. Fabbiano
Harvard-Smithsonian Center for Astrophysics
60 Garden St., Cambridge, MA 02138

H. Matsumoto and K. Koyama
Kyoto University, Kyoto 606-01, Japan

and G. Trinchieri
Osservatorio Astrofisico di Brera, Via Brera 28, Milano 20121, Italy
and
Harvard-Smithsonian Center for Astrophysics

April 8, 1996

Abstract

NGC 4382 is one of the E and S0 galaxies detected with the lowest X-ray to optical luminosity ratio. These galaxies have a peculiar X-ray (0.1-3 keV) spectrum, with a significant excess of counts in the lowest spectral channels (< 1 keV) relative to the spectral count distributions of X-ray brighter E and S0 galaxies. Analyzing the ROSAT PSPC observations of NGC 4382 (Fabbiano, Kim, and Trinchieri 1994), it was unclear whether this soft excess were due to a real very soft component in a multi-component spectrum, or reflected an extremely low metal abundance in a isothermal hot gas. Our ASCA observations show that the low-abundance single-temperature model does not fit well the X-ray spectrum, in agreement with our previous suggestions. A better explanation is a composite spectrum with a very soft component ($\sim$0.3 keV) in addition to a hard, likely stellar, component ($\sim$5 keV). In this model, the abundance cannot be constrained. However, other more complex spectral models cannot be excluded.

1. INTRODUCTION

The S0 galaxy NGC 4382 is in the Virgo cluster, but it differs from other Virgo early-type galaxies by being rather inconspicuous in X-rays. Its X-ray to optical flux ratio is among the lowest detected in E and S0's and is a factor of $\sim$100 smaller than those of X-ray bright Virgo and field galaxies of similar optical luminosity (Figure 1). Although its X-ray detection was first attributed to a hot ISM, and used to estimate a binding mass (Forman, Jones and Tucker 1985), it was soon realized that the X-ray emission may be dominated instead by a population of evolved stellar sources, similar to those present in the bulge of M31 (Trinchieri, Fabbiano and Canizares 1986; Canizares, Fabbiano and Trinchieri 1987). These sources have an X-ray spectrum typically harder than that of the hot ISM of X-ray bright E and S0s (Fabbiano, Trinchieri and Van Speybroeck 1987; Kim, Fabbiano and Trinchieri 1992a). Spectral observations could therefore establish the nature of the X-ray emission of NGC 4382 and of other similarly X-ray faint E and S0s.

The results of spectral analyses based on *Einstein* and ROSAT data present however a puzzling picture. Although NGC 4382 was too faint to warrant individual analysis of its *Einstein* IPC data, it belongs to the sample of E and S0s selected on the basis of their small X-ray to optical ratio, which have a peculiar soft excess in their average *Einstein* spectral count distribution (Kim, Fabbiano and Trinchieri 1992b). This spectrum is very different both from the $\sim$1 keV thermal spectrum of X-ray bright E and S0 galaxies, and from the harder spectrum expected from a collection of low-mass binaries. Subsequent ROSAT PSPC observations (Fabbiano, Kim and Trinchieri 1994) confirmed the *Einstein* results revealing a PSPC spectral count distribution in NGC 4382 significantly different from those of X-ray bright galaxies, with a relative excess of counts in the lower energy spectral channels.

However, the limited resolution and bandwidth of the PSPC do not allow us to distinguish between different sets of emission models. The PSPC data can be equally well fit with a very low metallicity plasma of kT$\sim$0.6 keV, a Bremsstrahlung emission of the same kT, or a two component model consisting of a solar abundance plasma with kT$\sim$0.2 keV plus a harder (>1 keV) component contributing similar amounts of the emission (Fabbiano, Kim and Trinchieri 1994). More complicated models however cannot be excluded (e.g., Pellegrini and Fabbiano 1994). Two or multi-component models are more appealing in terms of physical plausibility (Fabbiano, Kim and Trinchieri 1994), since they do not require assumptions about either a new population of X-ray sources or the presence of a metal-free (therefore primordial) plasma.

In order to establish the nature of the X-ray emission of this X-ray faint early type galaxy, we observed NGC 4382 with ASCA (Tanaka, Inoue, and Holt 1994). These higher spectral resolution data make the low-abundance single-temperature model very unlikely and confirm the existence of a complex emission spectrum,

including a very soft component.

In section 2, we describe the ASCA observations and data reduction (§2.1) and we present spectral analysis (§2.2) and results (§2.3). In section 3, we discuss the nature of the very soft component and the implications of our results

2. X-RAY OBSERVATIONS AND DATA ANALYSIS

2.1. Data Screening and Background Determination

NGC 4382 was observed on 1994 May 27-28 with ASCA using both SIS (Burke et al. 1991) and GIS (Ohashi et al. 1991). The observational log and basic parameters of the galaxy are given in Table 1. The data were screened using the screening package XSELECT/ASCASCREEN with the default selection criteria. This method excludes data affected by the South Atlantic Anomaly, Earth occultation, and regions of low geomagnetic rigidity. We also eliminated contamination by the bright Earth, removed hot and flickering pixels for the SIS data, and applied rise-time rejection to exclude particle events for the GIS data (Day et al. 1994). This screening was applied separately to data collected in each instrument mode, i.e., to 6 data sets (two GIS detectors; 1 and 2 CCD modes for two SIS detectors).

In Figure 2, images from the SIS1 2-CCD mode and GIS3 are shown; in Figure 3, the ROSAT PSPC image is shown for comparison. A strong source coincides with the optical position of NGC 4382. The ROSAT PSPC observation revealed several serendipitous sources within $\sim$15′ of NGC 4382 (Fabbiano, Kim and Trinchieri 1994). Sources are seen in the SIS and GIS images at 2.8′ NW, 7.0′ N, 13.7′ NW, and 15.9′ S (GIS only) from the center of NGC 4382. However, due to the poor point response function of the ASCA detectors, the corresponding source shapes are much broader and asymmetrical than in the PSPC. Furthermore, the surface brightness distribution appears different in the different detectors, because of the misalignment of the 4 telescopes associated with the detectors.

To generate spectra for further analysis, SIS data in 1 and 2 CCD modes were combined because the telescope pointings were the same for these two modes. This resulted in four data sets.

We used three different approaches for subtracting the field background contribution from the source counts: (1) we derived the background locally in a source free region in the same chip for the SIS data, and at a similar off-center distance for the GIS; (2) for the SIS 2 CCD observations only, we derived the background from the second – source free – chip; and (3) we used the 'deep blank sky data' (several PV phase observations combined) provided by the ASCA GOF. There are some disadvantages to all methods. In the first two methods, the background and source regions have different detector responses and the current available spectral package (XSPEC) ignores this difference. In the third method, although the source

and background regions are the same, the deep sky data do not correctly reflect temporal and spatial variations of the background of the observed field. Nevertheless the three estimates of the background produce consistent results in our spectral fitting analysis, and therefore these potential problems do not affect our results. In the following, we will report the results obtained with local background subtraction.

2.2 Spectral Analysis

The source spectrum was extracted from circles of radius 3′ and 5′ for the SIS and GIS data respectively. In both cases the circle was centered on the emission peak. These count extraction radii were determined by examining the radial profile of X-ray surface brightness in each detector. The extraction parameters are given in Table 2. We used XSPEC for the spectral analysis. For ASCA response files, the redistribution matrix (RMF) v0.6 for SIS and v3.1 for GIS were obtained from the ASCA GOF and the position-dependent effective area curve (ARF) for each detector was generated at the source position. We have also tried a new version v0.8 for SIS and v4.0 for GIS but no difference was found in our results. Prior to model fitting, we rebinned the data so that each spectral bin contains at least 20 counts.

In table 2, we also list counts and count rates for each detector. The counts rates are different for each detector, because of different detector responses. Spectral fitting done with the same source normalization (i.e., emission measure) are consistent with all the data except for that from GIS3. Counts in the GIS3 spectrum are larger than expected with its detector response, due most likely to incomplete detector calibration. An emission measure increase by a factor of 1.3 would be required to reproduce the GIS3 spectrum. However, this inconsistency does not affect the spectral fitting results because the SIS spectra mainly control the spectral fitting; therefore, we use the same emission measure for simultaneous fit of SIS and GIS spectra. We also fitted the SIS and GIS spectra separately. The results are similar except for the normalizations.

We tested the effect of using slightly different source radii (e.g., 4′ for SIS and/or GIS) on the spectral results, performing the same analysis. The results do not differ appreciably. We also repeated the analysis by explicitly including and excluding the source at 2.8′ NW from the center of NGC 4382. Again, we obtain consistent results.

2.3 Results

The results of the spectral analysis are summarized in Table 3 and Figures 4-6. A single temperature Raymond model (a revised version of Raymond and Smith 1977) with fixed solar abundance gives a very poor fit to the data. Not only is χ^2 too large, but also there is strong excess emission over the best fit model in the 0.5-1 keV energy range. This excess clearly indicates the presence of a secondary emission component. Allowing the metal abundance to vary freely, we obtained a somewhat

lower minimum χ^2. However, the reduction is not substantial, and moreover the excess in 0.5-1 keV still exists (see Figure 5). In this case the best fit abundance is almost zero, i.e., the model is close to pure Bremsstrahlung with no line emission.

Instead a two-component model, consisting of a low-temperature Raymond thermal model with solar abundance plus a higher temperature Bremsstrahlung model, fits the data well, without any significant residuals at any energies (see Figure 6). The significance of the secondary component determined by the F test is more than 99.9% . The best fit kT parameters are 0.3 keV for the soft thermal emission and ~6 keV for the Bremsstrahlung emission. The confidence ranges of the two temperatures are well determined (Table 3). In particular the temperature of the soft component is well constrained in a narrow range, 0.24-0.43 keV at 90% confidence for 3 interesting parameters (Avni 1976). The temperature of the hard component is constrained by the joint SIS-GIS fit to be between 3.6 and 10.4 keV. The acceptable ranges of the abundance and absorption column density are not well determined. If we use a Raymond model instead of a Bremsstrahlung model for the hard component, the result is almost the same, because emission lines are not significant at this high temperature in the detected energy range.

We has also used the ROSAT PSPC spectra taken from Fabbiano et al. (1994) and jointly fit the ASCA and PSPC spectra. The PSPC instrument has a larger effective area at the low energies, therefore the joint ASCA+PSPC fit can provide narrower constraints on the absorption column density and soft component. The results are listed in Table 3. While the best fit temperatures of the two components are almost the same, the absorption column density is lower and well constrained.

If we let the abundance vary, the best fit abundance is 2.5 times solar, although its error range is undetermined ($>$ 10% solar at 90% confidence).

In Table 4, we list fluxes and luminosities of each emission component and the total emission. These are absorption-corrected intrinsic quantities and determined with the spectral parameters of the joint ASCA+PSPC fit. The soft component contributes ~40% of the flux in the 0.1-2.0 keV range, consistent with the ROSAT results for the same spectral model, but it contributes only ~20% of the total emission in the 0.25-10 keV range. The total flux is 1.0×10^{-12} ergs cm^{-2}s^{-1} in the 0.25-10 keV range.

The best fit value of the absorption column density is 0.8×10^{20}. The allowed range at 90% confidence is $0.3 - 1.6 \times 10^{20}$ (Table 3). The line of sight value, 2.7×10^{20} (Table 1) is excluded at 99% confidence. This occurs only when we fit the PSPC and ASCA spectra simultaneously. There may be some relative calibration problem between the PSPC and ASCA. We have tried with different normalizations for the two data sets, but the discrepancy still remains. If the fact that N_H is lower than the galactic line of sight value is really significant, then a more complicated model is required, e.g., adding another soft component. By adding 0.1 keV component, the

allowed N_H range is $0.2 - 4 \times 10^{20}$.

For lower values of N_H, the additional component contributes negligibly to the total emission (i.e., the same as Table 3). For higher values N_H, the additional component increases to compensates for the larger absorption. This may suggest multi-temperature soft emission. However, this may be overinterpretation of the current data.

We considered the uncertainties in calibration and plasma emission codes to better understand the robustness of our results. The ASCA instruments are known to have some calibration problem. In particular, ASCA spectra of several galaxy clusters indicate large amount of excess absorption which is inconsistent with previous observations (L. David and A. Prestwich 1994, private communication; see also ASCANEWS communication of Dec. 11 1995). However, this calibration error will not remove the need for a very soft component, because our spectra have excess soft counts, not the deficit expected at the soft energies because of this calibration problem. Another known problem is that currently available plasma emission codes produce too much emission at the Fe-L 4 to 2 transitions at $\sim$1.5 keV (N. Brickhouse 1994, private communication; Fabian et al. 1994). Again this $\sim$1.5 keV line emission will not significantly affect the existence of very soft component. Even in a extreme case where all the emission lines are uncertain, the spectral fit with a single component model with almost zero abundance (therefore no lines) is still not acceptable.

3. DISCUSSION

Our ASCA observations of NGC 4382 help us constrain models of the X-ray emission of this galaxy, and by inference of low-X-ray luminosity early-type galaxies. The results of the spectral fit exclude a single-temperature low-metallicity model, and point to a multi-component emission, consisting of at least two components: a hard component (kT$\sim$4–13 keV), and a very soft component (kT$\sim$0.2–0.4 keV). The two components contribute to the flux in similar amounts in the 0.1-2 keV band, consistent with the ROSAT results (Fabbiano, Kim and Trinchieri 1994), but in a wider energy band (0.25-10 keV), the soft component amounts to only 1/4 of the total emission. An even softer component ($\lesssim$ 0.1 keV) may be present, but the present data and SIS soft-band calibration make this possibility rather uncertain.

The existence of a hard component in the emission of E and S0 galaxies, due to the integrated emission of low mass X-ray binaries, had been postulated early on (Trinchieri and Fabbiano 1985). This component was suggested by comparisons of the $L_X - L_B$ dependence of E and S0s with that of Spirals (Trinchieri and Fabbiano 1985; Canizares, Fabbiano and Trinchieri 1987; Fabbiano, Gioia and Trinchieri 1989; Eskridge, Fabbiano and Kim 1995), and was first glimpsed in the co-added *Einstein* IPC spectra of X-ray faint E and S0s (Kim, Fabbiano and Trinchieri 1992a and b). This component has now been detected with ASCA in virtually all early-type galaxies

(Matsushita et al. 1994), and its luminosity scales approximately linearly with the optical luminosity (T. Ohashi 1994, private communication), pointing to a stellar origin, as seen in spiral galaxies (Fabbiano and Trinchieri 1985; Fabbiano, Gioia and Trinchieri 1988). The X-ray to optical ratio of this component is consistent with that of spiral galaxies and in particular with bulge-dominated spirals, where the X-ray emission is likely to be dominated by a population of low-mass binaries (e.g., M31, Trinchieri and Fabbiano 1991).

The existence of a very soft emission spectrum in X-ray faint E and S0 galaxies was first seen with the *Einstein* IPC (Kim et al. 1992b), and later confirmed with the ROSAT PSPC (Fabbiano et al. 1994; Fabbiano and Schweizer 1995). ASCA confirms that this emission is truly due to a very soft emission component in a multi-component spectrum. The very soft component, characterized by $\sim$0.3 keV thermal emission, emits 2×10^{40} erg sec^{-1} in 0.25-10 keV (see Table 4).

Kim et al. (1992), Fabbiano et al. (1994) and Pellegrini and Fabbiano (1994) considered possible candidates for the very soft component. It is possible that X-ray faint E and S0 do not retain a hot ISM. In this case, candidates include stellar sources, such as M star coronae (Schmitt et al. 1990), RS CVn (Dempsey et al. 1993), and supersoft sources such as those discovered with ROSAT in nearby galaxies (e.g., Greiner, Hasinger and Kahabka 1991; Kahabka, Pietsch and Hasinger 1994). If the very soft component is totally or in part related with stellar sources, it should exist in all early type galaxies, although its contribution may be relatively small in X-ray bright early type galaxies where strong hot gaseous emission ($\sim$1 keV) dominates. However, hydrodynamic simulations (Pellegrini and Fabbiano 1994) suggest that the X-ray emission of X-ray faint E and S0 galaxies may be more complex than the simple two-temperature model we have here fitted to the data. X-ray faint early type galaxies may contain a hot ISM which is cooler than that present in X-ray bright E and S0s, depending on the potential and SNIa rate of the galaxy. In particular, Pellegrini and Fabbiano (1994) showed that the ROSAT PSPC spectrum of the X-ray faint E galaxy NGC 4365 could be modeled with a three component model including very soft and hard stellar components, plus a hot ISM component. These data were well fitted with a two-component thermal model, as is it the case for our ASCA data of NGC 4382. It may be interesting to do similar model comparisons for NGC 4382, but this is beyond the scope of the present paper. The spherically symmetric Pellegrini and Fabbiano (1994) models cannot be immediately adapted to an S0 galaxy.

4. CONCLUSIONS

We observed NGC 4382, one of X-ray faint early type galaxies, with ASCA SIS and GIS for $\sim$35 ksec. The X-ray flux is 1.0×10^{-12} erg sec^{-1} cm^{-2} in 0.25 - 10 keV, consistent with the previous ROSAT PSPC observations. The ASCA data allow us to reject a low-abundance single-temperature model for this galaxy. The data is well fitted with a two-component model consisting of a very soft component ($\sim$0.3

keV) in addition to a hard stellar component (~6 keV), possibly due to the low-mass X-ray binary population of this galaxy (e.g., see bulge of M31). The acceptable range of temperature (90% confidence) is 0.2-0.4 keV and 4-13 keV for the soft and hard components, respectively. The relative flux of the very soft component is about 1/2 of total X-ray emission in 0.1-2 keV range and 1/4 in 0.25-10 keV range. The data could also be fitted with more complex models. These data, while excluding a single thermal component low-abundance model, and requiring multi-component models, cannot be used to determine the metal abundance of the soft optically thin emission. Solar values cannot be excluded.

We propose to follow up this work with careful re-analysis of the ASCA data of E and S0 galaxies, once these become accessible in the public domain. AXAF data will be able to disentangle the spectral properties of these galaxies from spatial variations in the ISM and therefore give us a more realistic picture.

ACKNOWLEDGMENTS

We thank Martin Elvis for a critical reading of the manuscript, and Glen Mackie and Takaya Ohashi for useful discussions. This work was supported by NASA grant NAG5-2946 (ASCA), NAGW 2681 (LTSA), NASA contract NAS8-39073 (AXAF Science Center) and KOSEF international program. This research has made use of SIMBAD which is operated by the Centre de Donnees astronomiques de Strasbourg (CDS), France.

REFERENCES

Avni, Y. 1976, ApJ, 210, 642

Burke, B. E., Mountain, R. W., Harrison, D. C., Bautz, M. W., Doty, J. P., Ticker, G. R., & Daniels, P. J. 1991, IEEE Trans. ED-38, 1069

Canizares, C. R., Fabbiano, G. & Trinchieri, G. 1987, ApJ, 312, 503

Day, C., Arnaud, K., Ebisawa, K., Gotthelf, E., Ingham, J., Mukai, K., & White, N. 1994, "The ABC Guide to ASCA Data Reduction" NASA GSFC ASCA GOF

de Vaucouleurs, G., de Vaucouleurs, A., Corwin, H. G., Buta, R. J., Paturel, G., & Fouque, P. 1991, *Third Reference Catalogue of Bright Galaxies* (Spring-Verlag: New York)

Dempsey, R. C., Linsky, J. L., Schmitt, J. H. M. M., & Fleming, T. A. 1993, ApJ, 413, 333

Eskridge, P. B., Fabbiano, G., & Kim, D.-W. 1995, ApJS, 97, 141

Fabbiano, G., & Trinchieri, G. 1985, ApJ, 296, 430

Fabbiano, G., & Schweizer, F. 1995, ApJ, in press

Fabbiano, G., Gioia, I. M., & Trinchieri, G. 1989, ApJ, 347, 127

Fabbiano, G., Kim, D.-W. & Trinchieri, G. 1994, ApJ, 429, 94

Fabbiano, G., Trinchieri, G., & Van Speybroeck, L. 1987, ApJ, 316, 127

Fabian, A. C., Arnaud, K. A., Bautz, M. W., & Tawara, Y. 1994, ApJ, 436, L63

Forman, W., Jones, C., & Tucker, W. 1985, ApJ, 293, 102

Greiner, J., Hasinger, G., & Kahabka, P. 1991, AA, 246, L17

Kahabka, P., Pietsch, W., & Hasinger, G. 1994, AA, 288, 538

Kim, D.-W., Fabbiano, G., & Trinchieri, G. 1992a, ApJS, 80, 645

Kim, D.-W., Fabbiano, G., & Trinchieri, G. 1992b, ApJ, 393, 134

Matsushita, K., Makishima, K., Awaki, H., Canizares, C. R., Fabian, A. C., Fukazawa, Y., Loewinstein, M., Matsumoto, H. Mihara, T., Mushotzky, R. F., Ohashi, T., Ricker, G. R., Serlemitsos, P. J., Tsuru, T., Tsusaka, Y., & Yamazaki, T 1994, ApJ, 436, L41

Ohashi, T., Makishima, K., Ishida, M., Tsuru, T., Tashiro, M., Mihara, T., Kohmura, Y., & Inoue, H. 1991, Proc SPIE 1549, 9

Pellegrini, S. & Fabbiano, G. 1994, ApJ, 429, 105

Raymond, J. C., & Smith, B. W. 1977, ApJS, 35, 419

Schmitt, J., Collura, A., Sciortino, S., Vaiana, G., Harnden, F. R., & Rosner, R. 1990, ApJ, 365, 704

Stark, A. A., Gammie, C. F,. Wilson, R. W., Bally, J., Linke, R. A., Heiles, C., & Hurwitz, M. 1992, ApJS, 79, 77

Tanaka, Y., Inoue, H., & Holt, S. S. 1994, PASJ, 46, L37

Trinchieri, G., & Fabbiano, G., 1985, ApJ, 296, 447

Trinchieri, G., & Fabbiano, G., 1991, ApJ, 382, 82

Trinchieri, G., Fabbiano, G., & Canizares, C. R. 1986, ApJ, 310, 637

Table 1
Basic parameters

RA (J2000)[a]	12 25 24.7
DEC (J2000)[a]	18 11 27
B_T^o (mag)[a]	9.99
D (Mpc)[b]	27.0
D_{25} (arcsec)[a]	425
N_H (cm^{-2})[c]	2.7×10^{20}
ASCA Observed Date	May 27-28, 1994
ASCA Net Good Time (sec)	32000-35000[d]
Log Fx (IPC) erg sec^{-1} cm^{-2} [e]	$6.0 \times 10^{-13} \pm 0.5$
Log Fx (PSPC) erg sec^{-1} cm^{-2} [f]	$7.3 \times 10^{-13} \pm 0.5$

a. Right Ascension (RA), declination (DEC), total face-on B magnitude (B_T^o), and major isophotal diameter measured at B = 25 magnitude $arcsec^{-2}$(D_{25}) taken from de Vaucouleurs et al. 1991 (RC3)

b. Distance from Fabbiano et al. 1992.

c. Galactic line of sight H column density from Starks et al. 1992.

d. The net good times are 32.9ks for SIS0, 32.2ks for SIS1, and 35.0ks for GIS2 and GIS3.

e. IPC flux from Fabbiano et al. 1992. Fluxes were estimated in a energy range of 0.2–4.0 keV and kT=1keV was assumed. The count extraction radus is r=240″ and the error is a statistical one.

f. PSPC flux from Fabbiano et al. 1994. Fluxes were estimated in a energy range of 0.1–2.0 keV and a two-component model was used. The count extraction radius is r=220″ and the error is a statistical one.

Table 2
Counts

	X Y (det)[a]	r (″)	Exposure (sec)	Counts	bkgd	net	rate (cts/ks)
SIS0	113 111	180	32903.26	1178	405	773	23.49 ± 1.18
SIS1	111 118	180	32158.98	967	436	531	16.51 ± 1.13
GIS2	106 115	300	34983.24	876	421	455	13.01 ± 0.93
GIS3	109 113	300	34927.24	1073	420	653	18.70 ± 1.02

a. unbinned detector coordinates for GIS and binned (by factor of 4) detector coordinates for SIS.

Background region (in detector coordinates):
SIS0 BOX(102.50,68.50,79.00,21.00)+BOX(71,104,79.00,22.00,90.000)
SIS1 BOX(102.50,68.50,79.00,21.00)+BOX(71,104,79.00,22.00,90.000)
GIS2 CIRCLE(160,139,30)
GIS3 CIRCLE(157,140,30)

Table 3
Spectral Fit

1 Temperature (with solar abundance[a])				
	N_H (10^{20} cm^{-2})	kT (keV)	χ^2	degrees of freedom
SIS	0	5.1	197	79
GIS	0	4.2	113	88
SIS+GIS	0	4.7	310	170
SIS+GIS+PSPC	0.26	4.6	356	192

1 Temperature (with varying abundance)					
	N_H (10^{20} cm^{-2})	kT (keV)	Z (solar)	χ^2	degrees of freedom
SIS	0	2.5	0	161	78
GIS	0	4.4	0.03	107	87
SIS+GIS	0	3.3	0	274	169
SIS+GIS+PSPC	0.73	3.1	0	311	191

Ray + Brem (with solar abundance[a])					
	N_H[b] (10^{20} cm^{-2})	kT_1[b] (keV)	kT_2[b] (keV)	χ^2	degrees of freedom
SIS	6.7 (< 27.2)	0.30 (0.23-0.42)	4.9 (2.6-13.2)	88	77
GIS	11 (< 123)	0.30 (0.11-0.82)	6.1 (2.5-16.5)	87	86
SIS+GIS	6.9 (< 25.8)	0.31 (0.24-0.43)	5.6 (3.6-10.4)	179	168
SIS+GIS+PSPC[c]	0.80 (0.26-1.61)	0.33 (0.27-0.41)	6.4 (4.3-12.8)	196	190

a. The solar abundance is from Anders and Grevesse (1989), i.e., $[Fe]/[H] = 4.68 \times 10^{-5}$.

b. The acceptable range is in 90% confidence for 3 interesting parameters.

c. Varying the abundance, we obtain the best fit Z=2.45 (> 10%) solar at 90% confidence.

Table 4
Flux and Luminosity[a]

	soft component	hard component	total emission
F_X(0.1-2 keV)	2.5 ± 0.5	3.8 ± 0.7	6.3 ± 1.3
F_X(0.2-4keV)	2.2 ± 0.5	5.5 ± 1.1	7.8 ± 1.6
F_X(0.25-10keV)	2.2 ± 0.5	8.0 ± 1.5	10.1 ± 2.0
L_X(0.1-2keV)	2.1 ± 0.5	3.3 ± 0.6	5.5 ± 1.1
L_X(0.2-4keV)	2.0 ± 0.4	4.8 ± 0.9	6.8 ± 1.4
L_X(0.25-10keV)	1.9 ± 0.4	7.0 ± 1.3	8.8 ± 1.8

a. The flux is in unit of 10^{-13} erg sec^{-1} cm^{-2} and luminosity is in unit of 10^{40} erg sec^{-1}. The flux and luminosity are absorption-corrected intrinsic quantities. Distance = 27 Mpc. The error (1 σ) is calculated by estimating the acceptable range of normalization. The statistical error is negligible.

FIGURE CAPTIONS

Figure 1: The $L_X - L_B$ diagram of E and S0 galaxies. All data are from Fabbiano, Kim and Trinchieri (1992). The diagonal lines delimit the four spectral Groups (1-4) of Kim, Fabbiano and Trinchieri (1992b). Groups 4 and 3 galaxies have $\sim$1 keV average spectra in *Einstein*. Group 2 have hard spectra ($>$ 2 keV), and Group 1 have a spectrum that can be fitted with a mixture of a hard and a very soft ($\sim$0.2 keV) component. The locus of spiral galaxies and spiral bulges (dominated by discrete binary sources) in this plot corresponds with the Group 1 and 2 regions. The circle and triangle indicate detections and upper limits.

Figure 2: ASCA X-ray images. The images were taken (a) in a SIS1 2-ccd mode and (b) with GIS3. Both images were smoothed with a Gaussian of $\sigma = 30''$.

Figure 3: ROSAT PSPC image of NGC 4382. The ellipse indicates the optical galaxy at 25 B magnitude isophote. The image was smoothed with a Gaussian of $\sigma = 30''$.

Figure 4: Joint fit of 2 SIS and 2 GIS spectra. (a) SIS0; (b) SIS1; (c) GIS2; and (d) GIS3. The solid histogram indicates the best-fit one component Raymond thermal model with a fixed solar abundance. The bottom panel shows $\delta\chi$ = (observed - predicted) / (observed error).

Figure 5: Same as Figure 3 except for varying the abundance.

Figure 6: Same as Figure 3 except for a two component model.

Figure 7: χ^2 contour plots for (a) kT_1 and kT_2, (b) kT_1 and N_H, and (c) kT_2 and N_H. The 3 contours are 68%, 90% and 99% confidence levels with 3 interesting parameters.

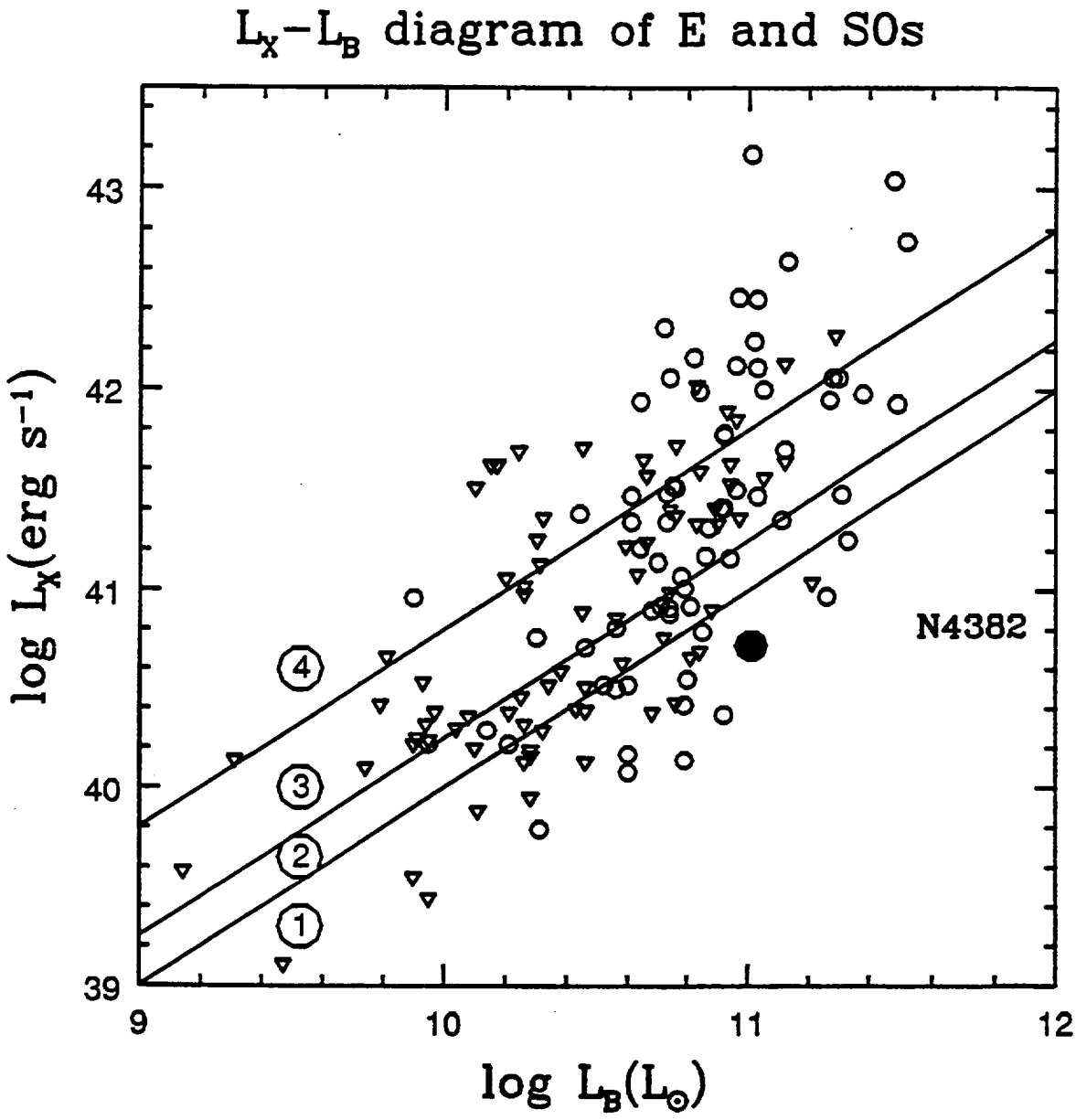
L_X–L_B diagram of E and S0s
43
42
41
40
39
9
10
11
12
log L_X(erg s^{-1})
log $L_B(L_\odot)$
N4382
4
3
2
1

FIG. 1

NGC 4382 PSPC

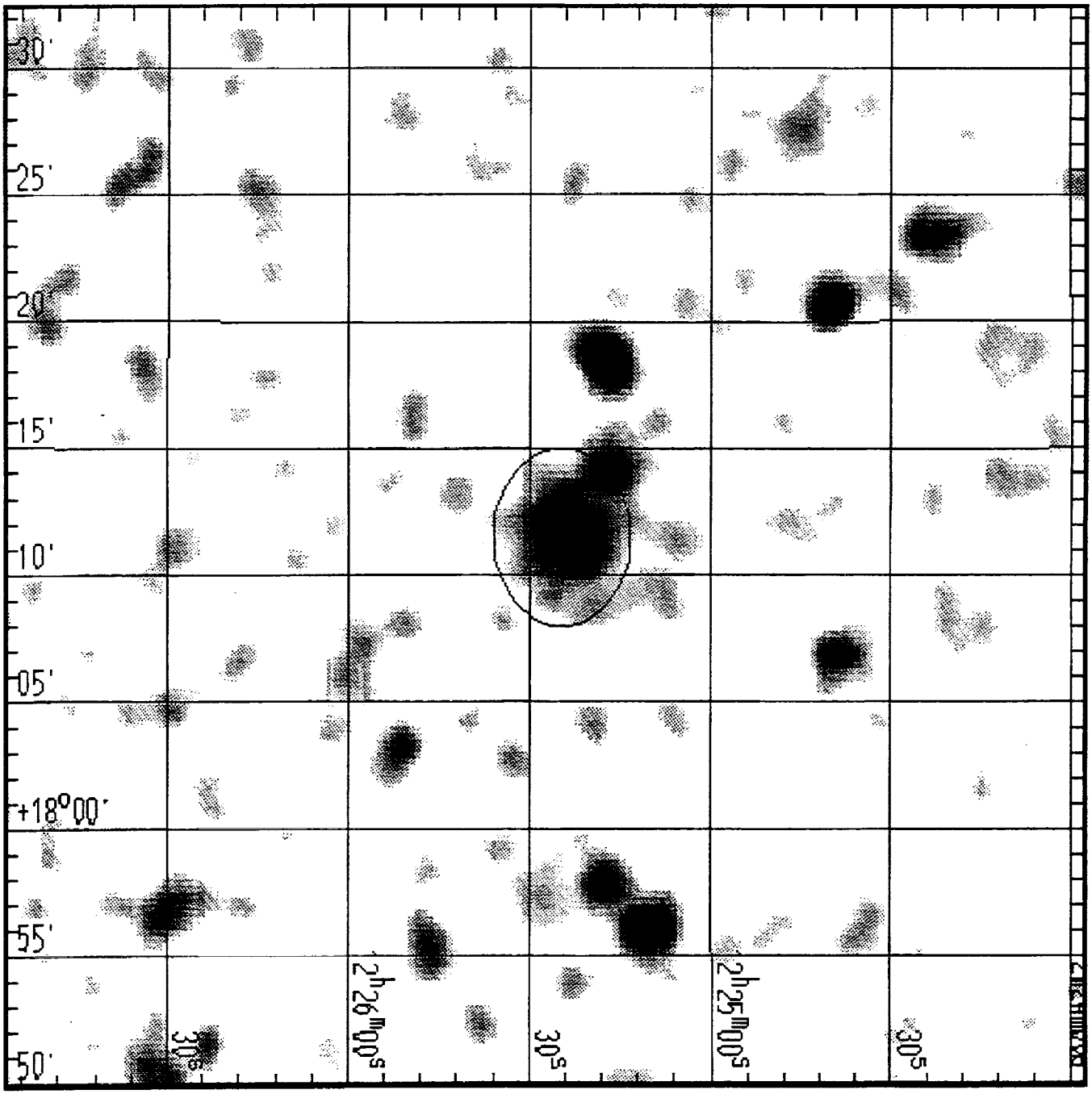

FIG. 3

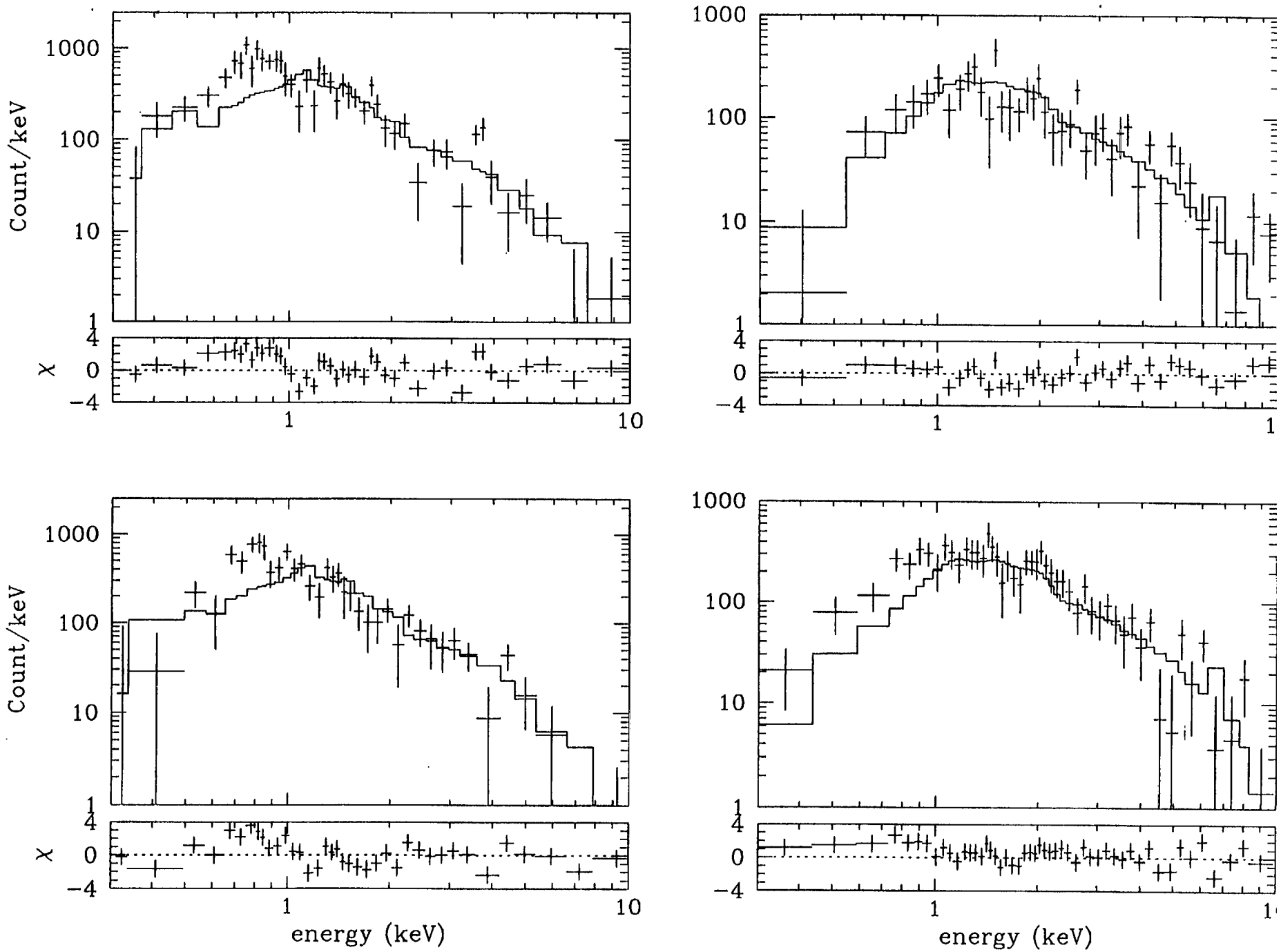

FIG. 4

NGC 4382 SIS1

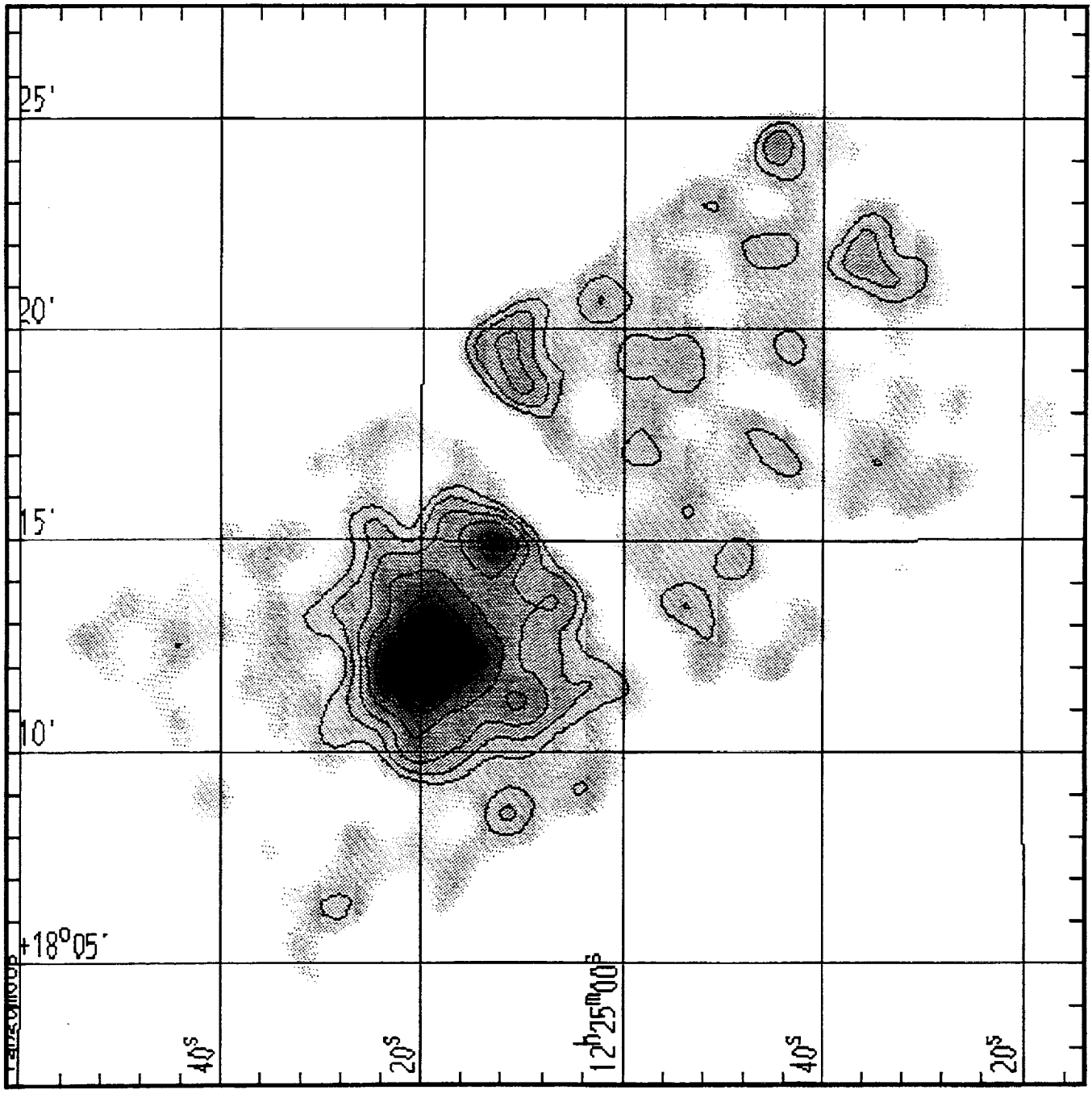

FIG. 2a

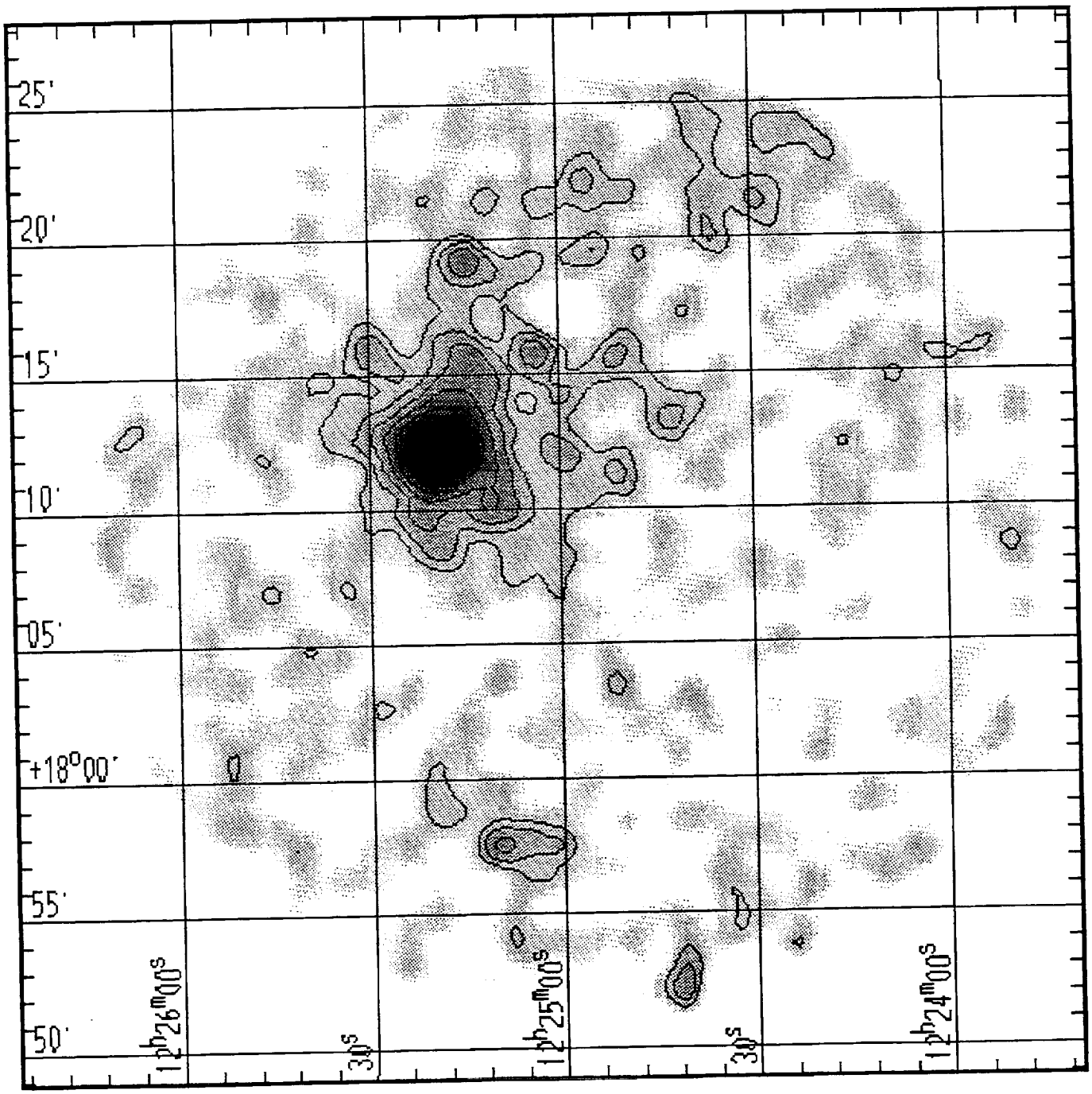
NGC 4382 GIS3
25'
20'
15'
10'
05'
+18°00'
55'
50'
12h26m00s
30s
12h25m00s
30s
12h24m00s

FIG. 2b

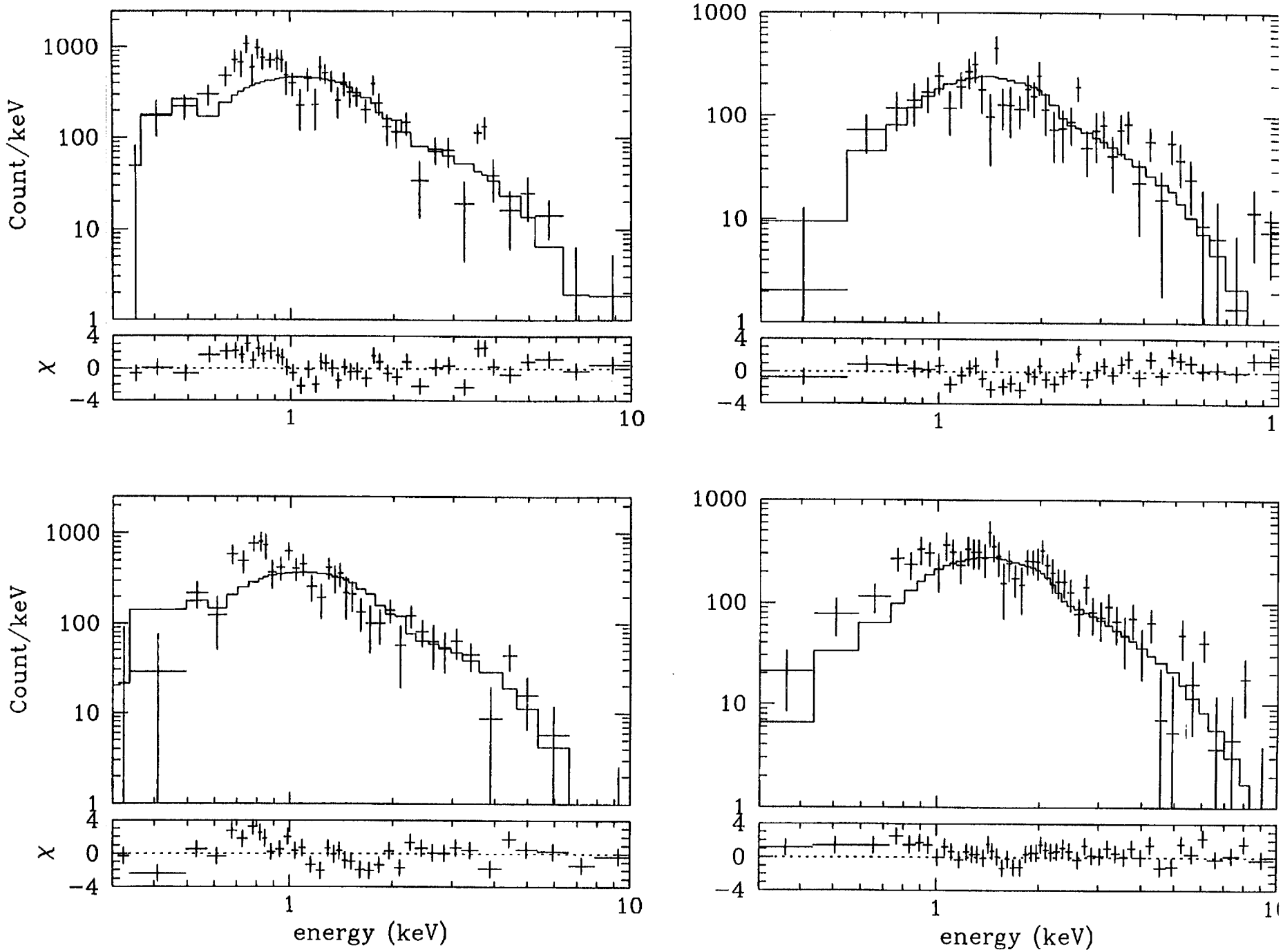

FIG. 5

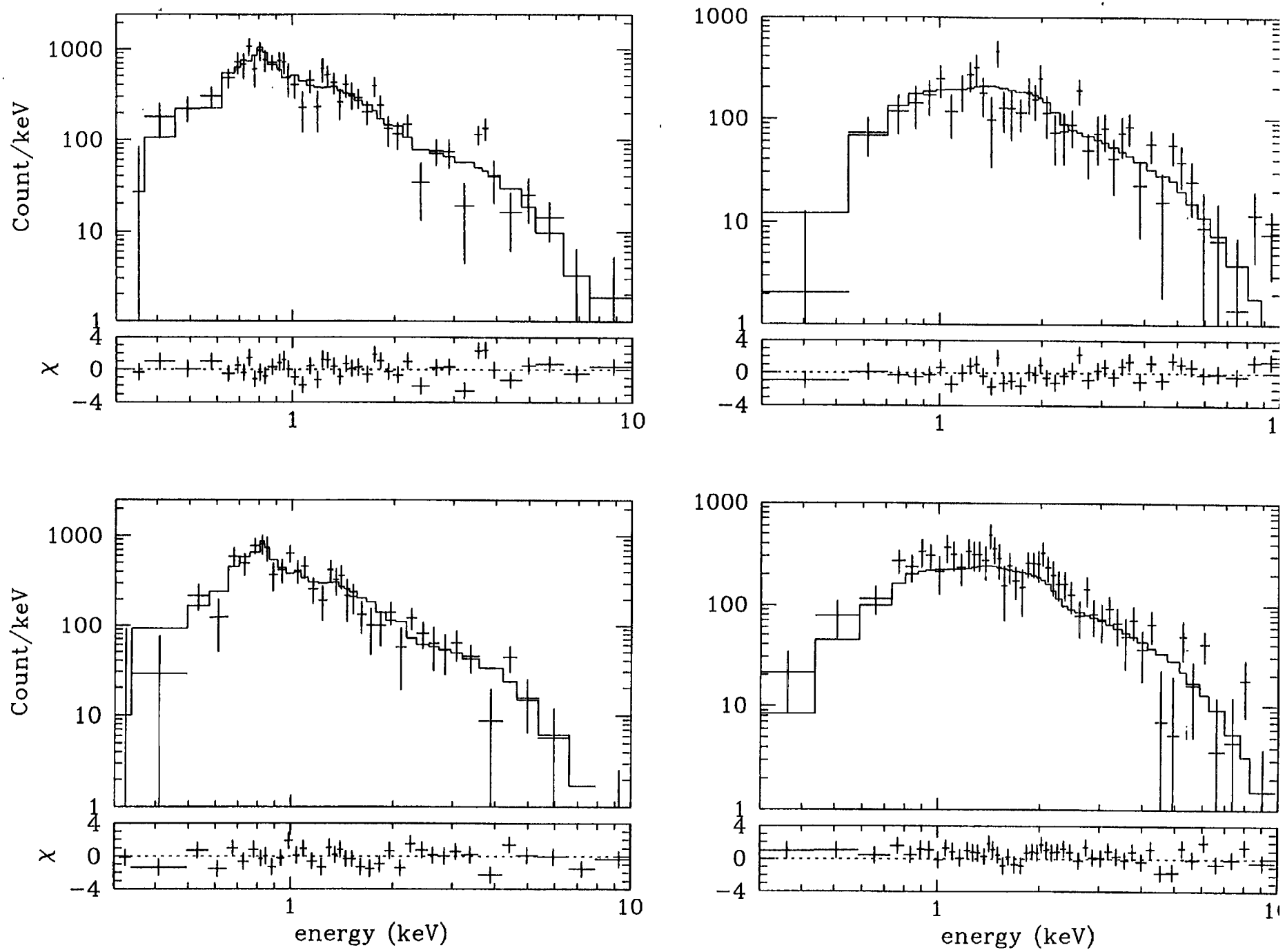

FIG. 6

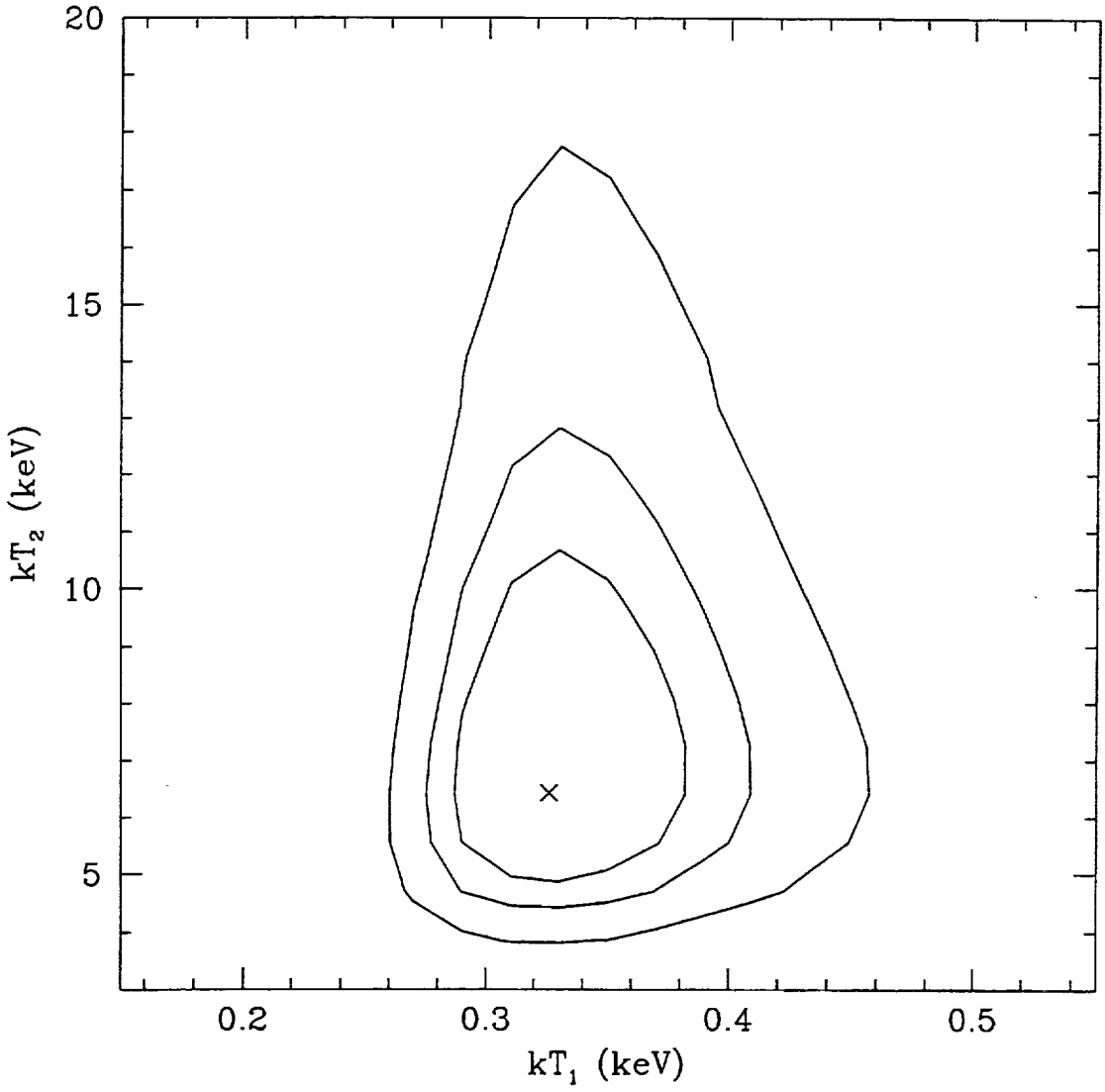

FIG. 7a

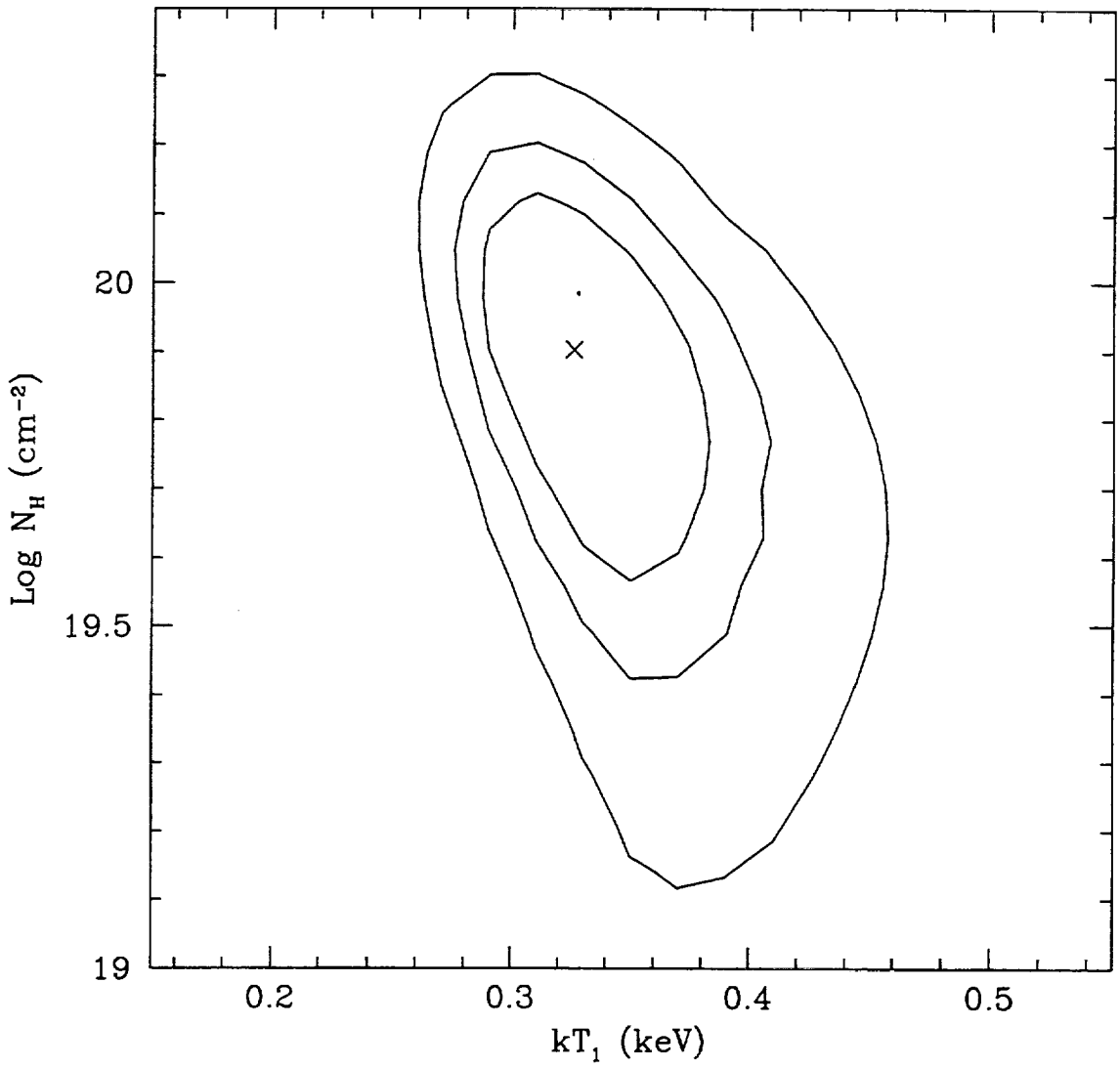

FIG. 7b

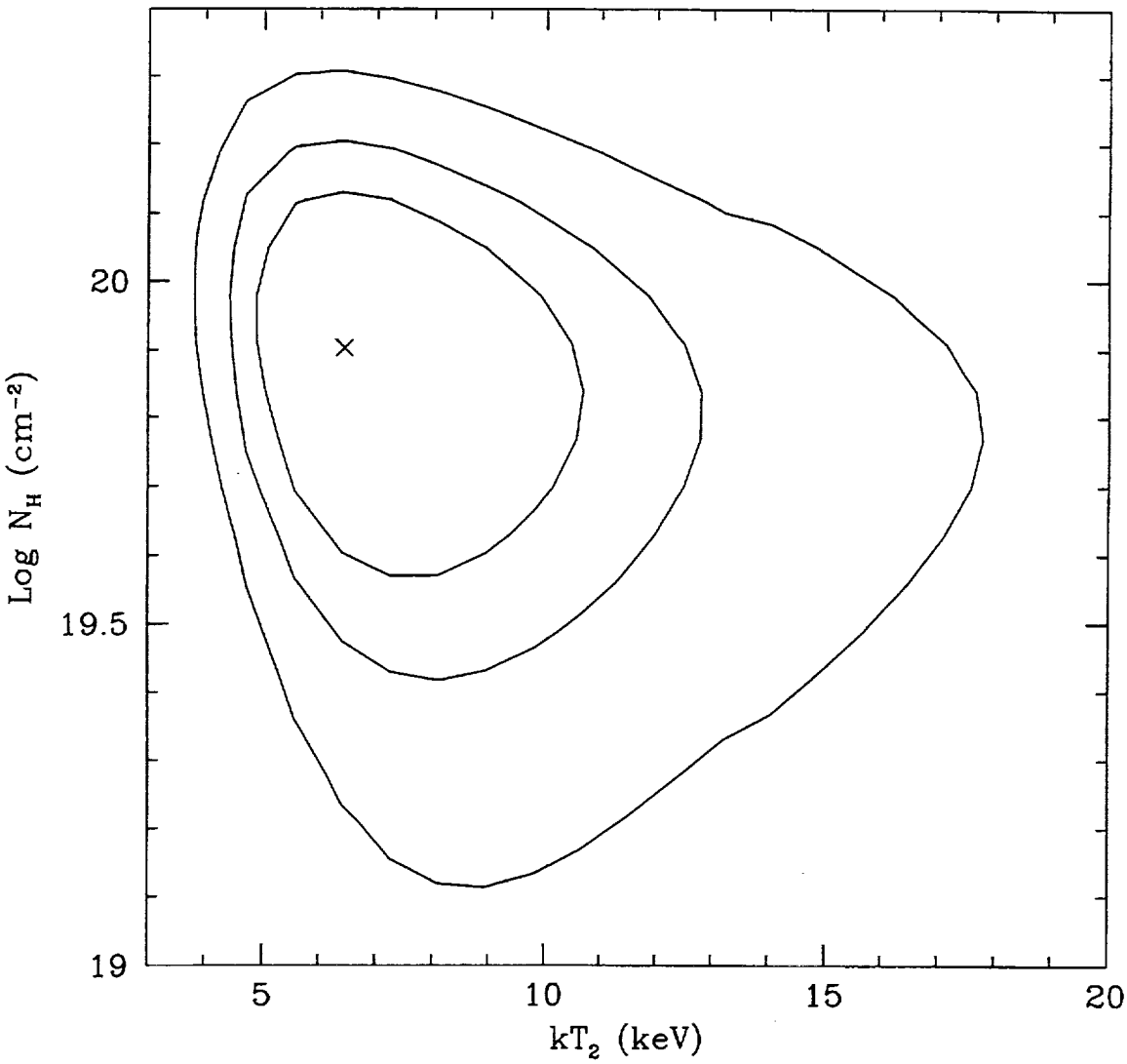

FIG. 7c

THE ASTROPHYSICAL JOURNAL, 428:555–573, 1994 June 20

ROSAT PSPC OBSERVATIONS OF NGC 4636: INTERACTION WITH VIRGO GAS?

G. TRINCHIERI
Osservatorio Astrofisico di Arcetri[1] and Harvard-Smithsonian Center for Astrophysics[2]
D.-W. KIM
Chungnam National University,[3] and Harvard-Smithsonian Center for Astrophysics[2]
G. FABBIANO
Harvard-Smithsonian Center for Astrophysics[2]
AND
C. R. C. CANIZARES
MIT[4]
Received 1993 August 30; accepted 1993 December 17

ABSTRACT

ROSAT PSPC observations of NGC 4636 have provided a deep image of the galaxy and its surroundings, which reveal the presence of emission well outside the optical galaxy. The source emission is measured out to $r \sim 18'$, where the instrument support structure prevents us at this time from following it farther out. The nature of this emission is not fully understood, but could be evidence that the Virgo cluster gas extends as far out as this galaxy (>3 Mpc from M87).

Spectral analysis of the X-ray emission suggests a relatively cool ($kT \sim 0.5$–0.9 keV) interstellar medium, with temperatures increasing with radius. However, the detailed properties of the interstellar gas cannot be unambiguously determined with the present data, since the results we obtain depend strongly on the choice of the spectral model. Comparison of the spectral distributions in concentric annuli clearly indicates significant differences with radius, which can be parameterized as a general increase of the temperature. For low cosmic abundance models, kT varies from ~ 0.55 keV in the inner $1'$ to ~ 0.8 keV at $r \sim 6'$–$8'$. Outside $8'$ the average temperature is higher than in the inner region ($kT \sim 0.8$–1.2 keV) and the low-energy absorption is significantly lower. For 100% cosmic abundance and galactic line-of-sight absorption, multi-temperature fits are required, suggesting the possibility that the interstellar medium is inhomogeneous.

Subject headings: galaxies: clusters: individual (Virgo) — galaxies: individual (NGC 4636) — galaxies: ISM — X-rays: galaxies

1. INTRODUCTION

Early *Einstein* observations of normal galaxies in the Virgo cluster have suggested that the emission of the brightest ellipticals could be attributed to the presence of hot gas radiating at $kT \sim 1$ keV (Forman et al. 1979; Trinchieri, Fabbiano, & Canizares hereafter TFC). Both the high X-ray luminosities and the soft spectra observed in the X-ray bright early-type galaxies have indicated the presence of an interstellar medium in these objects, previously thought to be devoid of gas (see Fabbiano 1989 and references therein).

This discovery has provided a potentially powerful tool for estimating galaxy masses (M) out to radii well outside the central regions, to which optical spectroscopic data have generally been restricted, and has led to the suggestion that large amounts of dark matter are a common feature of early-type systems (Forman, Jones, & Tucker 1985; Fabian et al. 1986). However, the combined spatial and spectral resolution of the *Einstein* X-ray data was not sufficient to yield an unequivocal determination of the masses in early-type galaxies (see TFC). In principle X-ray data could determine the temperature at each radius, and in particular at large radii where mass measurements are more interesting. Instead, only a gas temperature averaged over the entire source could be derived with the *Einstein* data, and even this mean depended on the assumption of a given (solar) metal abundance. Only estimates of radial temperature distributions have been attempted in a few cases (see Forman et al. 1985). Improved measurements are important. For example, a radially increasing temperature could indicate the presence of an external pressure and consequently relax the need for dark matter to confine the hot interstellar medium (e.g., Cowie & Binney 1977; Vedder, Trester, & Canizares 1988; Bertin, Pignatelli, & Saglia 1993).

Moreover the determination of the radial extent of the gas and to a lesser degree of the density gradient at large radii are also uncertain. In particular, in the observations of NGC 4636, emission observed at galactocentric radii of $\sim 6'$–$7'$ could have been due to an instrumental feature, and thus could not be unambiguously attributed to the source. In other cases, contamination from the emission of unconnected sources in the field could not be discarded. These uncertainties reflect directly in the evaluation of M.

To address this issue, deep observations of some of the more luminous galaxies have been obtained with the PSPC (Position Sensitive Proportional Counter) aboard the *ROSAT* satellite (Truemper 1983; Pfeffermann et al. 1987). The *ROSAT* band (~0.1–2 keV) is softer than the *Einstein* band (~0.2–3.5 keV)

[1] Currently at the Osservatorio Astronomico di Brera Via Brera 28, 20121 Milano, Italy.
[2] 60 Garden St., Cambridge, MA 02138.

THE ASTROPHYSICAL JOURNAL, 429:94–104, 1994 July 1

ROSAT PSPC OBSERVATIONS OF TWO X-RAY–FAINT EARLY-TYPE GALAXIES: NGC 4365 AND NGC 4382

G. FABBIANO
Harvard-Smithsonian Center for Astrophysics, 60 Garden Street, Cambridge, MA 02138

D.-W. KIM
Chungnam National University, Daejeon 305-764, South Korea, and Harvard-Smithsonian Center for Astrophysics

AND

G. TRINCHIERI
Osservatorio Astrofisico di Brera, Via Brera 28, Milano 20121, Italy, and Harvard-Smithsonian Center for Astrophysics

Received 1993 September 3; accepted 1993 December 23

ABSTRACT

We present the results of *ROSAT* PSPC observations of the two early-type galaxies NGC 4365 and NGC 4382. These galaxies are among those observed with *Einstein* to have the lowest X-ray to optical flux ratios of early-type galaxies. The PSPC data show that for radii $r > 50''$ the radial distributions of the X-ray surface brightness are consistent with the optical distributions of King (1978). We also find that these galaxies have X-ray spectra significantly different from those observed in X-ray–bright ellipticals, with a relative excess of counts detected in the softest spectral channels. This confirms earlier *Einstein* results. The characteristics of the *ROSAT* PSPC do not allow us to discriminate between possible spectral models. If we adopt a two-component thermal model on the grounds of physical plausibility, we find that the spectral data can be fitted with a very soft optically thin component, with $kT \sim 0.2$ keV, and a hard component with $kT > (1.0–1.5)$ keV. The hard component has a luminosity consistent with that expected from the integrated emission of a population of low-mass X-ray binaries in these galaxies; the nature of the very soft component is more speculative. Candidates include the coronal emission of late-type stars, supersoft X-ray sources, RS CVn, and perhaps a hot ISM. Alternatively, the spectral data may be fitted with a 0.6–1 keV bremsstrahlung spectrum (exponential plus Gaunt), and may suggest the presence of a totally new population of X-ray sources.

Subject headings: galaxies: elliptical and lenticular, cD — galaxies: individual (NGC 4365, NGC 4382) — radiation mechanisms: nonthermal — radiation mechanisms: thermal — X-rays: galaxies

1. INTRODUCTION

Observations of early-type galaxies with the *Einstein* satellite (Giacconi et al. 1979) have revealed that these galaxies can retain large amounts (up to $\sim 10^{11}\ M_\odot$) of hot ($T \sim 10^7$ K) interstellar medium (ISM; Forman, Jones, & Tucker 1985; Canizares, Fabbiano, & Trinchieri 1987). However, it was also observed that early-type galaxies of the same optical luminosity can have X-ray luminosities differing up to a factor of ~ 100 (e.g., Fabbiano, Kim, & Trinchieri 1992). While there are convincing observational and theoretical arguments suggesting that the X-ray emission of X-ray bright galaxies is dominated by the hot ISM, the origin of the emission of X-ray faint galaxies is less certain (Canizares et al. 1987; Fabbiano, Gioia, & Trinchieri 1989; see Fabbiano 1989 and references therein). These galaxies may have not been able to retain their hot ISM, which may have been either expelled through winds (e.g., Ciotti et al. 1991; David, Freeman, & Jones 1991) or stripped through interaction with a hot Intracluster Medium (e.g., White & Sarazin 1991).

A recent analysis of the *Einstein* IPC data of elliptical galaxies in different ranges of X-ray to optical ratio (L_X/L_B) has shown significant differences in the average spectral properties of the X-ray emission (Kim, Fabbiano, & Trinchieri 1992b), which may support these conclusions. While X-ray bright galaxies [$\log (L_X/L_B) > 30.3$, where L_X/L_B is in ergs $s^{-1}/L_\odot^{-1}$] have average spectra that can be fitted with thermal Raymond models with $kT \sim 1$ keV, with decreasing L_X/L_B the spectra [illegible] axes, which are significantly harder ($kT > 3$ keV), and whose emission is dominated by populations of evolved X-ray sources (see Fabbiano 1989). However, an unexpected very soft component of the X-ray emission is apparent in the average X-ray spectrum of the X-ray faintest galaxies [Group 1 in Kim et al. 1992b; $\log (L_X/L_B) = 29.3–30.0$] as a significant excess of counts in the lowest spectral channels.

To confirm the existence of this very soft emission in X-ray faint early-type galaxies, and to determine its characteristics, we have observed two of these galaxies, NGC 4365 and NGC 4382, with the *ROSAT* (Trümper 1983) PSPC (Pfeffermann et al. 1987). In this paper, we report the results of these observations, and we discuss briefly their implications. In the companion paper (Pellegrini & Fabbiano 1994), these results are compared with detailed model predictions.

2. OBSERVATIONS, DATA ANALYSIS AND RESULTS

Table 1 summarizes the characteristics of our two X-ray faint galaxies and gives the *ROSAT* PSPC observation log.

2.1. *Contour Plots*

The data were analyzed using the "xray" package of IRAF, developed at SAO for the analysis of X-ray data. Figures 1*a* and 1*b* show contours plots of the central parts of the two PSPC images, containing the target galaxies. Data from spectral channels 7 to 240 were used. The PSPC data were binned in 5″ pixels and smoothed with 15″ Gaussians to obtain these [illegible]

THE ASTROPHYSICAL JOURNAL, 429:105–118, 1994 July 1

THE VERY SOFT X-RAY EMISSION OF X-RAY–FAINT EARLY-TYPE GALAXIES

S. PELLEGRINI
European Southern Observatory, Karl Schwarzschild Strasse 2, D-85748 Garching bei München; and
Dipartimento di Astronomia, Via Zamboni 33, I-40126 Bologna

AND

G. FABBIANO
Harvard-Smithsonian Center for Astrophysics, 60 Garden Street, Cambridge, MA 02138
Received 1993 September 7; accepted 1994 February 2

ABSTRACT

A recent reanalysis of *Einstein* data, and new *ROSAT* observations, have revealed the presence of at least two components in the X-ray spectra of X-ray faint early-type galaxies: a relatively hard component ($kT > 1.5$ keV), and a very soft component ($kT \sim 0.2$–0.3 keV). In this paper we address the problem of the nature of the very soft component, and whether it can be due to a hot interstellar medium (ISM), or is most likely originated by the collective emission of very soft stellar sources. To this purpose, hydrodynamical evolutionary sequences for the secular behavior of gas flows in ellipticals have been performed, varying the Type Ia supernovae rate of explosion, and the dark matter amount and distribution. The results are compared with the observational X-ray data: the average *Einstein* spectrum for six X-ray faint early-type galaxies (among which are NGC 4365 and NGC 4697), and the spectrum obtained by the *ROSAT* pointed observation of NGC 4365. The very soft component could be entirely explained with a hot ISM only in galaxies such as NGC 4697, i.e., when the depth of the potential well—on which the average ISM temperature strongly depends—is quite shallow; in NGC 4365 a diffuse hot ISM would have a temperature larger than that of the very soft component, because of the deeper potential well. So, in NGC 4365 the softest contribution to the X-ray emission comes certainly from stellar sources. As stellar soft X-ray emitters, we consider late-type stellar coronae, supersoft sources such as those discovered by *ROSAT* in the Magellanic Clouds and M31, and RS CVn systems. All these candidates can be substantial contributors to the very soft emission, though none of them, taken separately, plausibly accounts entirely for its properties.

We finally present a model for the X-ray emission of NGC 4365, to reproduce in detail the results of the *ROSAT* pointed observation, including PSPC spectrum and radial surface brightness distribution. The present data may suggest that the X-ray surface brightness is more extended than the optical profile. In this case, a straightforward explanation in terms of stellar sources could be not satisfactory. The available data can be better explained with three different contributions: a very soft component of stellar origin, a hard component from X-ray binaries, and a ~ 0.6 keV hot ISM. The latter can explain the extended X-ray surface brightness profile, if the galaxy has a dark-to-luminous mass ratio of 9, with the dark matter very broadly distributed, and a SN Ia explosion rate of ~ 0.6 the Tammann rate.

Subject headings: galaxies: elliptical and lenticular, cD — radiation mechanisms: thermal — X-rays: galaxies

1. INTRODUCTION

After the launch of the *Einstein* satellite (Giacconi et al. 1979), it was first realized through X-ray measurements that elliptical galaxies may retain a large amount ($\sim 10^{8}$–$10^{11}\ M_{\odot}$) of hot ($T \sim 10^{7}$ K) interstellar gas (e.g., Forman, Jones, & Tucker 1985; Canizares, Fabbiano, & Trinchieri 1987; see the review of Fabbiano 1989). This conclusion was supported by the presence of X-ray emission displaced from the optical body in some cases, by the relatively soft (~ 1 keV) X-ray spectra of X-ray bright ellipticals, and by the steep correlation between X-ray and optical luminosity ($L_X \propto L_B^{1.5-2}$), see Figure 1. In contrast in spiral galaxies, where the X-ray emission can be attributed to a population of evolved stellar sources (see Fabbiano 1989, and references therein), the X-ray spectra tend to be harder, and $L_X \propto L_B$. Besides suggesting a steep relationship between L_X and L_B, the L_X–L_B diagram of early-type galaxies shows a substantial amount of scatter: the range of L_X for a given optical luminosity spans about two orders of magnitude.

The most successful models are those explaining the scatter in the L_X–L_B diagram in terms of different dynamical phases for the hot gas flows, ranging from winds to inflows (CDPR). These authors, assuming that the SN Ia explosion rate is declining with time slightly faster than the rate with which mass is lost by stars, find that in the beginning the energy released by SN Ia's can drive the gas out of the galaxies through a supersonic wind. As the collective SN Ia's energy input decreases, a subsonic outflow takes place, and this gradually slows down until a central cooling catastrophe leads to the onset of an inflow. An attractive feature of this scenario is that any of the three phases (wind/outflow/inflow) can be found

Chl *a* molecules and the two xanthophylls, seem to represent a central core of the complex. The internal 2-fold symmetry of this arrangement probably arose through duplication of a gene encoding an ancestral single-span polypeptide which proved effective in bringing Chl *a* into close contact with carotenoids. Helix C and the loops on the membrane surface show greater sequence variability within the family of Chl *a*/*b* binding proteins[41]. It is striking that the Chl *b* molecules in the complex seem to be bound by these parts of the polypeptide, which may be later additions. This may account for the variable Chl *b* content of related antenna complexes[42]. The atomic model of LHC-II presented here will be refined in future studies at higher resolution, to contribute to a more complete understanding of photosynthesis which supports all life on Earth. □

Received 23 November 1993; accepted 10 January 1994.

1. Cashmore, A. R. *Proc. natn. Acad. Sci. U.S.A.* **81,** 2960–2964 (1984).
2. Michel, H. P., Griffin, P. R., Shabanowitz, J., Hunt, D. F. & Bennett, J. *J. biol. Chem.* **266,** 17584–17591 (1991).
3. Deisenhofer, J., Epp, O., Miki, K., Huber, R. & Michel, H. *J. molec. Biol.* **180,** 385–398 (1984).
4. Deisenhofer, J., Epp, O., Miki, K., Huber, R. & Michel, H. *Nature* **318,** 618–624 (1985).
5. Krauss, N. *et al. Nature* **361,** 326–331 (1993).
6. Kühlbrandt, W. & Wang, D. N. *Nature* **350,** 130–134 (1991).
7. Kühlbrandt, W. & Downing, K. H. *J. molec. Biol.* **207,** 823–828 (1989).
8. Wang, D. N. & Kühlbrandt, W. *J. molec. Biol.* **217,** 691–699 (1991).
9. Wang, D. N. & Kühlbrandt, W. *Biophys. J.* **61,** 287–297 (1992).
10. Unwin, P. N. T. & Henderson, R. *J. molec. Biol.* **94,** 425–440 (1975).
11. Henderson, R., Baldwin, J. M., Downing, K. H., Lepault, J. & Zemlin, F. *Ultramicroscopy* **19,** 147–178 (1986).
12. Henderson, R. *et al. J. molec. Biol.* **213,** 899–929 (1990).
13. Fujiyoshi, Y. *et al. Ultramicroscopy* **38,** 241–251 (1991).
14. Glaeser, R. M., Tong, L. & Kim, S.-H. *Ultramicroscopy* **27,** 307–318 (1989).
15. Brünger, A. T. *J. molec. Biol.* **203,** 803–816 (1988).
16. Hoffmann, N. E. *et al. Proc. natn. Acad. Sci. U.S.A.* **84,** 8844–8848 (1986).
17. *International Tables for X-ray Crystallography* Vol. IV 71–175 (Kynoch, Birmingham, 1974).
18. Nussberger, S., Dörr, K., Wang, D. N. & Kühlbrandt, W. *J. molec. Biol.* **232,** 347–356 (1993).
19. Mullett, *J. J. biol. Chem.* **258,** 9941–9948 (1983).
20. Bennett, *J. Eur. J. Biochem.* **99,** 133–137 (1979).
21. Siefermann-Harms, D. *Biochim. biophys. Acta* **811,** 325–355 (1985).
22. Bassi, R., Pineau, B., Dainese, P. & Marquardt, J. *Eur. J. Biochem.* **212,** 297–303 (1993).
23. Juhler, R. K., Andreasson, E., Yu, S. G. & Albertsson, P. A. *Photosynth. Res.* **35,** 171–178 (1993).
24. Picorel, R., Bakhtiari, M., Lu, T., Cotton, T. M. & Seibert, M. S. *Photochem. Photobiol.* **56,** 263–270 (1992).
25. Plumley, F. G. & Schmidt, G. W. *Proc. natn. Acad. Sci. U.S.A.* **84,** 146–150 (1987).
26. Paulsen, H., Rümler, U. & Rüdiger, W. *Planta* **181,** 204–211 (1990).
27. Demmig-Adams, B. & Adams, W. W. A. *Rev. Plant Physiol.* **43,** 599–626 (1992).
28. Kearns, D. R. *Chem. Rev.* **71,** 395–427 (1971).
29. Cogdell, R. J. & Frank, H. A. *Biochim. biophys. Acta* **895,** 63–79 (1987).
30. Mauring, K., Renge, I., Sarv, P. & Avarmaa, R. *Spectrochim. Acta* **A43,** 507–529 (1987).
31. Dexter, D. L. *J. chem. Phys.* **21,** 836–850 (1953).
32. Eads, D. D., Castner, E. W., Alberte, R. S., Mets, L. & Fleming, G. R. *J. phys. Chem.* **93,** 8271–8275 (1989).
33. Pålsson, L. O., Spangfort, M. D., Gulbinas, V. & Gillbro, T. *FEBS Lett.* (in the press).
34. Ide, J. P., Klug, D. R., Kühlbrandt, W., Georgi, L. & Porter, G. *Biochim. biophys. Acta* **893,** 349–364 (1987).
35. Bowers, P. G. & Porter, G. *Proc. R. Soc.* **A296,** 435–441 (1967).
36. Kramer, H. & Mathis, P. *Biochim. biophys. Acta* **593,** 319–329 (1980).
37. van der Vos, R., Carbonera, D. & Hoff, A. J. *Appl. mag. Res.* **2,** 179–202 (1991).
38. Porra, R. J., Thompson, W. A. & Kriedemann, P. E. *Biochim. biophys. Acta* **975,** 384–394 (1989).
39. Matthews, B., Fenna, R. E., Bolognesi, M. C., Schmid, M. F. & Olson, J. M. *J. molec. Biol.* **131,** 259–285 (1979).
40. Eccles, J. & Honig, B. *Proc. natn. Acad. Sci. U.S.A.* **80,** 4959–4962 (1983).
41. Green, B. R., Pichersky, E. & Kloppstech, K. *Trends biochem. Sci.* **16,** 181–186 (1991).
42. Peter, G. F. & Thornber, J. P. *J. biol. Chem.* **266,** 16745–16754 (1991).
43. Hiller, R. G., Wrench, P. M., Gooley, A. P., Shoebridge, G. & Breton, J. *Photochem. Photobiol.* **57,** 125–131 (1993).
44. Ceska, T. A. *J. appl. Crystallog.* **27,** 200–201 (1994).
45. Brünger, A. T., Kuriyan, K. & Karplus, M. *Science* **235,** 458–460 (1987).
46. Born, M. & Wolf, E. *Principles of Optics* 5th edn 333–334 (Pergamon, Oxford, 1975).
47. Booy, F. P. & Pawley, J. B. *Ultramicroscopy* **48,** 273–280 (1993).
48. Butt, H.-J., Wang, D. N., Hansma, P. K. & Kühlbrandt, W. *Ultramicroscopy* **36,** 307–318 (1991).
49. Fujiyoshi, Y., Kobayashi, T., Ishizuka, T., Uyeda, N. & Harada, Y. *Ultramicroscopy* **5,** 459–468 (1980).
50. Evans, P. R. in *Crystallographic Computing* Vol. 5 (eds Moras, D., Podjarny, A. D. & Thierry, J. C.) 136–144 (Oxford University Press, Oxford, 1991).
51. Jones, T. A., Zou, J. Y., Cowan, S. & Kjelgaard, M. *Acta crystallogr.* **A47,** 110–119 (1991).
52. Sterling, C. *Acta crystallogr.* **17,** 1224–1228 (1964).
53. Kraulis, P. J. *J. appl. Crystallogr.* **24,** 946–950 (1991).

ACKNOWLEDGEMENTS. We thank K. Dörr for assistance in isolating and purifying the protein, K. Downing for the use of the electron cryomicroscope at the Lawrence Berkeley laboratory, P. Metcalf for advice on crystallographic refinement, H. Scheer and A. Hoff for discussion, and T. Gillbro for communicating results before publication.

Detection of soft X-rays from supernova 1993J six days after outburst

H.-U. Zimmermann*, W. Lewin†, P. Predehl*, B. Aschenbach*, G. Fabbiano‡, G. Hasinger*, L. Lubin§, E. Magnier†‖, J. van Paradijs‖, R. Petre¶, W. Pietsch* & J. Trümper*

* Max-Planck-Institut für Extraterrestrische Physik, Postfach 1603, D-85740 Garching, Germany
† Massachusetts Institute of Technology, Center for Space Research, Cambridge, Massachusetts 02139, USA
‡ Harvard-Smithsonian Center for Astrophysics, Cambridge, Massachusetts 02138, USA
§ Princeton University Observatory, Princeton, New Jersey 08544-1001, USA
‖ Astronomical Institute 'Anton Pannekoek', University of Amsterdam and Center for High-Energy Astrophysics, 1098 SJ Amsterdam, The Netherlands
¶ Goddard Space Flight Center, Greenbelt, Maryland 20771, USA

On 28 March 1993, a new supernova was discovered[1] in the nearby galaxy M81. The proximity of the event (the distance[2] to M81 is only 3.6 Mpc), and the fact that the supernova was detected at an early stage of its outburst[3], makes SN1993J an ideal candidate for the detailed study of the evolution of a supernova in all wavelength regimes. We report here the detection of soft X-ray emissions from SN1993J, six days after the initial discovery, and the subsequent evolution of the X-ray light curve over the next 41 days. The spectral characteristics of the emissions can be readily explained if the X-rays originate in strong shock fronts produced by the rapid expansion of the supernova ejecta into the slow, dense wind of a red supergiant progenitor star[4]. The low intrinsic absorption of the earliest emissions requires that any circumstellar material is ionized, probably by the intense radiation of the initial outburst. The decay of the X-ray luminosity with time should provide important constraints on the density profiles of both the circumstellar gas and the outermost layers of the supernova ejecta.

The mission programme of the X-ray observatory Rosat was interrupted on 3 April 1993 for a target-of-opportunity observation of SN1993J. Using the position sensitive proportional counter (PSPC) in the focal plane of the X-ray telescope, two observations were made between 10.00 and 12.00 UT for a total of 2,706 s. Using former Einstein[5] and Rosat observations of M81 a new source amidst the known bright X-ray sources in the field could be immediately identified with the supernova. The detection, a first estimate of the source intensity, spectral analysis results and the initial decrease of the X-ray intensity were reported[6]. Two days after the Rosat observation, Tanaka *et al.*[7] reported the detection of X-rays from SN1993J with the Japanese X-ray observatory ASCA. Additional Rosat PSPC observations of the supernova followed throughout April until 6 May. In addition to the PSPC observations, two observations

with the high resolution imager (HRI) detector of the Rosat telescope were carried out. Table 1 summarizes the individual observations with both detectors. The angular proximity between M81 and the Sun prevented further monitoring of the source beyond mid-May.

Figure 1 shows contour plots of the central region of M81 before and after the supernova outburst. Figure 1*a* originates from a 20×10^3 s observation taken with the Rosat PSPC in September 1992 before the supernova explosion. In Fig. 1*b*, resulting from the combination of all PSPC pointings on SN1993J (27.3×10^3 s), the supernova is clearly visible as a new bright source southwest of the nucleus. By measuring the angular distance of SN1993J relative to the known positions[5] of the nucleus of M81 and of the nearby source, we could verify that the X-ray and the optical[8] positions coincide within the 6-arcsec accuracy of our approach. Because of the narrow point spread function of the PSPC, the data of SN1993J are only slightly contaminated (by at most 3%) by the nearby southeastern source, which is of similar brightness (and spectral shape) as the supernova. Thus a significant influence of that source on the analysis of SN1993J is excluded.

Figure 2 shows the evolution of the count rate of SN1993J over the whole observation period of 41 d. Two of the data points (indicated by circles) have been derived from the HRI data and scaled to the PSPC data according to the spectral parameters discussed below (with PSPC rate equal to 2.76 times the HRI rate). The horizontal bars of the data points indicate the time span over which data have been averaged to obtain comparable statistics on most points. An exponential decay fits the data in Fig. 2 slightly better than a linear decrease. The resulting ($1/e$) time is 86.2 d (+33.7, −19 d at 90% confidence).

For a spectral analysis of the data, each observation was initially treated separately. Power law and thermal fits were tested on each data set. No statistically significant change of the spectral parameters with time could be established for either of the two models. The data were then added to form a composite spectrum with better statistics.

The fit of a power-law model to the mean spectrum (Fig. 3) yields a photon index of 1.0 ± 0.25 ($\chi^2_{red} = 0.99$; 13 degrees of freedom, d.f.). The low energy cut-off of the spectrum is due to photoelectric absorption in foreground diffuse matter, and corresponds to a neutral hydrogen column density N_H of $(5.9 \pm 0.7) \times 10^{20}$ cm^{-2}. For a fit to a thermal bremsstrahlung model the restricted energy range of the PSPC (0.1–2.4 keV) does not allow kT (where k is the Boltzmann constant and T is

TABLE 1 Rosat observations of SN1993J

Detector	Days (in 1993)	Observation time (s)	rate counts s^{-1}
PSPC	93.5	2,705	0.0790 ± 0.0055
PSPC	98.9	4,060	0.0734 ± 0.0043
PSPC	102.6	5,479	0.0609 ± 0.0034
PSPC	106.8	514	0.0614 ± 0.0121
HRI	109.2	13,210	0.0211 ± 0.0014
PSPC	113.1	5,464	0.0554 ± 0.0032
PSPC	125.3	9,051	0.0535 ± 0.0025
HRI	134.2	8,044	0.0159 ± 0.0016

Exposure times and uncorrected count rates (in the 0.1–2.4 keV band) for Rosat pointings on SN1993J with the position sensitive proportional counter (PSPC) and the high resolution imager (HRI) detectors. Using the measured spectral parameters, the PSPC rate equals 2.76 times the HRI rate.

temperature) to be constrained at the high temperature side. We find $kT > 7$ keV (or $T \gtrsim 80 \times 10^6$ K) at a 1σ confidence level. The corresponding N_H column density is $(5.9 \pm 1.1) \times 10^{20}$ cm^{-2} ($\chi^2_{red} = 1.05$; 13 d.f.). The galactic value of 4.3×10^{20} cm^{-2} in the direction towards M81, determined from radio measurements[9], shows that most of the absorbing material along the line of sight is located within our galaxy. Thus our measurement excludes the existence of large amounts of X-ray absorbing material near the source.

Assuming a distance[2] of 3.6 Mpc to M81 and the best-fit value for the power law model, the observed flux in the 0.1–2.4 keV band corresponds to an absorption corrected luminosity of $(2.94 \pm 0.20) \times 10^{39}$ erg s^{-1} on 3 April, and of $(1.64 \pm 0.17) \times 10^{39}$ erg s^{-1} in mid-May. Besides statistical uncertainties the luminosity has an additional error of ~25% due to the uncertainty of the spectral parameters.

Models for early X-ray emission from SN1993J have to be tested against the present findings of the very high temperature in the emission region, the low intrinsic absorption, the fact that X-rays were detected 6 days after the explosion, as well as against the slow decay of the soft X-ray luminosity. A rather obvious explanation for the present observations is provided by models where the interaction between the shock wave from the supernova and the circumstellar material, originating from the dense wind of a red supergiant progenitor star, heats matter to very high temperatures[4]. The soft X-ray luminosity requires high densities of the circumstellar matter, typical for the dense wind

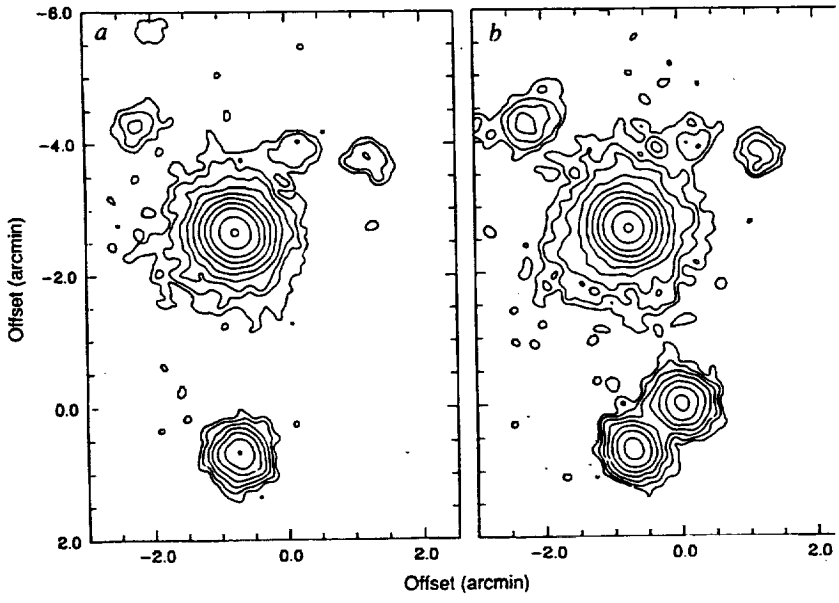

FIG. 1 Contour plots from weakly smoothed images of the central region of the galaxy M81. *a*, A 20×10^3 s exposure taken with the position sensitive proportional counter (PSPC) on the Rosat satellite in September 1992. *b*, The same region after the supernova explosion (27.3×10^3 s PSPC data). The distance between the M81 nucleus at the centre and the bright X-ray source at the lower rim is ~3 arcmin. The contours begin at 3 standard deviations above the background and go up in steps of a factor 2. The PSPC point spread function for a supernova-like spectrum has a half-energy radius of ~14 arcsec.

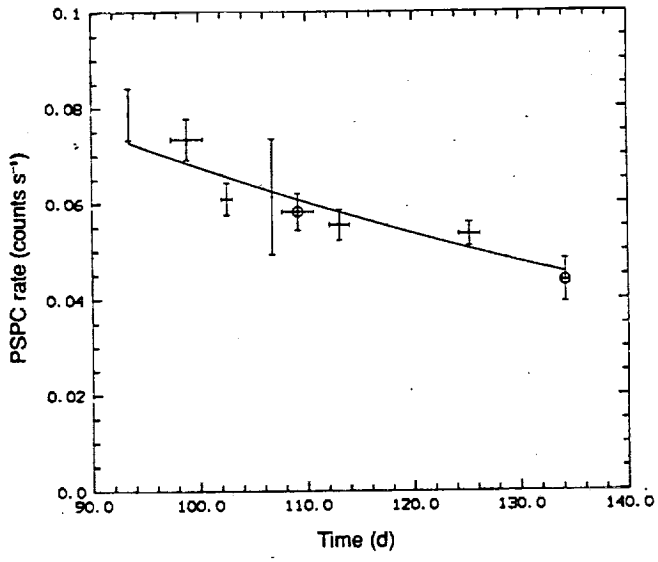

FIG. 2 Light curve of SN1993J as measured with the PSPC detector on Rosat in the 0.1–2.4 keV band. (The horizontal axis gives the days in 1993.) The two data points with circles represent the high resolution imager (HRI) rates that have been scaled by a factor of 2.76 (using the measured spectral parameters) to comparable PSPC rates. The line represents an exponential decay fit with a decay time of 86.2 d.

of red supergiants, as confirmed by detailed hydrodynamical calculations by Suzuki *et al.*[10]. The initial spectrum of SN1993J can be explained reasonably well by thermal bremsstrahlung emission from the supernova ejecta heated by the reverse shock to electron temperatures of the order of 3×10^8 K. But this model predicts a much faster decrease of the soft X-ray luminosity than observed, resulting in almost a factor of 2 difference at day 47 after the explosion. Tuning the circumstellar gas density profile and the density distribution in the outermost layers of the ejecta may help to overcome this discrepancy (K. Nomoto, personal communication).

Before SN1993J, the only supernova event from which low-energy X-rays had been seen was SN1980K in NGC6946, which was detected[11] at 5 standard deviations above background with the Einstein observatory 35 days after maximum optical light; 32 days later, the source was no longer visible. Canizares *et al.*[11] estimated a luminosity of 2×10^{39} erg s^{-1} (0.2–4 keV) during the first observation, remarkably close to the luminosity we find for SN1993J.

In marked contrast to SN1980K and SN1993J, only hard X-rays[12] (from the radioactive decay of Ni^{56}) but no early soft X-rays[13] (<2.5 keV) were seen from SN1987A, which exploded in the Large Magellanic Cloud, ~70 times as close as M81. The progenitor star of SN1987A was identified as a blue supergiant, an object class with typically thin and fast winds, which blow out a low-density bubble around the star. Here the circumstellar wind density is so low that the X-ray radiation from the shock interaction stayed below the detection limit (1.5×10^{36} erg s^{-1} at a distance of 50 kpc) of the Aschenbach *et al.*[13] observation.

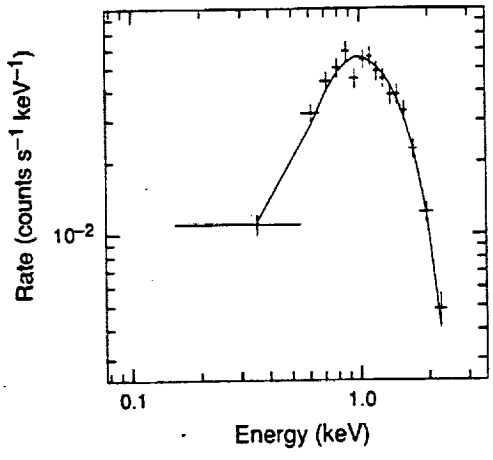

FIG. 3 Spectral fit of a power-law model of the form $f \propto E^{-\gamma}$ to the PSPC data of the supernova. Best fit values are $N_H = (5.9 \pm 0.7) \times 10^{20}$ cm^{-2} for the (cold) gas absorption along the line of sight and $\gamma = 1.02 \pm 0.25$ for the photon index.

Returning to SN1993J we note that the low intrinsic absorption observed already on day 6 after the explosion requires that the wind material of the red supergiant progenitor has been efficiently ionized, for example by an initial ultraviolet or X-ray flash[14]. The hydrogen column density in units of 10^{22} cm^{-2} outside the shock front along the line of sight, assuming a $1/r^2$ density distribution in the wind material, can be expressed as $N_{H,22} = 13 \times \dot{M}_{-5}/(v_{w,20} v_{s,4} t_d)^{-1}$. With the time after the explosion $t_d = 6$ in days, the wind velocity $v_{w,20} = 1$ in units of 20 km s^{-1}, the shock velocity $v_{s,4} = 3$ in units of 10^4 km s^{-1} and mass loss rates $\dot{M}_{-5}$ of 0.6 to 7.7 in units of 10^{-5} solar masses per year (required to achieve the observed luminosity, see also Suzuki[10]), we get $N_{H,22}$ values of 0.5–6. If the wind matter was neutral, soft X-rays would be completely absorbed by the outer layers of the wind, in contradiction to the observation. In fact the fits to the Rosat spectra show a 90% confidence upper limit of 0.05 for $N_{H,22}$, which means that the wind is optically thin against photoelectric absorption for photon energies >0.3 keV at least. Furthermore, our observations are consistent with no change of the absorption column density until the end of the observation period with the PSPC detector, that is day 39 after the outburst. This indicates that the degree of ionization, effective in the soft X-ray range, was essentially maintained.

After submission of this paper, SN1993J was re-observed by Rosat on 1 and 2 November 1993[15]. Since the last observation in May 1993, the PSPC count rate between 0.1 and 2.4 keV has decreased from 0.053 ± 0.0025 to 0.035 ± 0.0014 counts per second. The energy spectrum has become significantly softer, with $kT \approx 0.5$ keV for the fit to a thermal bremsstrahlung model. The low-energy X-ray absorption, as derived from the fit, has increased by a factor of ~5 compared to the May observation. □

Received 20 September; accepted 22 December 1993.

1. Ripero, J. *IAU Circ. No.* 5731 (1993).
2. Madore, B. F., Freedman, W. L. & Lee, M. G. *IPAC Preprint* No. 105 (1993).
3. Filippenko, A. V. & Matheson, T. *IAU Circ. No.* 5740 (1993).
4. Chevalier, R. A. *Astrophys. J.* **258** 790–797 (1982).
5. Fabbiano, G. *Astrophys. J.* **325**, 544–562 (1988).
6. Zimmermann, H.-U. *et al. IAU Circ. No.* 5748 (1993); *IAU Circ. No.* 5750 (1993); *IAU Circ. No.* 5766 (1993).
7. Tanaka, Y. and the ASCA team *IAU Circ. No.* 5753 (1993).
8. Hartwick, F. D. A., Balam, D. D., Zurek, D. & Robb, R. M. *IAU Circ. No.* 5731 (1993).
9. Dickey, J. M. & Lockman, F. J. *A. Rev. Astr. Astrophys.* **28**, 215–261 (1990).
10. Suzuki, T. *et al. Astrophys. J.* (submitted).
11. Canizares, C. R., Kriss, G. A. & Feigelson, E. D. *Astrophys. J.* **253**, L17–L21 (1982).
12. Itoh, M., Kumagai, S., Shigeyama, T., Nomoto, K. & Nishimura, J. *Nature* **330**, 233–235 (1987).
13. Aschenbach, B. *et al. Nature* **330**, 232–233 (1987).
14. Klein, R. I. & Chevalier, R. A. *Astrophys. J.* **223**, L109–L112 (1978).
15. Zimmermann, H.-U. *et al. IAU Circ. No.* 5899 (1993).

X-RAY PROPERTIES OF EARLY-TYPE GALAXIES

G. Fabbiano
Harvard-Smithsonian Center for Astrophysics

I. Outline

In this paper I will first review briefly the results of the X-ray observations of early-type galaxies with the *Einstein* satellite, published in the past ten years (see Fabbiano 1989 for a detailed review). I will then concentrate on more recent results stemming from a systematic re-analysis of the *Einstein* galaxy database, and I will also report on some very preliminary ROSAT results. Parts of this talk were given at the COSPAR Symposium in Washington DC in September 1992 and therefore there is a considerable overlap between this paper and that in the proceedings of the COSPAR meeting (Fabbiano 1992). Some of this material was also reviewed by Fabbiano and Kim (1992).

II. Summary of 'old' *Einstein* Results

Normal galaxies have been studied in X-rays only recently. The *Einstein Observatory* (Giacconi et al 1979) was the first X-ray experiment sensitive enough to detect a large number of normal galaxies and to give us X-ray images and spectra in the 0.2-4.0 keV energy range. These observations have shown that all galaxies are X-ray sources with luminosities in the range of $10^{39} - 10^{43}$ $ergs\ s^{-1}$ (see Fabbiano 1989 and references therein). There are however significant differences between spiral and elliptical galaxies (for the purpose of this paper the word 'elliptical' is used to include both E and S0 galaxies, unless otherwise indicated). In spiral galaxies, X-ray and optical luminosities are linearly correlated, and the X-ray luminosity typically does not exceed a few $10^{41} ergs\ s^{-1}$. Observations of nearby spirals, including the Galaxy, show that the emission in the *Einstein* range is dominated by bright X-ray sources (accretion binaries and supernova remnants). Bulge and disk X-ray emitting populations can be distinguished, both with direct observations of nearby galaxies, and because of sample differences in the properties of bulge-dominated and disk-dominated spirals (e.g. Fabbiano, Gioia, and Trinchieri 1988). Other sources, such as gaseous components associated with starburst activity, and small-scale AGN were also detected in spirals (e.g. NGC 253, M81).

Elliptical galaxies can be significantly more luminous in X-rays, reaching $\sim 10^{43}$ $ergs\ s^{-1}$. There is both imaging and spectral evidence that these X-ray luminous galaxies are dominated in X-rays by a soft (~ 1 keV) gaseous component, which has been suggested to be hot interstellar gas trapped in the gravitational field of the galaxy (e.g. Forman et al 1979; Forman, Jones and Tucker 1985; Trinchieri and Fabbiano 1985). The X-ray and optical luminosities of elliptical galaxies are

:.-L.: 1988, *ApJ* **335**, 940

1990, *ApJ* **361**, 220

.: 1993, *ApJS* , in press
ll, E., Dulk, G., and Linsky,

J.L.: 1985, in R.M. Hjellming

ApJL , submitted

:.S., Cash, W.Jr., and Snow,

.Jr.: 1992, *ApJS* **81**, 795

R., and Schmitt, J.H.M.M.:

R.A., Harnden, F.R.Jr., and

, and Rosso, C.: 1990, *A&A*

osner, R., and Vaiana, G.S.:

.R.Jr., and Rosner, R.: 1990,

988, *A&AS* **72**, 291
The Origin of Nonradiative
199

CORONAL STELLAR EMISSION IN GALAXIES

G. FABBIANO
Harvard-Smithsonian Center for Astrophysics

Abstract. The X-ray luminosity of galaxies is not dominated by their stellar coronal emission. However, stars are there and their presence must account for a fraction of the X-ray emission. Stellar coronal emission in the Galaxy may explain the Galactic Ridge. In nearby spirals, a fraction of the unresolved emission must be ascribed to stars. Even in more distant X-ray faint elliptical galaxies, there may be evidence for stellar emission.

Key words: Galaxies – Galactic X-ray emission

1. Introduction

In the optical band, studying galaxies is also studying stars. This is not true in X-rays, where the luminosity is dominated by different sources. In spiral galaxies a population of hard-spectrum discrete X-ray sources dominates the emission in the *Einstein* band ~(0.2–4 keV). These are likely to be X-ray binaries and young supernova remnants. A hot gaseous interstellar medium (ISM) may be also present, and has been convincingly detected in starburst galaxies. In X-ray-bright elliptical galaxies the X-ray luminosity is dominated by the emission of a hot ISM. However, emission from a population of low-mass binaries, similar to those in the bulge of M31, may be the dominant source of X-rays in X-ray-faint ellipticals (see Fabbiano 1989 and references therein; Fabbiano, Kim and Trinchieri 1992; Kim, Fabbiano and Trinchieri 1992a and b).

What is the role of stellar coronal emission in the X-ray luminosity of galaxies? Clearly it does not dominate the flux detected in the *Einstein* band: the X-ray to optical luminosity ratio expected from a 'normal' stellar population in spiral galaxies is smaller than the average measured value for the sample of galaxies observed with *Einstein* (see Fabbiano 1989). Moreover, the average X-ray spectrum of spiral galaxies is harder (kT>3 keV; Kim, Fabbiano, and Trinchieri 1992) than that expected from pure stellar emission for a measureable mix of stellar types (see Vaiana 1990). In elliptical galaxies this contribution would be even harder to discern.

However, the stellar contribution must be there at a certain level. As Pippo Vaiana was fond of saying, if there are $\sim 10^{11}$ suns in a spiral galaxy emitting 10^{28}ergs s^{-1} each, we have $\sim 10^{39}$ ergs s^{-1}, which is not far off the observed range of X-ray luminosity of spirals ($\sim 10^{39-40.5}$ergs s^{-1}).

In this talk I will review the evidence of stellar coronal emission in the Galaxy and in nearby spiral galaxies; I will then discuss the UV and X-ray observations of a starburst galaxy, where the X-ray emission of the young stellar population may be very significant; I will conclude with some recent puzzling results on X-ray faint elliptical galaxies that may suggest a detectable amount of stellar emission.

2. The Galaxy

Stars in the Galaxy could be detected in large numbers and studied with the *Einstein Observatory* (e.g. Linsky 1990; Vaiana 1990 and references therein). Although stars are individually faint X-ray sources, given to their large numbers they can be

J.F. Linsky and S. Serio (eds.), Physics of Solar and Stellar Coronae, 267–273.

Cambridge Astrophysics Series 26

X-Ray Binaries

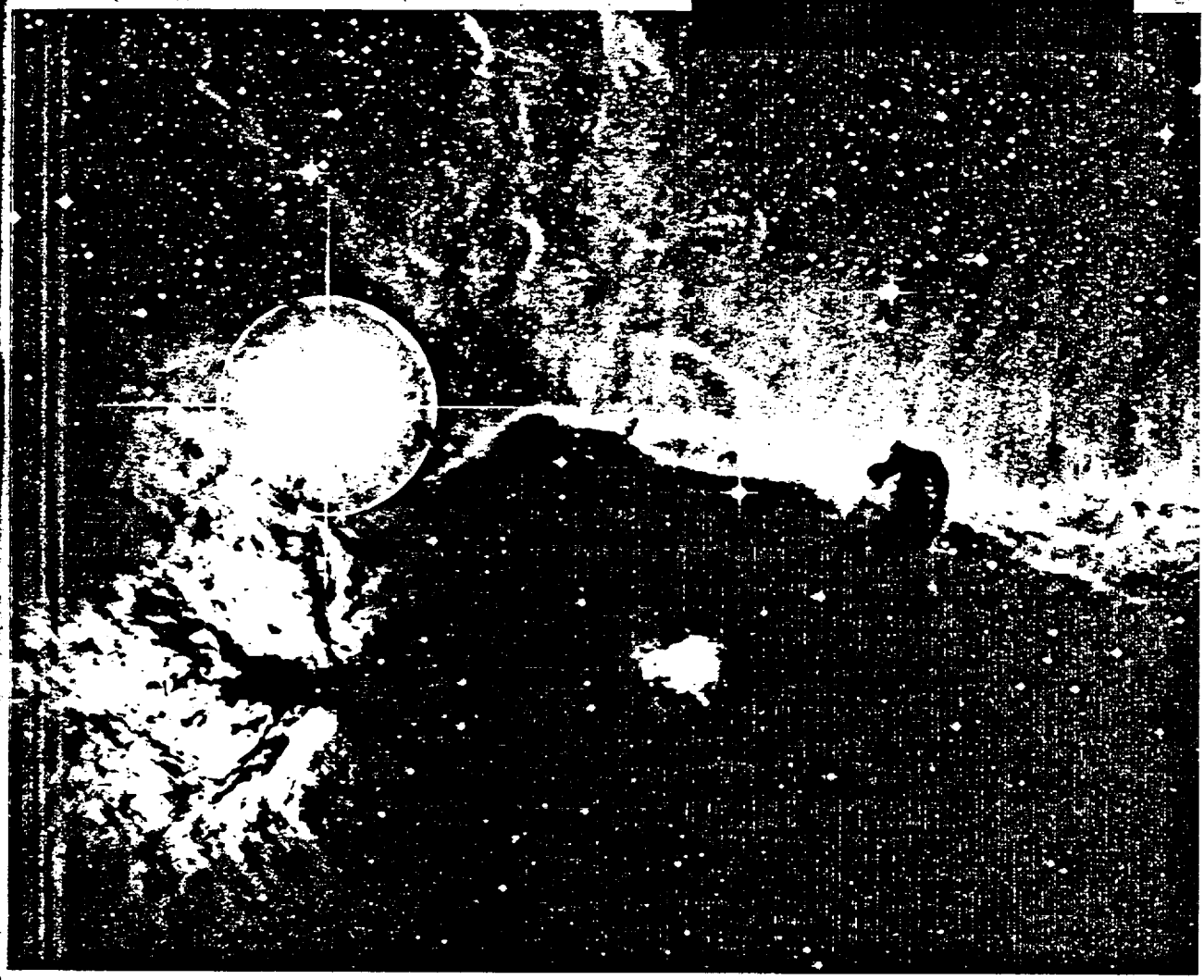

Edited by WALTER H. G. LEWIN,
JAN VAN PARADIJS and
EDWARD P. J. VAN DEN HEUVEL

9

Normal galaxies and their X-ray binary populations

G. Fabbiano
Harvard-Smithsonian Center for Astrophysics, 60 Garden Street, Cambridge, MA 02138, USA

9.1 Introduction

X-ray binaries (XBs) are an important component of the X-ray emission of galaxies. Therefore the knowledge gathered from the study of Galactic X-ray sources can be used to interpret X-ray observations of external galaxies. Conversely, observations of external galaxies can provide us with uniform samples of XBs, in a variety of different environments.

Although detailed spectral/variability studies are at the moment only feasible for Galactic X-ray sources and perhaps for X-ray sources in Local Group galaxies, the study of sources in external galaxies presents unique advantages. These sources within a given galaxy do not suffer from the uncertainty in distances that affects Galactic binaries. Moreover, except for very edge-on galaxies, these sources are not affected by large line-of-sight absorption, as are, for example, Galactic bulge sources. Furthermore, in external galaxies it is easy to associate sources with different galactic components (e.g. bulge, disk, spiral arms). Finally, different galaxies provide different laboratories in which to test theories of Galactic source formation and evolution with a variety of boundary conditions: different metallicity/stellar population, star-formation activity, galaxy structure. All considered, the best place to study the overall properties of Galactic sources is in external galaxies!

The study of galaxies in X-rays began with the *Einstein Observatory* (Giacconi *et al.* 1979) and will be undoubtly greatly expanded with *ROSAT* (Trümper 1983). A review of the *Einstein* results can be found in Fabbiano (1989); see also Fabbiano (1990a, 1990b). Enlarged compilations of the *Einstein* data (images, fluxes and spectra), including almost 500 galaxies, have been published recently (Fabbiano, Kim and Trinchieri 1992; Kim, Fabbiano and Trinchieri 1992a). These observations have shown that most of the X-ray emission of normal spiral galaxies (i.e. galaxies whose X-ray emission is not dominated by a point-like non-thermal nuclear source) in the *Einstein* band ($\sim 0.2-4.0$ keV) is due to the integrated contribution of galactic X-ray sources. Three components of the X-ray emitting population have been identified: bulge, disk and spiral arm sources. In starburst galaxies, a hot gaseous component is also present. Elliptical galaxies can be much more luminous in X-rays than spirals because they may retain a hot gaseous component, which dominates the X-ray emission. However, a good fraction of the elliptical galaxies observed with *Einstein* have relatively low X-ray luminosities. In these galaxies the X-ray emission may be dominated by a population of low-mass XBs (LMXBs).

In this chapter, largely based on the *Einstein* observations, I will concentrate on

THE ASTROPHYSICAL JOURNAL, 420:143–151, 1994 January 1

X-RAY CONTINUUM AND IRON K EMISSION LINE FROM THE RADIO GALAXY 3C 390.3

M. INDA,[1] K. MAKISHIMA,[1] Y. KOHMURA,[1] M. TASHIRO,[1] T. OHASHI,[2] P. BARR,[3] K. HAYASHIDA,[4] G. G. C. PALUMBO,[5] G. TRINCHIERI,[6] M. ELVIS,[7] AND G. FABBIANO[7]
Received 1993 February 8; accepted 1993 July 8

ABSTRACT

X-ray properties of the radio galaxy 3C 390.3 were investigated using the *EXOSAT* and *Ginga* satellites. Long-term, large-amplitude X-ray intensity changes were detected over a period extending from 1984 through 1991, and high-quality X-ray spectra were obtained especially with *Ginga*. The X-ray continuum spectra were described with power-law model with photon slope in the range 1.5–1.8, and the slope flattened as the 2–20 keV luminosity decreased by 40%. There was a first detection of the iron emission line from this source at the 90% confidence level. An upper limit was derived on the thermal X-ray component. X-ray emission mechanisms and possible origins of the long-term variation are discussed.

Subject headings: galaxies: individual (3C 390.3) — galaxies: active — X-rays: galaxies

1. INTRODUCTION

Radio galaxies occupy an important position as a possible parent population for quasars (QSOs) and BL Lac objects (Brown & Murphy 1987; Barthel 1989). In fact, certain models (called "Unified Scheme"; see Orr & Brown 1982) claim that a group of radio galaxies that are seen nearly end-on to their radio jets should become a highly relativistically beamed luminous class of active galactic nuclei (AGNs). In order to test the Unified Scheme, it is important to better understand the X-ray characteristics of radio galaxies and compare them with those of other types of AGN, because X-ray emission is thought to be directly related to the emission mechanism of the central engine of the AGN.

3C 390.3 is a broad-line radio galaxy at $z = 0.057$. In the radio, it is classified as F-R II (lobes with leading edge hot spots; Fanaroff & Riley 1974), and has a prominent double-lobed morphology, together with a compact nucleus which shows evidence of superluminal motion (Alef et al. 1988). The optical spectrum, which classifies it as an N galaxy (Burbidge & Burbidge 1971; Penston & Penston 1973), shows broad Hα and Hβ lines whose double-peaked structure provides evidence for an accretion disk (Perez et al. 1988). Since its first X-ray detection by *Uhuru* (Giacconi & Gursky 1974; Forman et al. 1978), 3C 390.3 has also been known to have an X-ray luminosity as large as $L_X \sim 10^{44}$ ergs s^{-1}. The galaxy has been subsequently monitored in X-rays by several satellites, up to the most recent observations with *EXOSAT* (Shafer, Ward, & Barr 1985, hereafter SWB85), and the new results from *Ginga* that we are presenting here. The *HEAO 1* data indicate X-ray spectra of power-law form with photon index $\Gamma = 1.65\,(+0.50, -0.25)$ in 2–50 keV (error is 90% confidence level) and $\Gamma = 1.40 \pm 0.37$ in 12–165 keV (error is 1 σ uncertainty) (Rothschild et al. 1983; Mushotzky 1984), which are typical of an AGN, and has a 2–10 keV luminosity of $L_X = 10^{43.8}$ ergs s^{-1}. A continuous decline of 3C 390.3 has been observed over a period of ~ 15 yr up to ~ 1984, in the optical blue continuum (from 14.8 to 16.6 mag; Barr et al. 1980; Lloyd 1984; SWB85), in the optical broad-line components (Oke 1986), in ultraviolet lines (Clavel & Wamsteker 1987), and in X-rays (SWB85).

Here we report on the X-ray observations of 3C 390.3 made with the *EXOSAT* and *Ginga* satellites, and present high-quality X-ray spectra obtained with *Ginga*. In § 2 and § 3 we describe our observations and results respectively, followed by the discussion in § 4.

2. OBSERVATIONS

2.1. *EXOSAT Observations*

A total of six *EXOSAT* observations of 3C 390.3 were performed between 1984 and 1986. Data from the first two observations have already been reported (SWB85); processed data from all six observations are publicly available in the *EXOSAT* data base. However, for a weak source like 3C 390.3, where the hard X-ray data are background-noise dominated, it is often possible to obtain significantly better reduced data than available in the archive by interactive reanalysis of the raw data. Therefore, we have systematically reanalyzed all data from the Medium Energy proportional counter array (ME; Turner, Smith, & Zimmerman 1981) to obtain a uniform sample of X-ray spectra.

Observations were performed on 1984 day 153, day 259; 1985 day 33, day 311; and 1986 day 76, day 77. Both observations in 1984 were affected by solar activity; on day 153, 63 minutes of data were not used due to background variations, while on day 259 the ME data were completely unusable due to solar flaring. We therefore exclude 1984 day 259 data from the present analysis. The useful data on 1985 day 33 were truncated by 3 hours due to spacecraft pointing problems. Only 54 minutes of useful data were obtained on 1985 day 311 due to background variations.

[1] Department of Physics, University of Tokyo, 7-3-1 Hongo, Bunkyo-ku, Tokyo, Japan 113.
[2] Department of Physics, Tokyo Metropolitan University, 1-1 Minami-Osawa, Hachioji, Tokyo, Japan 192-03.
[3] *EXOSAT* Observatory, Astrophysics Divisions, Space Science Department, ESTEC, NL-2200 AG Noordwijk, The Netherlands.
[4] Department of Earth and Space Science, Osaka University, 1-1 Machikane-yama, Toyonaka, Osaka, Japan 560.
[5] Dipartimento di Astronomia, Università di Bologna, Via Zamboni 33, 40126 Bologna, Italy.
[6] Osservatorio Astrofisico di Arcetri, Largo Enrico Fermi 5, 50125 Firenze, Italy.

THE ASTROPHYSICAL JOURNAL, 434:67–81, 1994 October 10

HIGH-RESOLUTION OPTICAL AND UV OBSERVATIONS OF THE CENTERS OF NGC 1316 AND NGC 3998 WITH THE *HUBBLE SPACE TELESCOPE*[1]

G. FABBIANO, C. FASSNACHT,[2] AND G. TRINCHIERI[3]
Harvard-Smithsonian Center for Astrophysics, 60 Garden Street, Cambridge, MA 02138

Received 1993 August 2; accepted 1994 April 21

ABSTRACT

B and UV high-resolution images obtained with the *HST* FOC reveal centrally increasing surface brightness and UV-bright point sources at the nuclei of the early-type galaxies NGC 1316 and NGC 3998. Model fitting of the surface brightness distribution does not exclude a central flattening, which could however be the result of extinction and/or of improper evaluation of the point-source component. The present data, while not requiring the presence of central massive black holes in these two galaxies, make them possible candidates. Follow-up work is needed to study this point further. The presence of unresolved nuclei gives model-dependent support to this quest, if these sources are due to small AGN. These UV-bright sources could belong to the low-luminosity end of active nuclear emission.

Subject headings: galaxies: active — galaxies: individual (NGC 1316, NGC 3998) — galaxies: nuclei — ultraviolet: galaxies

1. INTRODUCTION

The study of the light distribution in the central regions of elliptical galaxies can give us important clues on their formation and growth, and on the presence of a large central mass concentration. These studies, however, have typically been hampered by the effect of seeing (e.g., Schweizer 1981). *HST*, even with its aberrated optics, gives us a direct way to infer the distribution of light in the central regions of galaxies, down to radii well below 1".

NGC 1316 and NGC 3998 are two early-type galaxies (S0), which exhibit nuclear activity. NGC 1316 is a nearby radio galaxy (Fornax A), with a core-jet-lobes structure (Geldzahler & Fomalont 1984). NGC 3998 hosts a compact radio source (see Fabbiano, Gioia, & Trinchieri 1989). The central regions of both galaxies have low-ionization emission-line spectra (Baum, Heckman, & Van Breugel 1992; Heckman, Balick, & Crane 1980; Keel 1983), and there is evidence for circumnuclear emission-line disks (Ford et al. 1986; M. Frank 1993, private communication; F. Bertola 1993, private communication). NGC 3998 has also been studied in the IR as part of a sample of LINERs (Willner et al. 1985); UV observations with *IUE* (Reichert et al. 1992) suggest the presence of a nuclear point source, with strong broad Mg II (2800 Å) emission. Both galaxies have been observed in X-rays with *Einstein* (e.g., Fabbiano, Kim, & Trinchieri 1992; Kim, Fabbiano, & Trinchieri 1992). The ~5" resolution observation of NGC 1316 shows that the X-ray emission is extended, and there is no evidence of a strong nuclear point source. The X-ray emission of NGC 3998 is unresolved; however, this galaxy was observed only at low spatial resolution (~40") with *Einstein*. A study of the optical surface brightness of the central regions of NGC 1316 (Schweizer 1981) led to the detection of a small bright core, and to the suggestion of a heavily absorbed nucleus.

The presence of nuclear radio sources in NGC 1316 and NGC 3998 makes them likely candidates for hosting central massive black holes. Accretion onto massive black holes has been invoked as the energy source of quasars and active galactic nuclei (Rees 1984). Based on a correlation between the core radio luminosity of quasars and bright 3CR galaxies, and their X-ray luminosity (Fabbiano et al. 1984), one can predict X-ray luminosities for the active nuclei. These estimates are below the detected *Einstein* luminosities of these galaxies which are likely to be dominated by an extended gaseous component (Fabbiano, Gioia, & Trinchieri 1989). Predictions on the X-ray emission of an active nucleus can be turned into limits on the mass of a central black hole, following Fabian & Canizares (1988), who consider accretion from the hot ISM as the fueling mechanism for the nuclear black hole. For NGC 1316 and NGC 3998 these limits suggest black hole masses between 10^8 and 10^9 $M_\odot$ (see Fabbiano et al. 1989).

In this paper we report the results of high-resolution observations of NGC 1316 and NGC 3998 with the *HST* FOC in the optical and UV. There were two motivations for these observations: we wanted to find or set limits on the luminosity of nuclear point sources, which could be the optical-UV counterparts of the radio-emitting nucleus; and we wanted to study the surface brightness distributions in the inner regions of these galaxies to seek the dynamical signature of a central mass concentration.

The presence of a large central mass concentration would have visible effects on the radial distributions of both stellar surface brightness and velocity dispersion, which should be increasing at smaller radii. Although a number of ellipticals can be fitted with King profiles (e.g., King 1978), even before space observations it was known that some galaxies presented deviations from a flat-core King distribution in their inner regions (see Lauer 1985). Direct evidence of massive black holes has been sought with high-resolution observations of the inner regions of nearby galaxies both from the ground (e.g., Young et al. 1978; Sargent et al. 1978; Dressler 1980; Dressler

[1] Based on observations with the NASA/ESA *Hubble Space Telescope*, obtained at the Space Telescope Science Institute, which is operated by AURA, Inc. under NASA contract NAS5-26555.

THE ASTROPHYSICAL JOURNAL SUPPLEMENT SERIES, 80:531–644, 1992 June

AN X-RAY CATALOG AND ATLAS OF GALAXIES

G. FABBIANO,[1] D.-W. KIM,[1] AND G. TRINCHIERI[1,2]
Received 1991 May 20; accepted 1991 September 4

ABSTRACT

We present an X-ray catalog and atlas of galaxies observed with the *Einstein Observatory* imaging instruments (IPC and HRI). The catalog comprises 493 galaxies, including targets of pointed observations, and RSA or RC2 galaxies serendipitously included in *Einstein* fields. A total of 450 of these galaxies were imaged well within the instrumental fields, resulting in 238 detections and 212 3 σ upper limits. The other galaxies were either at the edge of the visible field of view or confused with other X-ray sources. For these we also give a rough measure of their X-ray emission. The atlas shows X-ray contour maps of detected galaxies superposed on optical photographs and gives azimuthally averaged surface brightness profiles of galaxies detected with high signal-to-noise ratio.

Subject headings: atlases — catalogs — Galaxy: structure — X-rays: galaxies

1. INTRODUCTION

The *Einstein Observatory* (Giacconi et al. 1979) has given us for the first time the capability to study galaxies in the soft X-ray band (0.2–3.5 keV). The focusing optics of the *Einstein* mirror combined with the imaging capabilities and sensitivity of its instruments has led to the detection of the X-ray emission of normal galaxies at least as far as the Virgo Cluster and in some cases has given us detailed information on the morphology of the X-ray emission and on its spectral characterists. These results suggest that the X-ray emission of normal spiral galaxies in the *Einstein* band is dominated by the integrated output of evolved stellar sources, such as supernova remnants and close accreting binaries with a compact stellar remnant. Bright E and S0 galaxies are dominated by the emission of a hot interstellar medium, and a similar gaseous emission is associated with starburst nuclei (see Fabbiano 1989 for a review).

Although many of the *Einstein* observations of galaxies have been published, including the nearest best studied objects, there are many observations in the *Einstein* data bank that have never been published. These include both galaxies observed as the field target, and galaxies included serendipitously in fields pointed at other astrophysical objects. Moreover, slightly different analysis techniques have been used in different papers, resulting in a certain nonuniformity of the reported fluxes. For these reasons, we have undertaken a systematic analysis of all the galaxies observed as part of the *Einstein* mission with either the Imaging Proportional Counter (IPC) or the High Resolution Imager (HRI). We have also searched for X-ray emission from galaxies included in either A Revised Shapley-Ames Catalog of Bright Galaxies (Sandage & Tamman 1981, hereafter RSA) or the Second Revised Catalog of Bright Galaxies (de Vaucouleurs, de Vaucoulers, & Corwin 1976, hereafter RC2) that might have been included in the *Einstein* field of view of observations of unrelated targets. This search, combined with the target galaxies, has resulted in 493 galaxies observed in X-rays with *Einstein*. By comparison, only data relative to less than 200 galaxies have been previously reported (Fabbiano 1989 and references therein).

In this paper we report the selection criteria and observation parameters (§ 2), and we describe the data analysis techniques (§ 3). We give X-ray fluxes or upper limits for all these galaxies, together with detailed analysis of separate components for complex objects (§ 4). For the detected galaxies, we present X-ray surface brightness contours overlaid onto optical images, and when appropriate we give X-ray surface brightness profiles (§ 5). We then discuss our results in comparison with published work (§ 6). In a companion paper (Kim, Fabbiano, & Trinchieri 1992a, hereafter Paper II), we report the results of a systematic spectral analysis of this sample. Average spectral properties of different types of galaxies and their implications for the emission mechanisms are discussed in Kim, Fabbiano, & Trinchieri (1992b, hereafter Paper III).

2. THE SAMPLE

The galaxies used for this work (see Table 1 of the catalog, located after the text of this paper) include all the bright galaxies targets of *Einstein* observations, and all other galaxies in RSA or RC2 serendipitously included in *Einstein* fields. Galaxies of all morphological types, normal galaxies, starburst galaxies and mergers, and also galaxies with active nuclei (e.g., Seyfert galaxies) are included. In the latter, the X-ray emission is typically dominated by a pointlike nuclear source. Galaxies at the center of rich clusters (e.g., M87, NGC 1275), where the X-ray emission is clearly dominated by the hot intracluster medium (e.g., Fabricant, Lecar, & Gorenstein 1980), are excluded from this catalog. Also excluded are NGC 4476 and NGC 4478; these two galaxies are in a region of the sky which is totally dominated in X-rays by the gaseous halo of M87. Early-type galaxies in groups are, however, included, even if the group potential could account for a larger gaseous halo and brighter X-ray sources (e.g., Kriss, Cioffi, & Canizares 1983). Galaxies in clusters are also included, when the X-ray emission is clearly associated with the individual galaxy. In Table 1 we do not list the *Einstein* observations of M31, M32, LMC, and SMC, although their X-ray fluxes are included in Table 3.

[1] Harvard-Smithsonian Center for Astrophysics, 60 Garden Street, Cambridge, MA 02138.

[2] Postal address: Osservatorio Astrofisico di Arcetri, Largo Enrico Fermi 5, I-50125 Firenze, Italy.

ADS Astronomy Abstract Service

Title:	The insignificance of 'heating flows' in 'cooling flow' clusters of galaxies
Authors:	CANIZARES, CALUDE R.; MARKERT, THOMAS H.; MARKOFF, SERA; HUGHES, JOHN P.
Affiliation:	AC(MIT, Cambridge, MA) AD(Harvard-Smithsonian Center for Astrophysics, Cambridge, MA)
Journal:	Astrophysical Journal, Part 2 - Letters (ISSN 0004-637X), vol. 405, no. 1, p. L17-L20.
Publication Date:	3/1993
Category:	Astrophysics
Origin:	STI
Bibliographic Code:	1993ApJ...405L..17C

Abstract

This paper considers the possibility that 'cooling flow' clusters are really 'heating flow' clusters in which cold gas clouds evaporate in the hot intracluster medium. Total X-ray luminosity was calculated as a function of the total evaporation rate. X-ray line emissivity for evaporating clouds was also calculated using a nonequilibrium ionization code. The calculated X-ray luminosity and X-ray line emissivity are approximately 1000 times smaller than for cooling clouds. Other comparisons were made using measured line fluxes for M87 and Perseus cluster. Results indicate that evaporative heating flow models require mass fluxes much greater than cooling flow models to explain the same X-ray emission. This requirement exceeds any plausible mass source. These conclusions are very general and serve to reject all heating flow models as viable alternatives to cooling flows.

THE ASTROPHYSICAL JOURNAL SUPPLEMENT SERIES, 80:645–681, 1992 June

THE X-RAY SPECTRA OF GALAXIES. I. SPECTRAL FITS OF INDIVIDUAL GALAXIES AND X-RAY COLORS

D.-W. KIM AND G. FABBIANO
Harvard-Smithsonian Center for Astrophysics, 60 Garden Street, Cambridge, MA 02138
AND
G. TRINCHIERI
Osservatorio Astrofisico di Arcetri and Harvard-Smithsonian Center for Astrophysics, 60 Garden Street, Cambridge, MA 02138
Received 1991 June 12; accepted 1991 October 30;

ABSTRACT

We have systematically investigated the X-ray spectra of normal galaxies, by using the Imaging Proportional Counter (IPC) data in the *Einstein* data bank. In addition to the standard model fitting technique, we introduce X-ray colors in order to extract spectral information from the fainter X-ray sources. We present spectral parameters for 43 galaxies and X-ray colors for 127 galaxies.

Subject heading: X-rays: galaxies

1. INTRODUCTION

Since the launch of the *Einstein* satellite in 1978 (Giacconi et al. 1979), X-ray observations have added important information to our knowledge of normal galaxies (see Fabbiano 1989 for a review). Most of the work done so far, however, has been concentrated on the analysis of imaging data. Spectral parameters [i.e., hydrogen absorption column density and emission temperature (or power-law index)] can be extracted for sources observed with the Imaging Proportional Counter (IPC), but have been published only for a limited number of normal galaxies (for six elliptical galaxies, Trinchieri, Fabbiano, & Canizares 1986; for 13 spiral galaxies, Fabbiano & Trinchieri 1987; for the bulge of M31, Fabbiano, Trinchieri, & Van Speybroeck 1987; for N1399, Killeen & Bicknell 1988; for M33, Trinchieri, Fabbiano, & Peres 1988; for M81, Fabbiano 1988a; for M101, Trinchieri, Fabbiano, & Romaine 1990; and for the starburst galaxies NGC 253 and M82, Fabbiano 1988b). Forman, Jones & Tucker (1985) gave temperature ranges for eight early-type galaxies, but not fitting N_H, for which they assumed the Galactic line-of-sight value. An extensive IPC spectral survey of Seyfert galaxies has been recently published (Kruper, Urry, & Canizares 1990, hereafter KUC). The X-ray emission of these galaxies is dominated by their active nuclear source (AGN).

Spectral information is essential for a more concrete understanding of the nature of the X-ray sources and of the emission mechanisms in galaxies. Because different types of galaxies are likely to consist of different mixtures of X-ray emitting components, which may have different spectral characteristics, searching for differences in their spectral properties may help us identifying the dominant component for a given class of galaxies. We have performed a systematic spectral analysis of all the galaxies in the catalog of Fabbiano, Kim, & Trinchieri (1992, hereafter Paper I) and we present the results in this paper. For galaxies detected with high signal-to-noise ratio we present the results of a two-parameter χ^2 fit of emission models to the data. However, most galaxies observed with the *Einstein* Observatory IPC do not have enough counts for us to apply this model fitting technique. To extract X-ray spectral information from faint sources, we have introduced and calibrated two X-ray colors so that two important parameters—emission temperature (or power-law index) and hydrogen column density responsible for the low-energy cutoff—can be determined. X-ray colors, although with a different definition from ours, have been used by Cordova et al. (1990) to find very soft X-ray sources.

Galaxies from Paper I observed with the *Einstein* IPC are included for this spectral study if detected with more than 30 net counts. Galaxies which have ambiguous sources (i.e., the X-ray emission could be due to interlopers) or were partly hidden by the detector supporting structure are excluded. These galaxies are listed in Tables 3 and 6 of Paper I. We describe the standard model fitting technique and present the results in § 2. We describe the X-ray colors and present the results in § 3. We include notes on individual galaxies in § 4. In a forthcoming paper, we will discuss the average spectral properties of different types of galaxies and their implications on the X-ray emission mechanisms (Kim, Fabbiano, & Trinchieri 1992, hereafter Paper III).

2. STANDARD MODEL FITTING

2.1. *Analysis and Results*

In the standard model fitting method [for example, see *Einstein* Revised User's Manual (Harris 1984, hereafter RUM)], a two-parameter model (e.g., kT and N_H for a bremsstrahlung spectrum with low-energy cutoff; α and N_H for a power-law spectrum with low-energy cutoff) is convolved with the instrumental response of the *Einstein* IPC for a range of spectral parameters, and then compared with the observed distribution of counts in the IPC pulse height (PH) channels using the minimum χ^2 technique. We restricted our fits to PH channels corresponding to energies in the range of $\sim$0.2 to $\sim$4 keV, because the uncertainties in the calibration of the IPC beyond either end is considerably larger (Harnden et al. 1984). We also exclude the PH channel 1, regardless of its energy, because the calibration of PH channel 1 is far more uncertain than that of the other PH channels. The exact energy range depends on

THE ASTROPHYSICAL JOURNAL, 393:134–148, 1992 July 1

THE X-RAY SPECTRA OF GALAXIES. II. AVERAGE SPECTRAL PROPERTIES AND EMISSION MECHANISMS

D.-W. KIM
Chungnam National University, Daejeon 305-764, South Korea; and Harvard-Smithsonian Center for Astrophysics, 60 Garden Street, Cambridge, MA 02138

G. FABBIANO
Harvard-Smithsonian Center for Astrophysics, 60 Garden Street, Cambridge, MA 02138

AND

G. TRINCHIERI
Osservatorio Astrofisico di Arcetri, Largo E. Fermi 5, 50125 Firenze, Italy; and Harvard-Smithsonian Center for Astrophysics, 60 Garden Street, Cambridge, MA 02138

Received 1991 September 25; accepted 1992 January 9

ABSTRACT

We have systematically investigated the X-ray spectra of normal galaxies, by using the Imaging Proportional Counter (IPC) data in the *Einstein* data base. We find that on the average the X-ray emission temperature of spirals is higher than that of ellipticals. This is consistent with our understanding that accreting binaries are a major source of X-rays in spirals, while a hot interstellar medium (ISM) is present in ellipticals. The X-ray spectra of Sa galaxies are intermediate between those of ellipticals and spirals, suggesting that these galaxies contain hot gaseous emission as well as emission from accreting binaries. We confirm that the X-ray to optical ratio is an important indicator of the presence of a hot gaseous component in early-type galaxies. In particular we find that the emission temperature becomes higher with a decreasing X-ray to optical luminosity ratio in E and S0 galaxies. This result is what we would expect if the emission of X-ray faint early-type galaxies consists of a large evolved stellar component, while the gaseous emission becomes dominant in X-ray brighter galaxies. The group with the lowest L_X/L_B does not follow this trend. In these galaxies we find a *very soft* ($kT \sim 0.2$ keV) X-ray component, amounting to about half the total X-ray emission, in addition to the hard X-ray component. Possible explanations for this component include the integrated emission of M stars and a relatively cool ISM. A *very soft* component is also found in several spiral galaxies. This result may indicate that some spirals contain hot gaseous components similar to those seen in NGC 253 and M82.

Subject headings: galaxies: elliptical and lenticular, cD — galaxies: spiral — radiation mechanisms: miscellaneous — X-rays: galaxies

1. INTRODUCTION

Based on the results from the *Einstein Observatory* (Giacconi et al. 1979), it is now known that normal galaxies of all morphological types are sources of X-ray emission with luminosities in the range of 10^{38}–10^{42} ergs s^{-1} (see Fabbiano 1989 for a review). The imaging data and the results of the spectral fits of a relatively small number of galaxies have suggested that different sources are responsible for the X-ray emission in galaxies of different morphological types. While in spiral galaxies accreting binaries are a major source of X-ray emission (see Fabian 1981; Helfand 1984; Fabbiano & Trinchieri 1985, 1987), in bright elliptical galaxies hot gaseous emission can be the dominant source of X-rays (Forman, Jones, & Tucker 1985; Trinchieri & Fabbiano 1985; Canizares, Fabbiano, & Trinchieri 1987). Supernova remnants or masssive young stars may dominate in blue starburst galaxies, together with emission from outflowing gaseous plumes in some cases (Fabbiano, Feigelson, & Zamorani 1982; Stewart et al. 1982; Watson, Stanger, & Griffiths 1984; Fabbiano & Trinchieri 1984; Fabbiano 1988b; Fabbiano, Heckman, & Keel 1990).

The purpose of this paper is to study the average spectral properties of reasonably large samples of galaxies of different types and to use these results to constrain the X-ray emission chieri 1992), whose spectral parameters and/or X-ray colors have been tabulated by Kim, Fabbiano, & Trinchieri (1992, hereafter Paper I). Most of these galaxies were not detected with enough statistics to yield meaningful spectral parameters, when analyzed singly. To overcome this problem, we have studied the distribution of X-ray colors, and we have derived and compared combined spectra for given classes of galaxies. The analysis methods are described and justified in § 2. The sample selection is discussed in § 3.

First, we investigate the differences in the average X-ray spectra of galaxies of different morphological types (§ 4). In particular, we examine the average spectral properties of spiral and elliptical galaxies, and we take a closer look at S0 and Sa galaxies, intermediate in disk-to-bulge ratio, to determine the relative importance of stellar sources and hot gaseous ISM in their X-ray emission.

Second, we address the question whether E and S0 galaxies with relatively faint X-ray emission retain a hot gaseous ISM as do X-ray luminous elliptical galaxies (§ 5). If the spectra of less luminous ellipticals differ from those of the bright galaxies, this may imply a global difference between the two subsamples in the process of formation and evolution. If early-type galaxies with hot gaseous components can be properly selected by their X-ray spectra, they can then be used to further investigate the